

THE STRUCTURE AND EVOLUTION OF STARS OF
VERY LOW MASS

by

Dwight Thomas Hoxie

A Dissertation Submitted to the Faculty of the
DEPARTMENT OF ASTRONOMY

In Partial Fulfillment of the Requirements
For the Degree of

DOCTOR OF PHILOSOPHY

In the Graduate College
THE UNIVERSITY OF ARIZONA

1 9 6 9

THE UNIVERSITY OF ARIZONA

GRADUATE COLLEGE

I hereby recommend that this dissertation prepared under my
direction by Dwight Thomas Hoxie
entitled The Structure and Evolution of Stars of Very Low
Mass
be accepted as fulfilling the dissertation requirement of the
degree of Doctor of Philosophy

Ray J. Weymann
Dissertation Director

March 5, 1969
Date

After inspection of the final copy of the dissertation, the
following members of the Final Examination Committee concur in
its approval and recommend its acceptance:*

R. E. Williams

March 5, 1969

Donald J. Taylor

March 5, 1969

T. L. Swihart

5/5/69

Boald K. Wangness

5 March 1969

Ray J. Weymann

March 5 1969

*This approval and acceptance is contingent on the candidate's adequate performance and defense of this dissertation at the final oral examination. The inclusion of this sheet bound into the library copy of the dissertation is evidence of satisfactory performance at the final examination.

STATEMENT BY AUTHOR

This dissertation has been submitted in partial fulfillment of requirements for an advanced degree at The University of Arizona and is deposited in the University Library to be made available to borrowers under rules of the Library.

Brief quotations from this dissertation are allowable without special permission, provided that accurate acknowledgment of source is made. Requests for permission for extended quotation from or reproduction of this manuscript in whole or in part may be granted by the head of the major department or the Dean of the Graduate College when in his judgment the proposed use of the material is in the interests of scholarship. In all other instances, however, permission must be obtained from the author.

SIGNED: Dwight Thomas Hoxie

ACKNOWLEDGMENTS

The author wishes to express his gratitude to the following persons who have contributed both materially and spiritually to the completion of this work:

To Dr. Ray J. Weymann who initially suggested the problem and who, as advisor, provided much of the impetus and guidance and contributed greatly to solving many of the seemingly insurmountable problems encountered along the way;

To Dr. Bart J. Bok, Director of Steward Observatory, for his interest and encouragement and for arranging for financial support during the final stages of this work;

To my wife, Janelle, for her endurance, her encouragement, and especially for the many hours she spent at various typewriters and keypunches;

To the University of Arizona Computing Center and personnel, especially Mrs. Vinnie Bradford, Dave McQueeney, and Ernest Payne, for their assistance with the computer programs and for making available the facilities of the IBM 7072 and CDC 6400 computer systems;

To Drs. P. Demarque, H. DeWitt, R. Emrick, H. Graboske, H. Mahmoud, E. Schatzman, M. Schwarzschild, T. Swihart, D. Taylor, M. Vardya, R. Wangsness, and R. Williams for helpful discussions at various stages of this work;

Finally, to my mother without whose encouragement and support over so many years neither the initiation nor the completion of this work would have been possible.

TABLE OF CONTENTS

	Page
LIST OF ILLUSTRATIONS	vii
LIST OF TABLES	ix
ABSTRACT	x
CHAPTER	
1. INTRODUCTION	1
2. HISTORICAL BACKGROUND	7
3. OBSERVATIONAL DATA FOR LOW MASS STARS	23
4. THERMODYNAMIC, OPACITY, AND NUCLEAR ENERGY GENERATION DATA FOR THE STELLAR INTERIOR	43
4.1 Thermodynamic Properties of an Interacting Hydrogen-Helium Plasma	44
4.1.1 Debye-Hückel Region	49
4.1.2 Monte-Carlo Region	51
4.1.3 Ion-Pair Model	53
4.2 Pressure Ionization of Hydrogen and Helium	57
4.3 Pressure Dissociation of Molecular Hydrogen	72
4.4 Interior Opacity	75
4.5 Nuclear Energy Generation Rate	76
4.6 Constitutive Data Table	78
4.6.1 $T > 5000$ °K	79
4.6.2 $T < 5000$ °K	86
5. ATMOSPHERIC MODELS FOR LOW MASS STARS	97
5.1 Equation of State, Adiabatic Gradient, and Radiative Opacity	98
5.2 Radiative Region	103
5.3 Convective Transition Region	109
5.4 Computation of Atmospheric Data Table	112

TABLE OF CONTENTS--Continued

CHAPTER	Page
6. CONSTRUCTION OF THE THEORETICAL EVOLUTIONARY STELLAR MODELS	117
6.1 Polytropic Evolutionary Models	120
6.2 Calculation of the Detailed Evolutionary Models	135
6.3 Comparison and Discussion of the Theoretical and Empirical Main Sequence Properties	147
6.3.1 Theoretical Models	152
6.3.2 Empirical Data	155
6.4 Stars Below the Main Sequence Limiting Mass	160
6.5 The Shape of the Mass Function	162
APPENDIX A. DEBYE-HÜCKEL THEORY FOR AN IONIZED, PARTIALLY DEGENERATE PLASMA	165
REFERENCES	179

LIST OF ILLUSTRATIONS

Figure	Page
1. Adopted transformation between R-I and $(R-I)_E$	30
2. Adopted bolometric correction (B.C.) and effective temperature (T_e) calibration for the M dwarf stars	31
3. Adopted $(R-I)_E$, M_V relation	32
4. Adopted sun-Sirius mass-luminosity relation	34
5. Empirical main sequence locus in the H-R diagram	37
6. Adopted B-V, M_V relation from Eggen (1968)	39
7. Mass function for the solar neighborhood	41
8. Domain of the constitutive data table in the $\log \rho$, $\log T$ plane	91
9. The magnitude of the pressure correction as a function of the pressure and temperature in a hydrogen-helium plasma	92
10. $\log T_{\text{mxl}}$ as a function of g_{srf} with T_e as parameter	114
11. $\log P_{\text{mxl}}$ as a function of g_{srf} with T_e as parameter	115
12. Polytropic evolution in the H-R diagram	129
13. Behavior of central values of the temperature and the density for the polytropic evolutionary models	133
14. Evolution of the detailed 0.1 and 0.07 M_\odot models in the H-R diagram	143
15. Comparison of the evolutionary behavior of detailed 0.1 M_\odot model with that calculated by Ezer and Cameron (1966)	145

LIST OF ILLUSTRATIONS--Continued

Figure	Page
16. Comparison of theoretical and empirical mass-luminosity relations	148
17. Comparison of theoretical and empirical mass-radius relations	149
18. Comparison of the theoretical and empirical main sequence loci in the H-R diagram	150
19. Comparison of the empirical and theoretical mass-radius relations with the data for the eclipsing binary systems	158

LIST OF TABLES

Table	Page
1. Observational Data for Low Mass Binary Pairs	27
2. Adopted Mean Empirical Main Sequence Properties of the Low Mass Stars	36
3. Rosseland Mean Atmospheric Opacities (Log $\bar{\kappa}_R$)	104
4. Theoretical Main Sequence Properties of the Polytropic Models	131
5. Detailed Evolution at $0.1 M_\odot$	141
6. Detailed Evolution at $0.07 M_\odot$	142

ABSTRACT

Both an "idealized" and a "detailed" approach are employed to calculate the pre-main sequence evolutionary behavior and main sequence structure of very low mass stars of nearly solar composition ($X = 0.739$, $Y = 0.240$, $Z = 0.021$). The "idealized" approach is based on the assumptions that during the Hayashi contraction phase as well as during main sequence hydrogen burning such objects are in convective equilibrium throughout and that the interiors are composed of a completely ionized, partially degenerate ideal gas. Under these assumptions the interior structure may be represented by a polytrope of index $n = 1.5$. Using a simple interpolation formula to represent the nuclear energy generation rate due to the He^3 terminated proton-proton chain and a set of model atmospheres calculations, a semi-analytic formulation for calculating the evolutionary behavior of these "idealized" polytropic models is derived and employed to calculate the pre-main sequence evolutionary behavior of objects in the mass range 0.14 - $0.02 M_{\odot}$. From these calculations it is found that the lower limiting mass below which objects fail to achieve sufficiently high interior temperatures to produce enough nuclear energy release to stabilize on the main sequence is $0.085 M_{\odot}$. This value for the main sequence limiting

mass is in good agreement with values determined theoretically by previous investigators.

The validity of the assumptions entering into the polytropic representation of very low mass objects is tested through the calculation of "detailed" evolutionary sequences at 0.1 and 0.07 M_{\odot} . The "detailed" models are constructed explicitly through numerical solution of the equations of stellar structure. An improved calculation of the nuclear energy generation rate is undertaken in these models and the condition for convective equilibrium is tested at each point within the interior. The hydrogen-helium ionization-dissociation zone is treated in detail through application of approximate treatments for the pressure ionization of hydrogen and helium and the pressure dissociation of molecular hydrogen. In addition the effect on the overall structure due to departures from ideal gas behavior arising from the electrostatic interactions between charged particles within the ionized interior are explored. From the results of these model calculations it is concluded that the polytropic models should provide a reasonable approximation to the structure and evolution of very low mass main sequence objects. The 0.07 M_{\odot} object fails to reach the main sequence and the electrostatic interaction effects begin to influence significantly the evolutionary track in the H-R diagram shortly after the central temperature reaches its maximum value.

The same set of atmospheric models is used in conjunction with both the "idealized" and "detailed" models. In constructing these atmospheric models the Eddington graybody approximation is used to treat the outermost radiative region while a simple version of the mixing length theory is used to treat the underlying superadiabatic convective zone. Water vapor is included as a source of atmospheric opacity.

The currently available data regarding the masses, radii, luminosities, and effective temperatures for the low mass stars are reviewed. From these data a set of mean empirical main sequence properties of the low mass stars of presumed solar composition is adopted and compared with the main sequence properties defined by the theoretical models. It is found that while the models appear to reproduce satisfactorily the adopted empirical mass-luminosity relation, there is a considerable lack of agreement between the theoretical and empirical mass-radius relations and therefore between the respective main sequence locii in the H-R diagram as well. Several possible inadequacies of the models as well as the empirical data are discussed but no completely satisfactory explanation for the apparent discrepancy between theory and observation is found.

CHAPTER 1

INTRODUCTION

Because of the observed existence of massive highly luminous stars whose ages are very much less than that of the galaxy, we conclude that star formation is a continuing process and that stars form out of the interstellar medium. While our understanding of the instabilities which lead to the formation of objects of stellar mass is far from complete (cf. Spitzer 1968), we have reason to believe (Hayashi 1966) that once a proto-star is formed it will undergo rapid dynamical collapse until the dissociation of molecular hydrogen as well as the ionization of atomic hydrogen and helium are complete throughout the bulk of the interior and the interior opacity has risen to such values as to inhibit the outward flow of the thermal energy. At this point essentially stellar conditions obtain, the central temperature will be of the order of 10^5 °K and the radius of an object of mass M will be of the order of $50 (M/M_{\odot}) R_{\odot}$ (Hayashi 1966). At this point the object will enter into a period of relatively slow Helmholtz-Kelvin contraction. The characteristic feature of this phase of stellar evolution is that at any instant of time the object may be regarded as being in a state of quasi-hydrostatic

equilibrium with the rate of contraction being determined by the condition that the rate of gravitational energy release be just sufficient to maintain the stellar luminosity.

As the contraction proceeds, the interior values of temperature and density rise, and for normal stars a point will be reached at which the temperature in the central regions becomes high enough to initiate thermonuclear hydrogen burning. With a portion of the star's energy demands being met by nuclear energy generation, the contraction will slow, and when the nuclear energy release becomes sufficient to maintain the luminosity, the contraction will cease altogether. At this instant the star will be in steady-state thermal and mechanical equilibrium and will have arrived at its position on the zero-age main sequence.

While it is true that in most instances continued gravitational contraction will be accompanied by a rise in the interior temperature, indefinitely high values of temperature can in fact never be obtained. This is a consequence of the onset of electron degeneracy which will occur for an object of any given mass should the interior density become sufficiently high. By electron degeneracy we refer to the condition prevailing at high electron densities under which the electrons must be treated explicitly as Fermi-Dirac particles obeying the Pauli

exclusion principle. In this circumstance the compression of the free electrons into ever shrinking geometric volumes as a result of continued contraction can be accomplished, according to the exclusion principle, only by making states of higher (kinetic) energy available to the electrons.

When the degree of degeneracy becomes sufficiently high, a point will be reached beyond which further contraction can occur only at the expense of the thermal energy of the non-degenerate ions. At this point the temperature, which is a measure of the thermal (kinetic) energy of the ions, will reach a maximum value and will decrease with further contraction. We anticipate that there exists some limiting stellar mass below which a sufficiently high degree of electron degeneracy is achieved during the course of the gravitational contraction that the interior temperature never reaches a sufficiently high value to produce enough thermonuclear hydrogen burning to stabilize the object on the main sequence (Kumar 1963; Hayashi and Nakano 1963; Ezer and Cameron 1966). Objects less massive than this limiting mass never reach the main sequence but are doomed to undergo continued slow contraction towards completely degenerate configurations, thus prematurely entering into the final white dwarf stage of stellar evolution.

It is our intention to investigate this aspect of stellar evolution and to attempt a determination of the

limiting mass below which objects fail to reach the main sequence. To accomplish this we shall construct evolutionary sequences of stellar models for objects of various masses undergoing pre-main sequence gravitational contraction. We shall follow the evolution of objects more massive than the hypothesized limiting mass to the point at which it is certain that the main sequence stage is reached; while for objects less massive than the limiting mass, we shall continue to follow their evolutionary course until their radii have approached the nearly constant values appropriate to completely degenerate configurations.

A further consequence of the high densities and relatively low temperatures expected in the interiors of low mass stars is that, in determining the thermodynamic properties of the gaseous interior, the ideal gas approximation of non-interacting particles breaks down and the interactions between particles must be taken explicitly into account. In a gas consisting of a mixture of ions and electrons, we expect that the electrostatic interactions between the charged particles will provide the major contribution to departures from ideal gas behavior. We shall, in an admittedly very approximate way, attempt to incorporate corrections to the ideal gas thermodynamic functions to account for the electrostatic interactions and shall further endeavor to assess the extent to which these affect the overall structure of the models for low mass stars.

We also expect that in high density gases neighboring particles will so perturb the potential field in which the outer bound electrons of a given ion move as to result in an effective lowering of the energy required to remove these electrons from the ion. This leads to the phenomenon of pressure induced ionization which is expected to affect greatly the ionization equilibrium within the deeper regions of the stellar interior. We shall develop a simplified treatment of pressure ionization which will be employed in determining the ionization equilibrium of hydrogen and helium throughout the stellar interior. We shall also employ an approximate theory to account for the analogous effect of the pressure dissociation of molecular hydrogen.

From the computation of an evolutionary sequence of stellar models for an object of given mass and chemical composition, we obtain predicted values of the radius, luminosity, and the effective temperature as functions of time. We can display the evolutionary path described by the models in the theoretical H-R diagram, that is, in a plot of luminosity versus the effective temperature. It is our hope that such predicted behavior will, in fact, represent the evolutionary behavior of real stars. To test the adequacy with which the theoretical models do represent real stars, we require observationally determined values of the masses, radii, luminosities and chemical

compositions. Ideally we would also like information regarding the evolutionary behavior, but, of course, most stages of stellar evolution are prohibitively long to be followed directly by observational means.

In the following chapter we review the historical developments associated with the construction of stellar models for low mass stars and in Chapter 3 we discuss the observational data concerning the masses, luminosities and effective temperatures for such stars. In Chapter 4 we consider the thermodynamic properties of an interacting hydrogen-helium plasma while in Chapter 5 we present the results of model atmosphere integrations appropriate to low mass stars. We utilize the latter to obtain the surface boundary condition needed in the integration of the equations of stellar structure. Finally in Chapter 6 we describe the model calculations of both an idealized and a detailed approach to the problem. In this last chapter we also compare the theoretical results with the available observational data and attempt an assessment of the possible observational consequences resulting from the existence of a lower limiting mass for main sequence stars.

CHAPTER 2

HISTORICAL BACKGROUND

The construction of a stellar model involves the simultaneous solution of a set of four first order, non-linear differential equations. These equations must be solved numerically and to do so by hand computation is, indeed, a formidable task; although techniques have been devised to reduce the required labor (see Schwarzschild 1958). Prior to the development of high-speed computers, emphasis in stellar model calculations was placed on the construction of static equilibrium models of main sequence stars. An initial reconnaissance of the problem of computing such models for red dwarf stars is undertaken by Williamson and Duff (1949a, b) who attempt to fit models to the observational values of mass, radius and luminosity given by Chandrasekhar (1939) for the stars Krüger 60A (M3), α^2 Eridani C (M5e) and YY Geminorum (M0). It is assumed that these stars can be represented by spherically symmetric models consisting of central cores in convective equilibrium surrounded by outer radiative envelopes. It is further assumed that the carbon cycle is the process of energy generation. It is found, however, that the results

obtained are unsatisfactory in that they are not entirely consistent with the initial assumptions.

Aller (1950) attempts to assess the relative contributions of the carbon cycle and the proton-proton chain in providing the luminosities of low mass stars. Using models taken to be homologous to Schwarzschild's (1946) model of the sun, he seeks values of the abundances of hydrogen and helium for which the computed luminosity is equal to that observed and for which the models satisfy the mass-luminosity relation. Kuiper's (1938) values of the masses, radii and luminosities of the stars Krüger 60A and ϵ^2 Eridani C are employed and it is found that consistent models can be obtained only for rather low hydrogen abundances. It is acknowledged, however, that assuming these stars to be homologous to the sun may be a poor assumption and that little confidence can be placed in the results predicted by such models.

Employing the results of Salpeter's (1952) calculation of the energy generation rate for the proton-proton chain, Aller et al. (1952) construct a model for the star Krüger 60A under the assumption that it is homologous to the sun and that the proton-proton chain provides the energy output. The mass, radius and luminosity are taken from Kuiper (1938) and the chemical compositions are taken to be $X = 0.34$ and $Y = 0.64$, where X and Y are the fractional abundances by mass of hydrogen and helium,

respectively. No satisfactory solution is obtained as the model predicts an appreciably higher luminosity than observed.

Basic to the models proposed by Williamson and Duff (1949a, b) and by Aller and his associates (Aller 1950; Aller et al. 1952) is the assumption that these stars can be represented by models consisting of convective cores overlaid by radiative envelopes. Naur and Osterbrock (1953) show that stars of later type than the sun, and the sun as well, are expected to be in radiative equilibrium in their central regions. Furthermore Stromgren (1952) suggests that the zone in the outer regions of the star in which hydrogen is undergoing ionization will be expected to be in convective equilibrium and will, further, be expected to extend deep into the interiors of the late type stars.

Osterbrock (1953) undertakes the task of computing new models for red dwarf stars incorporating these features. His models consist of central radiative cores surrounded by convective envelopes overlaid in turn by thin radiative atmospheres. He further assumes that the proton-proton chain is the only source of energy generation. The calculations are particularized to the values of the mass, radius and luminosity given by Kuiper (1938) for the average component of the binary system YY Gem. Models are constructed by fitting together at the outer boundary of the radiative core inward integrations from the surface with

outward integrations from the center. A family of models is obtained which depends upon the hydrogen and helium abundance parameters, X and Y . It is found that satisfactory models for YY Gem as well as the K1 dwarf α Centauri B can be obtained using values of X and Y typical of the sun. However, it is further found that such models will not adequately represent stars of later spectral type than M0 for any reasonable values of the abundances. It thus appears that further revision of the models is required to extend the model calculations to stars of later type.

In two papers Limber (1958a, b) continues the attack on the problem of the internal structure of M dwarf stars. In the first of these papers Limber (1958a) reassesses the observational data regarding the masses, radii, and luminosities of low mass stars. In view of revisions in these data as well as Osterbrock's (1953) work, he concludes that the envelope convective zones in middle and late M dwarfs will be expected to extend to the centers of these stars and, thus, that these stars must be regarded as wholly convective structures.

In the second paper Limber (1958b) attempts to construct models for completely convective stars. He includes electron degeneracy inasmuch as it affects the interior equation of state and shows that the interior can be represented by a polytrope of index 1.5 throughout the bulk of the star in which hydrogen and helium are completely

ionized. The polytrope, and thus, the interior, solution is completely determined upon specification of the mass, radius, and chemical composition of the configuration. The luminosity of the model is obtained through a subsidiary integration of the equation of thermal equilibrium. For this purpose Limber (1958b) represents the nuclear generation rate by interpolation formulae based upon Salpeter's (1952) work on the proton-proton chain. Limber (1958b) tabulates luminosities and effective temperature as a function of the radii for models in the mass range from $1.0 M_{\odot}$ to $0.091 M_{\odot}$.

From the polytrope solutions alone one obtains a mass, radius and luminosity relation for a given set of chemical composition parameters X and Y , for which Limber (1958b) chooses the values $X = 0.75$ and $Y = 0.23$. Considering the composition as fixed, we see that associated with a given mass there will be a continuous sequence of models of differing radii and luminosities. Hence, a model of given mass will define a line in the H-R diagram. If the theory is adequate, the observational values of luminosity and effective temperature for a star of given mass should fall along the corresponding theoretical line within the expected probable errors in the theory and the observation. Limber compares his results with the observational data for the stars Krüger 60A and 60B and finds that the discrepancies between the theory and the

observations are larger than the expected errors. He concludes, however, that the models can be described as being at least consistent with the observations.

One difficulty encountered with the polytrope models, as mentioned above, is that they alone do not permit a determination of both the radius and luminosity upon specification of the mass and chemical composition, a result which we expect from the Russell-Vogt theorem. The reason for this is that in obtaining the polytrope solution only one of two outer boundary conditions is actually invoked. The second boundary condition can be expressed through the relation between the pressure and the temperature as the surface of the star is approached. In the completely ionized interior the pressure, P , and temperature, T , satisfy the adiabatic relation, $P = KT^{2.5}$, where K is a constant. To satisfy the second boundary condition we perform an inward integration through the outer radiative atmosphere and the ionization zone to the point in the interior at which ionization is complete and demand the value of the constant, K , obtained at this point be equal to that at the center. Limber undertakes such a calculation using the observational data for the mass, radius, and luminosity of Krüger 60A. An approximate atmospheric integration is performed using the graybody relation between temperature and optical depth and assuming the atmosphere to be composed entirely of atomic hydrogen with

the H^- ion being the only source of opacity. The atmospheric integration is halted once convection sets in, and the values of pressure and temperature appropriate to the bottom of the ionization zone are obtained by requiring that the entropy computed at the base of the atmosphere be equal to that at the bottom of the ionization zone. From this condition the value of the adiabatic constant, K , appropriate to the atmosphere-envelope integration is evaluated. It is found that in using the observational data for Krüger 60A the agreement between the interior and the atmosphere-envelope solutions is quite poor. Limber (1958b) emphasizes the approximate nature of the atmospheric integration and points out several possible sources of uncertainty. He also attempts to determine the effect of the hydrogen ionization zone on the radius. In this calculation he includes a very approximate correction for the effect of pressure ionization of hydrogen and concludes that the inclusion of the ionization zone will result in an increase in the radius of the model by less than one per cent.

Limber (1958b) also delineates in the mass-radius plane the domain appropriate to the completely convective models. The physical effects restricting the applicability of the models include the occurrence of energy transport by electron conduction and radiation as well as the occurrence of complete degeneracy within the interior. From his plot it is apparent that as one proceeds along the main sequence

from early to late M dwarfs the radiative cores will disappear, and the stars become wholly convective. Electron conduction may become an important energy transport mechanism in the central regions of those stars of lowest mass. The circumstance of nearly complete electron degeneracy in the interiors of these stars will probably not occur in objects undergoing steady-state hydrogen burning, but would determine the limiting radii of those objects having exhausted their store of hydrogen or in those not passing through the hydrogen burning stage.

Recognizing that the polytrope models of fixed mass and composition but with decreasing radii can be used to simulate the stage of gravitational contraction, Kumar (1963) attempts to determine the limiting mass below which hydrogen burning will not be expected to occur. The procedure involved is essentially that of extending Limber's (1958b) calculations to objects of lower mass. Kumar considers two possible chemical compositions which he takes to be representative of Population I and II objects, respectively. It is found that as a given object approaches the limiting radius appropriate to a completely degenerate configuration, the central temperature passes through a maximum value and begins to decrease. Kumar concludes that the maximum value of the central temperature reached by Population I objects less massive than $0.07 M_{\odot}$ and Population II objects less massive than $0.09 M_{\odot}$ will be

insufficiently high to produce enough hydrogen burning to meet the energy demands of these objects. These values of the limiting mass must be regarded as being rather tentative, however, as Kumar does not obtain complete stellar models in which both of the outer boundary conditions are satisfied. To accomplish this it would be necessary to attach appropriate stellar atmospheric models to the interior solutions.

Hayashi and Nakano (1963) have investigated specifically the pre-main sequence contraction phase for stars of low mass. Historically the first attempt to depict in the H-R diagram the evolutionary tracks followed by contracting stars was undertaken by Henyey, LeLevier, and Levéé (1955). Under the assumption that such objects were wholly in radiative equilibrium, they found that the contracting stars move towards the main sequence along upwardly inclined tracks originating in the lower right hand portion of the H-R diagram, that is, the region of low luminosities and effective temperatures. However, Hayashi and Hōshi (1961) point out that the outer regions of contracting stars are expected to be in convective equilibrium as a result of the lowered adiabatic gradient prevailing in the region in which hydrogen and helium are undergoing ionization. By employing the outer boundary condition appropriate to stars with convective envelopes, Hayashi (1961) obtains pre-main sequence tracks which differ

considerably from those of Henyey et al. (1955). Subsequent work by several authors, e.g., Hayashi, Hōshi, and Sugimoto (1962), Weymann and Moore (1963), Iben (1965) and M. Hayashi (1965), have confirmed Hayashi's (1961) results.

According to Hayashi (1961) the initial collapse of a pre-stellar object will carry it to a position of high luminosity in the H-R diagram. At this point the object will be wholly convective and will enter the phase of slow luminosity-controlled Helmholtz-Kelvin contraction. As the contraction proceeds the object will descend vertically in the H-R diagram, moving towards the main sequence at almost constant effective temperature. For stars more massive than $0.26 M_{\odot}$, according to Hayashi and Nakano (1963), a radiative core will develop and expand radially outward during the course of the contraction. If the radiative core achieves appreciable extent, the track will turn abruptly to the left and subsequent evolution will occur in accordance with that predicted by Henyey et al. (1955). The track will terminate on the main sequence when the temperature in the interior achieves sufficiently high values to initiate hydrogen burning.

Applying these results to low mass stars, Hayashi and Nakano (1963) compute a series of contracting models for stars in the mass range $0.6 M_{\odot}$ to $0.05 M_{\odot}$ in which they include the effects of electron degeneracy within the interiors as well as the presence of molecular hydrogen in

the envelopes. Objects less massive than $0.26 M_{\odot}$ are found to remain wholly convective throughout the contraction phase, and the interior regions of these objects in which ionization is complete are represented by a polytrope of index 1.5. The outer boundary condition for the models is obtained in a manner very similar to that described by Limber (1958b) by noting that within the interior the pressure, P , and the temperature, T , satisfy the adiabatic relation $P = KT^{2.5}$, where K is a constant. This relation will hold for a specific value of K throughout the region in which ionization is complete. A complete model is obtained by requiring that the value of K obtained from an integration through the atmosphere and envelope to the point at which ionization is complete agree with that obtained from the interior. For the purpose of this calculation it is assumed that above the photosphere, defined as that point in the star at which the optical depth $\tau = 2/3$, the atmosphere is isothermal. It is further assumed that the temperature gradient in the envelope region underlying the photosphere, in which molecular hydrogen is undergoing dissociation and hydrogen and helium are undergoing ionization, is equal to the adiabatic gradient. To perform the integration through the envelope, Hayashi and Nakano (1963) resort to the expediency of simply calculating the entropy at the photosphere and requiring that the value so obtained be equal to that in

the interior in which ionization is complete. From this result the value of K appropriate to the atmosphere-envelope integration is obtained, and by fitting this to the interior value, the appropriate radius and luminosity of each model is determined.

For objects of low mass, the energy generation is provided by the proton-proton chain which, at the low temperatures prevailing in the interiors of these objects, will terminate with the production of He^3 rather than going to completion with the production of He^4 . In this case the rate of energy generation will be about half that of the complete chain. Expressing the energy generation rate as an interpolation formula in powers of the temperature and the density, Hayashi and Nakano (1963) find that the limiting mass below which objects will fail to enter the main sequence phase of steady state hydrogen burning is $0.08 M_{\odot}$ for Population I objects and $0.12 M_{\odot}$ for Population II objects. Because of the increasing effects of electron degeneracy in less massive objects, the evolutionary tracks turn away from the main sequence, and such objects continue to contract towards completely degenerate configurations. It should be noted that this result is in quite good agreement with that found by Kumar (1963).

Hayashi and Nakano (1963) also compare their models with the observational data given by Limber (1958a) for the stars Krüger 60A and 60B and Ross 614B. A plot in the H-R

diagram of the predicted luminosities and effective temperatures against the observed values shows the models and the observation to be discrepant in that for Krüger 60A and B the models have higher effective temperatures than the observed values, while the model for Ross 614B has both a higher effective temperature and luminosity. It is deemed likely that these discrepancies resulted from the very approximate treatment accorded the determination of the outer boundary condition for the model calculations. In the first place the atmosphere will not be isothermal, and the effects of non-grayness of the atmosphere should be taken into account as well. Also Hayashi and Nakano (1963) consider absorption due to the H^- ion to be the only source of atmospheric opacity, and in so doing they may have severely underestimated the total opacity. Indeed, it is found that by arbitrarily multiplying their opacity values by a factor of five, they can significantly reduce the discrepancy between their models and the observations.

Below the point in the atmosphere at which convection sets in there will lie a transition region in which the outward flux of energy will be transported both by convection and radiation. In this region the adiabatic gradient may be a poor approximation to the actual temperature gradient and it is necessary to resort to some approximate technique, such as the mixing length theory, in order to estimate the true temperature gradient.

Hayashi and Nakano (1963) neglect the effect of this region on the models but calculate that the true and adiabatic gradient differ by about 10% in their models for stars of $0.26 M_{\odot}$ and $0.1 M_{\odot}$. They estimate however, that the inclusion of this effect in the models will lead to an inappreciable reduction of the effective temperatures.

The method employed to determine the appropriate value of the parameter K from the atmosphere calculation which matches that of the interior, that is, of requiring the entropy at the top of the convective region be equal to that at the point at which ionization is complete, neglects the effect of the thickness of this region on the radius. Hayashi and Nakano (1963) estimate that for a star of $0.26 M_{\odot}$ the neglect of this effect will be insignificant. In computing the entropy in the region of complete ionization, they include the effects of electron degeneracy and assume that hydrogen is completely ionized; however, they completely neglect the ionization of helium. In so doing they may have underestimated the electron density and, thus, the entropy, to which the electrons make an increasingly greater contribution as they become increasingly degenerate. Nakano (1966) asserts, however, that the neglect of the electrons contributed by the ionization of helium will have little effect on the overall models.

More recently Ezer and Cameron (1966) have reported the results of the computation of evolutionary sequences of

models for stars in the mass range $0.4 M_{\odot}$ to $0.1 M_{\odot}$. They use the Population I composition $X = 0.739$ and $Y = 0.240$ and find that the evolutionary behavior of their models during the phase of gravitational contraction is essentially the same as that predicted by Hayashi and Nakano (1963). However, they find that the limiting mass below which objects fail to reach the main sequence is $0.1 M_{\odot}$, a value somewhat higher than that found by Hayashi and Nakano (1963) and Kumar (1963) for Population I objects.

It is our purpose in the present work to expand and improve upon the theoretical calculations of Kumar (1963), Hayashi and Nakano (1963), and Ezer and Cameron (1966) regarding the structure and evolution of very low mass stars. Specifically, we construct a set of evolutionary stellar models in which we determine the outer boundary condition through the construction of approximate model atmospheres in which we provide for the effects of water vapor opacity. In these atmospheric calculations we also include a treatment, based on a simple version of the mixing length theory, of the convective transition region immediately underlying the outermost radiative layers. We incorporate approximate treatments of the pressure dissociation of molecular hydrogen and the pressure ionization of hydrogen and helium in treating the structure of the hydrogen-helium ionization-dissociation zone. In addition we investigate the effects of non-ideal gas behavior

within the stellar interior on the overall structure and evolution of these stars. Finally we review the currently best available empirical data for the main sequence properties of the low mass stars and attempt an assessment of the adequacy of the model calculations through comparison of the theoretical results with these empirical data.

CHAPTER 3

OBSERVATIONAL DATA FOR LOW MASS STARS

It is to gain an understanding of the physical state of the interior regions of stars as well as of their evolutionary behavior and the processes governing this behavior that we attempt the construction of time dependent stellar models. In order to judge the adequacy with which the theoretical models represent the structure and evolution of real stars, we must compare the theoretical predictions with the observed properties of real stars. Because of the prohibitively long time scales associated with most evolutionary changes, the evolutionary behavior of individual stars is inaccessible to direct observation. However, we can determine observationally the masses, radii, luminosities, and effective temperatures of individual stars. Our empirical knowledge of stellar evolution consists largely of inferences derived from the color-magnitude diagrams of star clusters and the observed distribution of field stars in the H-R diagram.

In Section 6.2 we calculate the pre-main sequence evolutionary behavior as well as the initial main sequence properties of stars having masses in the range 0.1^4 to $0.085 M_{\odot}$, and it is these results which we desire to

compare with observational data. Because of the very long main sequence lifetimes associated with stars of low mass, we expect that by far the majority of the M dwarf stars in the solar neighborhood are main sequence objects. Furthermore because of the slowness with which such observable properties as the luminosity and radius change during main sequence hydrogen burning, we expect that currently observed values depart inappreciably from the initial main sequence values. Consequently we presume that the mean properties of any observed sample of M dwarf stars in the solar vicinity define those properties associated with the zero-age main sequence.

We must anticipate, of course, some departures by individual stars from such mean relations due, for example, to differences in evolutionary ages, since any arbitrarily chosen sample of M dwarf stars may contain some possibly young objects still undergoing pre-main sequence contraction. A far more likely source of intrinsic scatter, however, may be due to the presence within the sample of different population types having different initial chemical compositions. As an example Eggen (1963) finds that the dwarf stars of the Hyades and Pleiades clusters populate a distinctly different mass-luminosity relation from that defined by the sun and the members of the Sirius common motion group. The Hyades-Pleiades stars are considerably younger than the sun and Eggen (1963) suggests that this

observational difference is explicable in terms of the Hyades stars' having a greater helium abundance than the sun-Sirius stars. In addition to these possible sources of intrinsic scatter, we must expect some accidental scatter about any observationally defined mean relation due to the limitations on the accuracy with which observational measures can be made.

In the present study we are concerned with stars having a chemical composition appropriate to that of the sun and we would prefer to define all means over a sample of stars having nearly this same composition. It is not possible in general, to determine M dwarf compositions directly through observation. We can, however, distinguish population types for these stars as above or, for example, by their kinetic properties. From subsidiary considerations we may be able to associate differences in chemical compositions with the different population types, and thus, determine or at least estimate, the quantitative effects of compositional differences on the observable stellar properties. As a consequence we should exercise some caution in applying the observationally derived mean relations defined over an arbitrary sample of stars to stars having a specific, but perhaps unknown, composition or in utilizing such mean relations with which to compare the results of theoretical calculations employing a fixed composition.

In Table 1a we list the masses, luminosities, effective temperatures, and radii for those K and M dwarf stars which are members of binary pairs for which reliable masses have been determined. In Table 1a we list the data for the low mass components of visual binaries from the compilations of Eggen (1965, 1967). In addition we give the values of the photometrically determined B-V and $(R-I)_E$ color indices for those stars for which these data are available. Here we adopt the convention of using the subscript E to designate the R-I index as measured by Eggen (1968) on the I,R system defined by Kron, Gascoigne, and White (1957). The quantity R-I without a subscript designates the R-I index measured on the photometric system defined by Johnson (1964). In Table 1b we list the corresponding quantities for the components of the eclipsing system YY Gem. Here the mass and radii are taken from Popper (1967), $(R-I)_E$ and B-V from Eggen (1968), and M_V from Johnson (1964). The value of M_{bol} and T_e is based on the bolometric correction of -1.31 adopted for YY Gem by Johnson (1966).

The bolometric corrections and effective temperatures were obtained for the stars of Table 1a from the main sequence bolometric correction and effective temperature calibration proposed by Johnson (1966, Table II). Regarding these data as functions of the R-I index, we transform them to functions of the $(R-I)_E$ index using the correlation

Table 1. Observational Data for Low Mass Binary Pairs

ADS	Name	Sp	M_V	$m(0)$	B-V	$(R-I)_E$	M_{bol}	Log T_e	Log (R/R_\odot)
a. Data for visual binary components									
	1729AB	K8	+7.0	0.7	--	+0.42	--**	--	
	1865AB	dM2	8.5	0.45	+1.39	0.66	+7.4	3.578	-0.14
UV Ceti	AB	M5e	15.5	0.03	--	(1.66)*	11.3	3.43	-0.62
Ross	614A	dM4e	12.9	0.14	--	+1.38	10.1	3.471	-0.47
	B	M8	16.4	0.08	--	(1.72)	12.0	3.42	-0.75
	6554AB	dK2	6.2	0.75	0.85	0.28	--	--	--
	6664AB	dM0	8.5	0.50	1.49	0.66	7.4	3.578	-0.14
	7114BC	dM1	6.1	0.35	--	(0.28)	--	--	--
	7284AB	dK4	6.7	0.70	1.02	0.36	--	--	--
	8048BC	MOV	9.0	0.19	1.38	0.75	7.7	3.558	-0.16
	8166AB	K0	6.2	0.35	0.75	0.28	--	--	--
	8635AB	K8	6.9	0.60	1.08	0.405	--	--	--
	8680AB	K5	6.8	0.6	1.02	0.385	--	--	--
	8901AB	K5	5.9	0.85	0.72	0.27	--	--	--
	9031AB	dK6	7.0	0.6	1.12	0.425	--	--	--
	9352AB	dM0	8.0	0.6	1.29	0.57	7.2	3.604	-0.11
	9716AB	dK4	5.9	0.7	0.92	0.275	--	--	--
	10075AB	dK2	6.4	0.65	0.86	0.315	--	--	--
	10158AB	dK6	6.7	0.38	1.00	0.37	--	--	--
	10188AB	dK6	6.7	0.77	1.04	0.38	--	--	--
-8°	4352AB	dM3e	10.7	0.37	1.60	1.08	8.7	3.511	-0.27
+45°	2505AB	dM4	10.9	0.31	1.49	1.08	8.9	3.511	-0.31
	10585AB	dM0	7.4	0.70	1.14	0.48	--	--	--
+27°	2853AB	K5	7.2	0.60	1.16	0.47	--	--	--
	10786BC	dM4	10.9	0.36	1.50	1.10	8.9	3.509	-0.30
	11046A	KOV	5.7	0.90	0.76	(0.20)	--	--	--
	B	dK6	7.5	0.65	1.15	(0.52)	6.8	3.620	-0.10

Table 1.--Continued

15972A	M4	10.7	0.29	--	(1.06)	8.7	3.514	-0.27
B	M6	12.4	0.17	--	(1.31)	9.8	3.484	-0.43
<u>b. Data for eclipsing binary systems</u>								
YY Gem AB	M0.5V	+9.11	0.58	+1.50	+0.78	+7.80	3.578	-0.222

*Values of R-I contained within parentheses are obtained from measured M_V and Figure 3.

**Data on M_{bol} , $\log T_e$, and R/R_\odot given only for objects with $(R-I)_E > 0.50$.

shown in Figure 1 between the $R-I$ and $(R-I)_E$ indices. This correlation is based on the individual measures of 17 stars observed in common by Johnson (1965, Table 1) and Eggen (1968, Table 1) and is substantially in agreement with the transformation between Johnson's $R-I$ index and that of Kron *et al.* (1957) as determined by Johnson *et al.* (1966). The resulting relations between the bolometric corrections and the effective temperatures and $(R-I)_E$ are shown in Figure 2.

The bolometric corrections and effective temperatures for the stars of Table 1a which have direct $(R-I)_E$ measures available were obtained from Figure 2. Values of $(R-I)_E$ for those stars not having direct measures were obtained from their observed M_V and the relation between M_V and $(R-I)_E$ shown in Figure 3. This relation was adapted from the data of Eggen (1968) and the stars of Table 1 for which direct $(R-I)_E$ measures are available. In Figure 3 these stars are shown by filled circles except for YY Gem which is shown by a cross. For comparison we show in Figure 3 by a dashed line the M_V , $(R-I)_E$ relation we obtain from transforming the M_V , $R-I$ relation adopted by Johnson (1965, 1966) for the main sequence M dwarf stars. The $(R-I)_E$ values listed in Table 1a which were obtained from Figure 3 are shown in parentheses and were used with Figure 2 to obtain the bolometric corrections and effective temperatures. We assume that the $(R-I)_E$ measure listed by

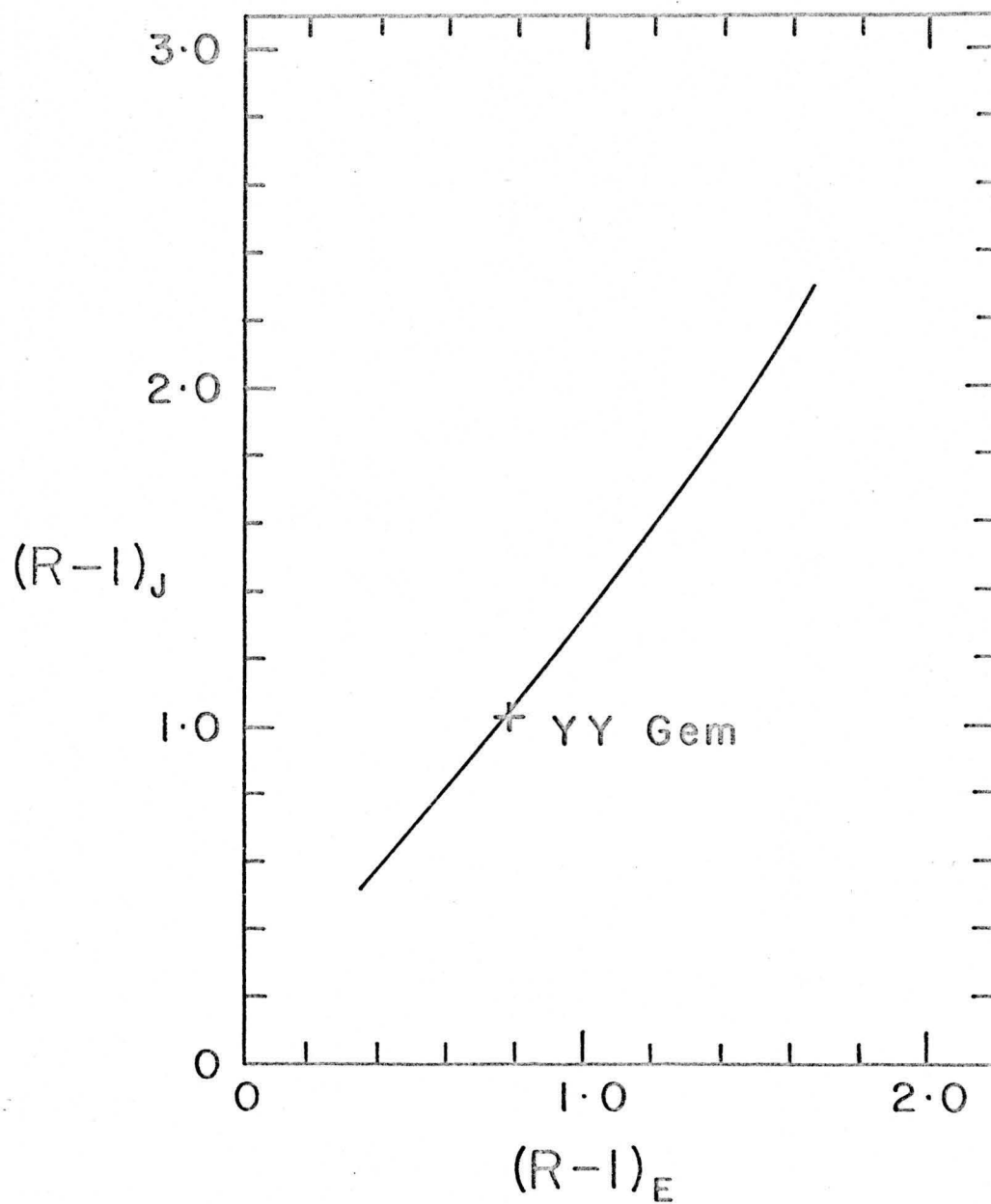


Fig. 1. Adopted transformation between $R-I$ and $(R-I)_E$.

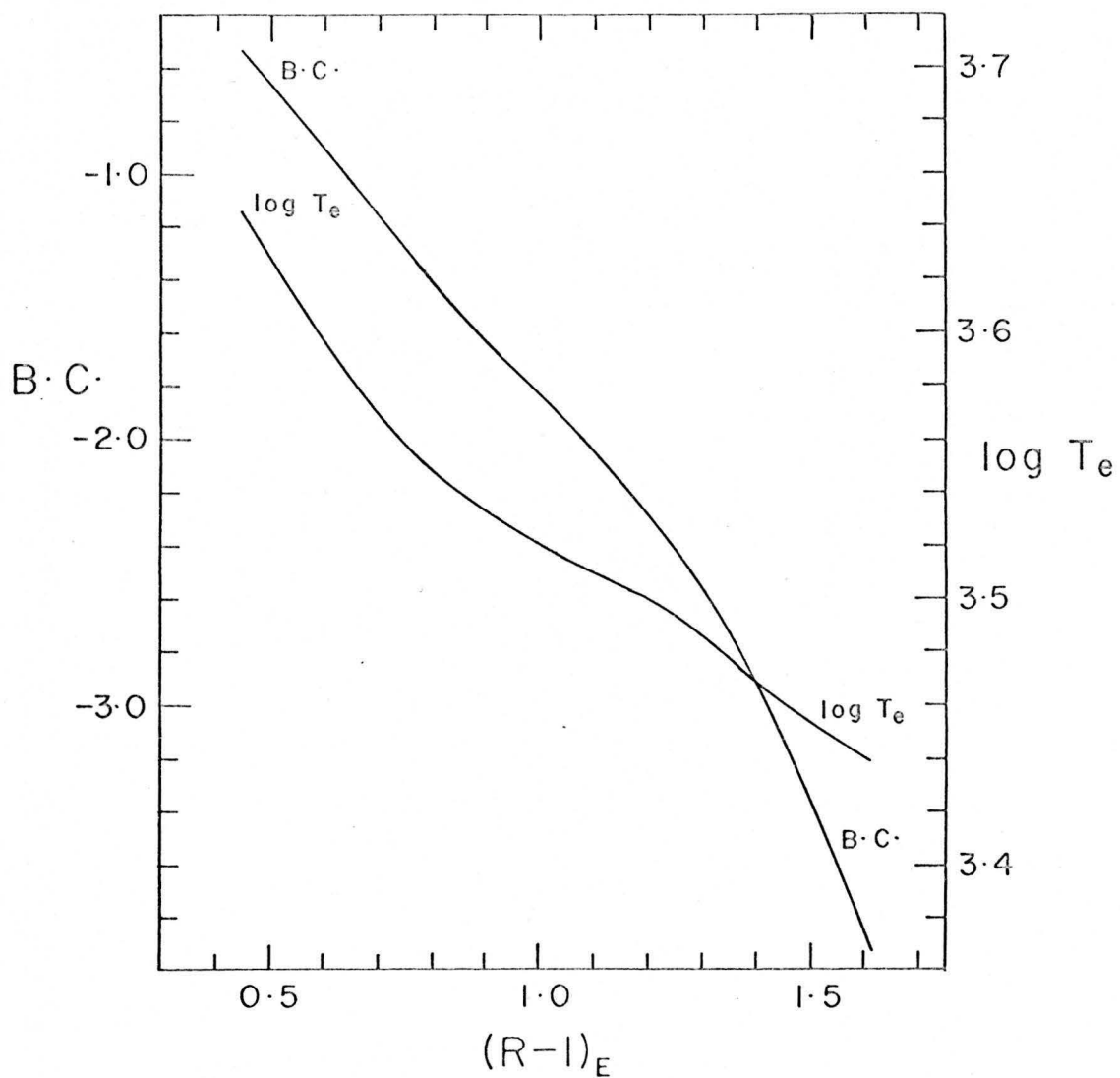


Fig. 2. Adopted bolometric correction (B.C.) and effective temperature (T_e) calibration for the M dwarf stars.

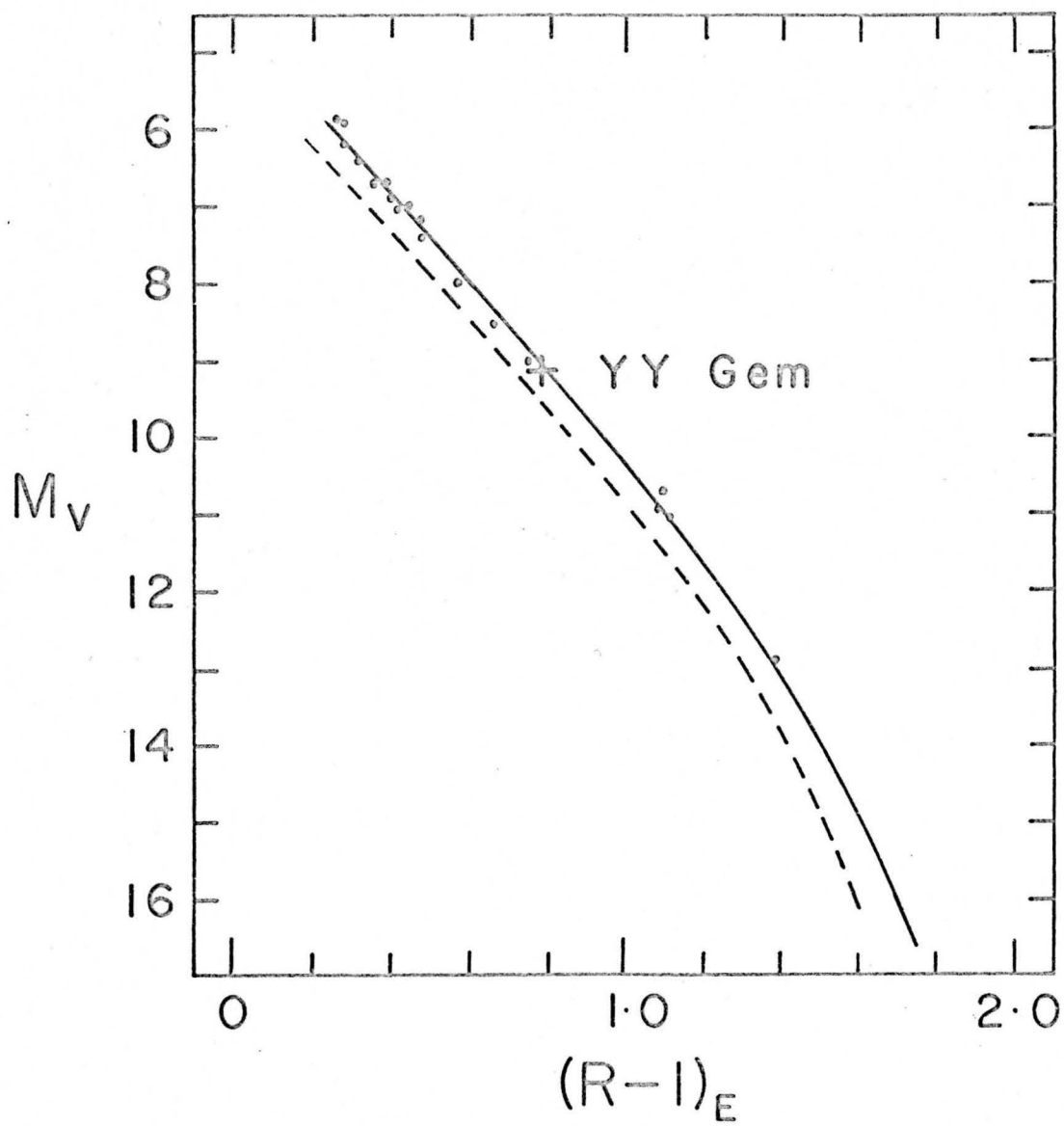


Fig. 3. Adopted $(R-I)_E$, M_V relation.

Eggen (1967, Table 15) for the system Ross 614AB applies to the A component alone.

The radii given in Table 1a were computed from the defining relation for the effective temperature, T_e , that is, $L = 4\pi\sigma R^2 T_e^4$, where L is the luminosity, R is the radius, and σ is the Stefan-Boltzmann constant. From this relation we obtain, taking $M_{bol} = 4.84$ for the sun (Johnson 1964),

$$\text{Log } (R/R_\odot) = 8.495 - 0.2 M_{bol} - 2 \log T_e \quad (3.1)$$

In Figure 4 we show the placement of the stars of Table 1 in the $\log m, M_V$ plane, where m denotes the mass in M_\odot and M_V is, of course, the absolute visual magnitude. The widely discrepant objects ADS 7114BC, 8048BC, 8166AB, 10158AB, and UV Ceti all appear to obey the Hyades mass-luminosity relation defined by Eggen (1963, 1965). The remaining objects in the sample of Table 1a define the low mass limit of the sun-Sirius mass-luminosity relation of Eggen (1963, 1965). We represent this relation by the following linear relation, which we show plotted by the solid line in Figure 4:

$$M_V = -11.91 \log m + 4.84 \quad (3.2)$$

From Figure 4 we see that equation (3.2) fits the plotted points reasonably well although the object YY Gem, shown by the cross in Figure 4, may be somewhat discrepant. Because

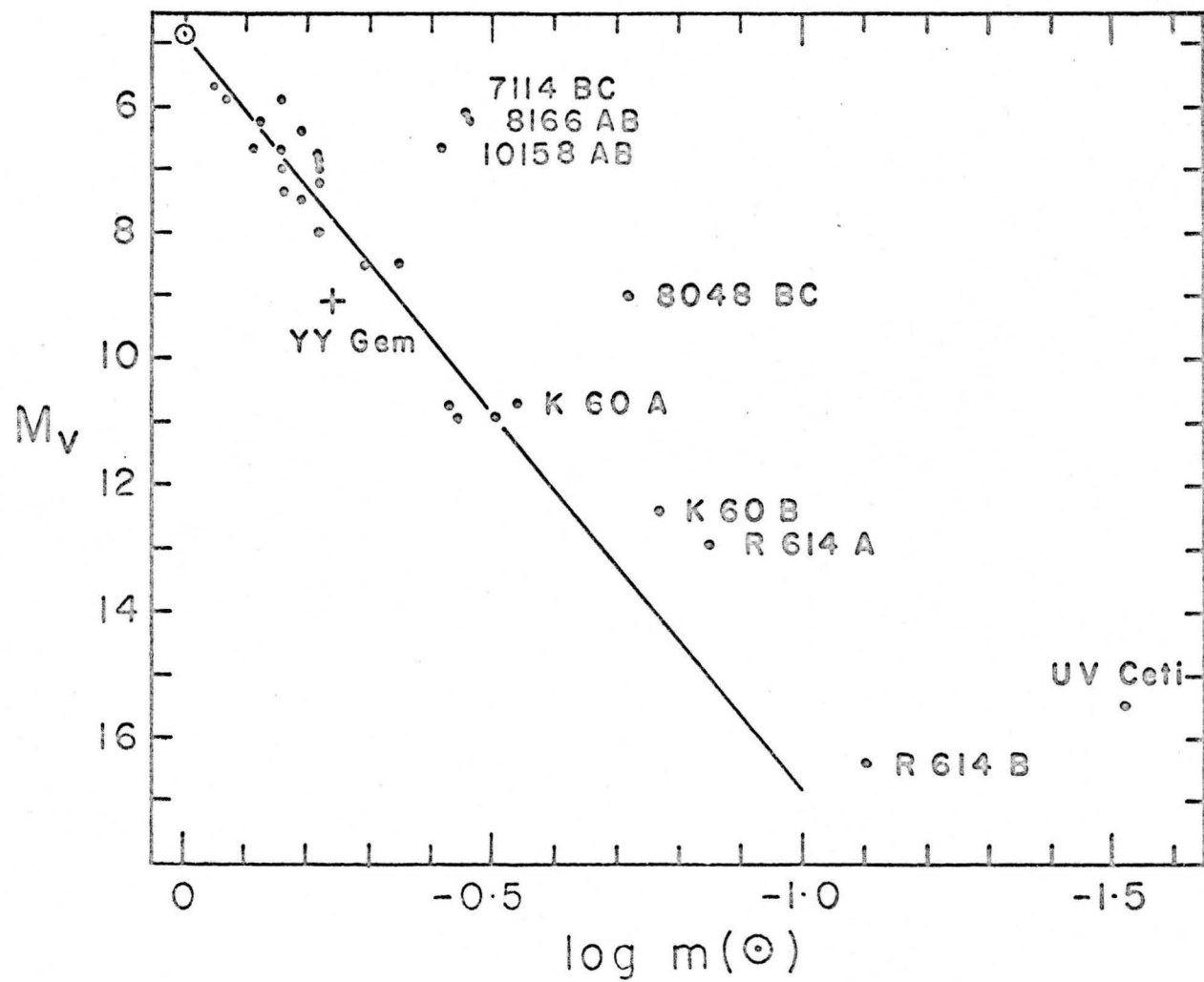


Fig. 4. Adopted sun-Sirius mass-luminosity relation.

of the lack of data below $0.3 M_{\odot}$, we must regard equation (3.2) to be a somewhat provisional extrapolation in this region of mass.

We assume that the sample of sun-Sirius stars as defined by Eggen is a representative sample of main sequence objects of solar composition. In all further discussion we employ the term "sun-Sirius" to designate such a sample of stars. We additionally assume for the present that equation (3.2) is valid over the range of mass appropriate to the main sequence M dwarf stars of solar composition.

Using equation (3.2) we derive a set of mean relations between the masses, bolometric magnitudes, radii, and effective temperatures for our sample of sun-Sirius stars. For a given mass we obtain M_V from equation (3.2), the corresponding $(R-I)_E$ index from Figure 3, and the bolometric correction and effective temperature from Figure 2. We calculate the radii from equation (3.1). In Table 2 we present the resulting relations for objects having masses in the range from 0.63 to $0.12 M_{\odot}$. In addition we give the corresponding approximate spectral types from the spectral type, effective temperature calibration for the main sequence M dwarfs given by Johnson (1966). In Figure 5 we show the resulting locus of the empirical main sequence in the H-R diagram. For comparison we show the positions of the stars of Table 1 (by filled circles except

Table 2. Adopted Mean Empirical Main Sequence
Properties of the Low Mass Stars

Log $m(\odot)$	M_V	$(R-I)_E$	M_{bol}	Log T_e	Log (R/R_\odot)	Sp
-0.2	7.22	0.47	6.63	3.637	-0.105	K5
-0.3	8.41	0.65	7.37	3.582	-0.143	M0
-0.4	9.60	0.87	8.03	3.536	-0.183	M2
-0.5	10.80	1.08	8.80	3.512	-0.289	M3
-0.6	11.99	1.26	9.53	3.492	-0.395	M5
-0.7	13.18	1.41	10.21	3.466	-0.479	M6
-0.8	14.37	1.54	10.82	3.447	-0.563	M7
-0.9	15.56	1.65	11.46	3.435	-0.667	M8

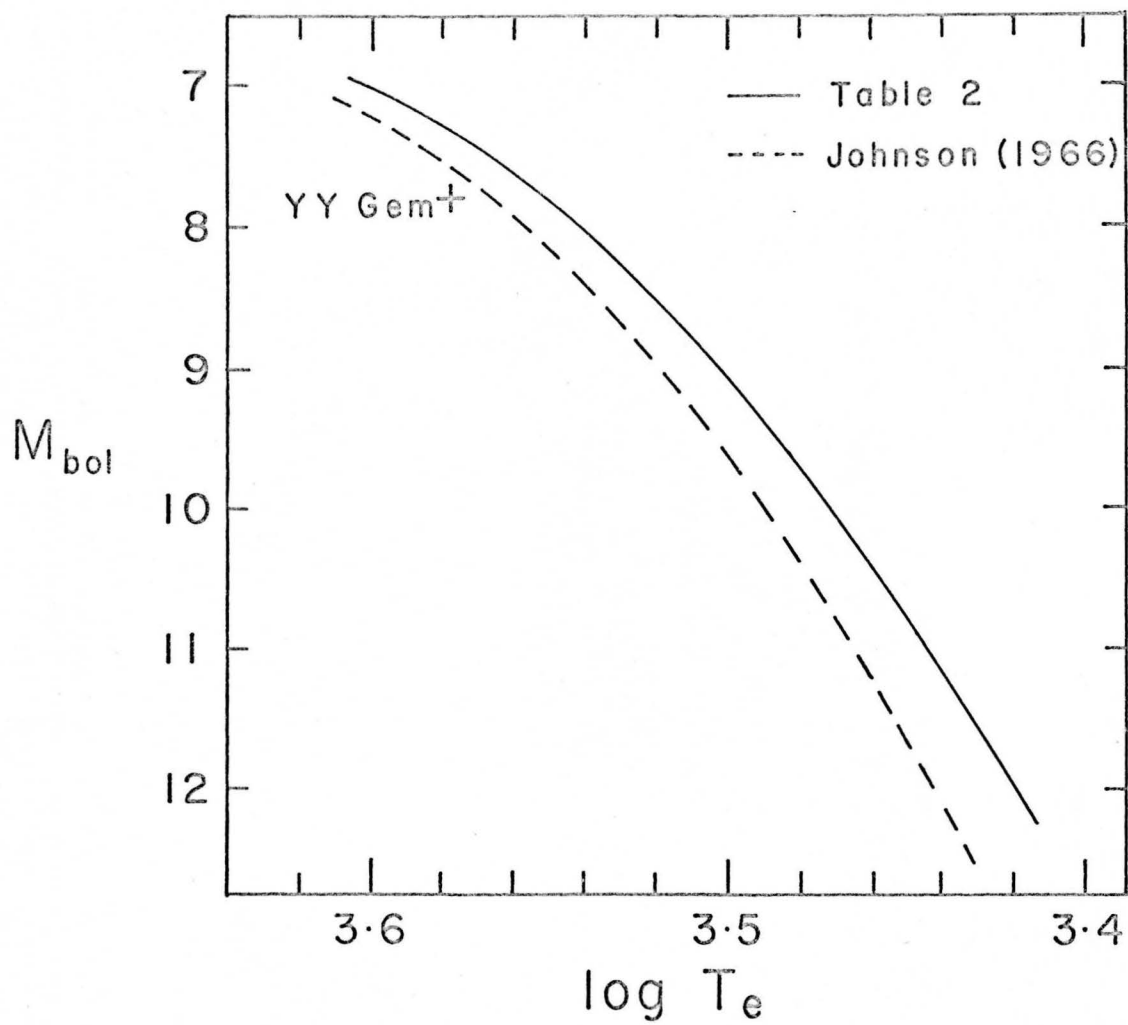


Fig. 5. Empirical main sequence locus in the H-R diagram.

for YY Gem which we show by a cross) and the mean relation (dashed line) adopted by Johnson (1966). The discrepancy between our adopted main sequence locus and that proposed by Johnson reflects the small discrepancy shown in Figure 3 between our adopted M_V , $(R-I)_E$ relation and that which we derive from Johnson's data. We display the resulting mass-luminosity relation and mass-radius relation in Figures 16 and 17, respectively, in which we compare our theoretically predicted relations with these empirically based relations.

It is also of interest to determine the mass function, that is, the distribution of stars with mass, in the solar neighborhood. If there is in fact a lower limiting mass for main sequence objects, we would expect to observe a sharp decrease in the numbers of stars having masses less than this limiting mass. Using the results of his partially completed proper motion survey, Luyten (1968) tabulates the numbers of stars per one magnitude interval in M_{pg} observed within 10 parsecs of the sun. From a plot of 201 red dwarf stars having $B-V > 1.30$ (extracted from the data of Eggen 1968, Table 1), we obtain the mean M_V , $B-V$ relation for the M dwarf stars shown in Figure 6 (solid line). For comparison we show the positions in this diagram of the stars of Table 1 (filled circles) having $B-V$ measures available as well as the mean relation (dashed line) adopted by Johnson (1966). Adopting the zero-point

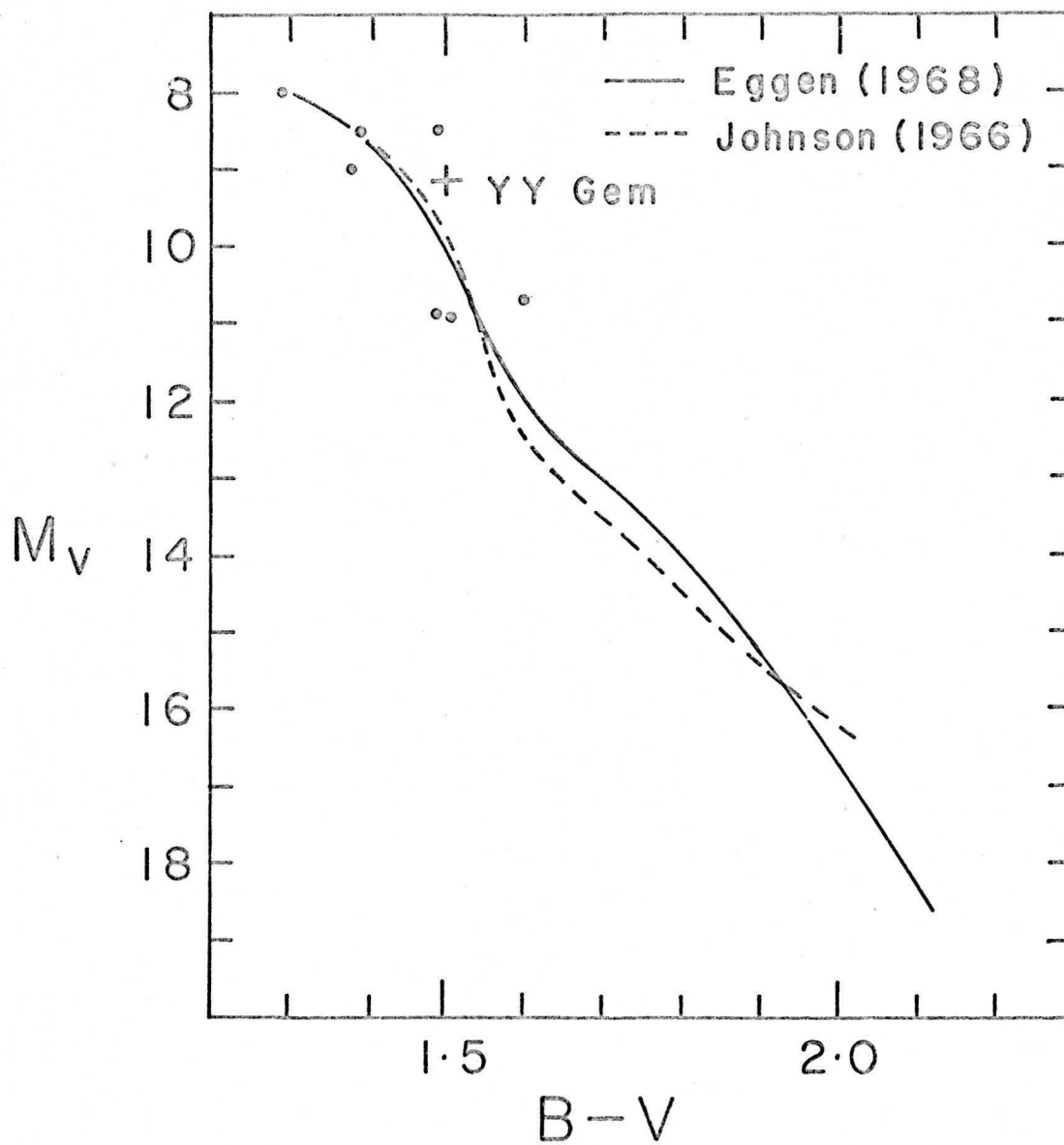


Fig. 6. Adopted $B-V$, M_V relation from Eggen (1968).

difference between M_{pg} and the absolute B magnitude quoted by Allen (1963, p. 197), we obtain

$$M_{pg} = M_V + (B-V) - 0.11$$

Using this relation together with Figure 6 we convert Luyten's luminosity function to a function of M_V . Assuming that the faint component of Luyten's sample is composed entirely of M dwarf stars of solar composition, we use equation (3.2) to obtain the empirical mass function shown in Figure 7. Here we plot the actual number of stars observed within ten parsecs of the sun as a function of stellar mass. The dashed portion of the curve in Figure 7 indicates that region over which Luyten (1968) suggests the data to be observationally incomplete.

Luyten (1968) finds the luminosity function to peak at $M_{pg} = 15.7$ which leads to the occurrence of a rather sharp maximum in the mass function at a mass of about $0.16 M_{\odot}$. As may be seen in Figure 7 there is a quite rapid decline in the numbers of stars as we proceed to lower masses. It is tempting to attribute this behavior of the mass function to the existence of a lower limiting mass for main sequence objects. However, as we shall see in Chapter 6, the main sequence limiting mass appears to occur at a somewhat lower mass than the maximum observed in the mass function. Considering that equation (3.2) may not be accurate for very low mass objects as well as the

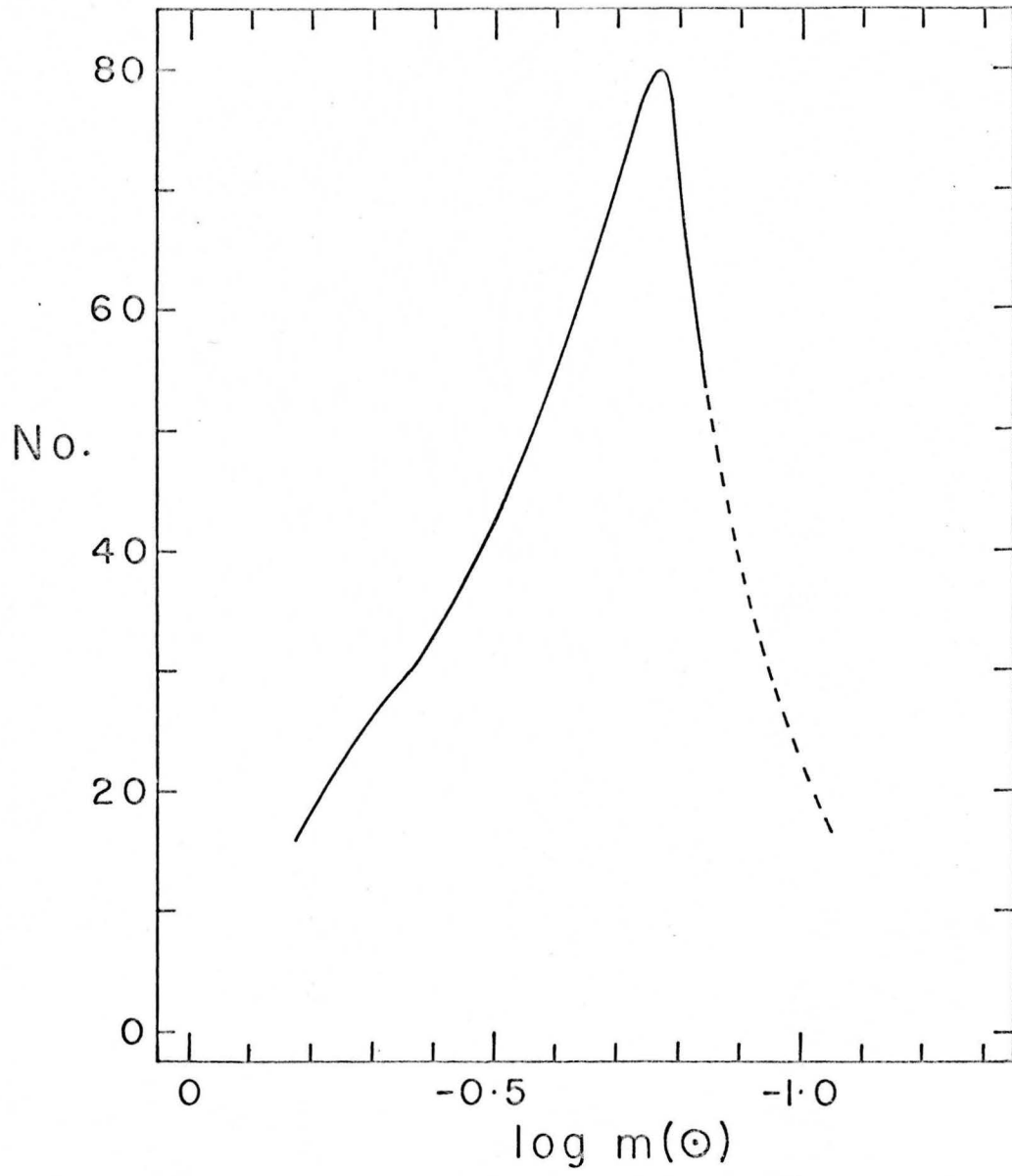


Fig. 7. Mass function for the solar neighborhood.

assumptions involved in deriving the original luminosity function (Luyten 1968) and the considerable scatter exhibited in the plot of M_V versus $B-V$ for the M dwarf stars, we are certainly justified in questioning the accuracy with which the above mass of $0.16 M_\odot$ has been determined. For example, Luyten (1968) estimates that the peak in the luminosity function is determined within a magnitude (photographic) which would imply that the maximum in the mass function, under the assumed validity of equation (3.2), lies between 0.21 and $0.12 M_\odot$. We withhold further comment on the implications of Figure 7 as well as the rest of the empirical data presented in this chapter until Section 6.3-6.5 at which point we consider these data in light of the theoretical calculations of the structure of low mass main sequence stars.

CHAPTER 4

THERMODYNAMIC, OPACITY, AND NUCLEAR ENERGY GENERATION DATA FOR THE STELLAR INTERIOR

Supplementing the equations of stellar structure are the constitutive data by which we refer to those quantities entering into the equations of structure which depend upon the chemical composition. Included among these quantities are the equation of state, the opacity, the nuclear energy generation rate, the internal energy per gram, if the star is undergoing gravitational contraction, and the adiabatic temperature gradient, if convection is a possible mode of energy transport within the stellar interior. These data must be supplied for each value of the pressure and temperature encountered in the numerical solution of the equations of structure.

To compute the thermodynamic quantities, that is, the equation of state, the internal energy and the adiabatic gradient, we consider in Section 4.1 the thermodynamic properties of a mixture of hydrogen and helium including an approximate treatment for the departures from perfect gas behavior arising from the Coulomb interactions between ionized particles. In computing the equilibrium abundances of the particles (neutral atoms, ions, free electrons, and molecules) composing such a mixture, we

desire to take into account the phenomena of pressure ionization and dissociation. In Section 4.2 we derive an approximate model for the pressure ionization of hydrogen and helium and in Section 4.3 we describe a provision for including the pressure dissociation of molecular hydrogen following Vardya (1965). We approach the problem of pressure ionization from the standpoint that the micro-fields established by free ions and electrons in the neighborhood of the incompletely ionized particles will so perturb the bound state energy levels as to lower the effective ionization energies as well as to render the internal partition functions dependent upon the free electron number density. We develop a procedure by which the partition functions as well as the lowering of the ionization potentials may be evaluated for inclusion in the Saha ionization equation.

In Section 4.4 we discuss the procedures for computing the opacity and in Section 4.5 the nuclear energy generation rate. We conclude this chapter with a description in Section 4.6 of the numerical procedures employed in supplying the constitutive data to the computer program which is used in computing the stellar models.

4.1 Thermodynamic Properties of an Interacting Hydrogen-Helium Plasma

Historically the first successful attempt to account, in an approximate way, for the effects of

electrostatic interactions between the charged particles in ionic systems was the treatment of strong electrolyte solutions developed by Debye and Hückel (1923). The Debye-Hückel (DH) theory has been carried over to the domain of high temperature plasmas where it has been utilized to estimate the departures from the ideal gas thermodynamic functions resulting from Coulomb interaction effects. Because of the approximations employed in the DH theory, however, it is applicable only at sufficiently low densities that the interactions remain small; at higher densities the DH treatment tends to overcorrect for these effects.

A completely general treatment of systems of interacting particles entails the solution of the quantum mechanical manybody problem. Although the complexity of this problem as yet prohibits the obtaining of general solutions applicable to any system of interest, it has been subject to attack at several points along its periphery. One of the more promising analytic methods is that which has evolved from Mayer's (see Mayer and Mayer 1940 and Brout and Carruthers 1963) expansion of the thermodynamic functions of a system of interacting particles as a power series in the density (the virial expansion). The coefficients of the powers of the density appearing in this expansion are expressed in terms of the so-called cluster integrals, the evaluation of which proceeds from the properties of the canonical ensemble. In its original form

this approach is applicable only to classical systems for which the potential between a pair of particles decreases more rapidly than the cube of the particle separation. Montroll and Ward (1958) and Glassgold, Hechrothe, and Watson (1959) have generalized Mayer's treatment through the grand canonical ensemble and the techniques of quantum field theory for application to quantized systems of particles interacting through inverse-square forces. While it is possible to extend these developments to more complicated systems (DeWitt 1961, 1965), they have yet to yield results by which the thermodynamic functions for real systems may be easily evaluated.

A number of investigations of the practical consequences of the Coulomb interaction effects in plasmas beyond the DH limit have adopted what we may designate a model approach. We refer to the approximate procedure by which the system under consideration is replaced by an idealized but representative model, which, for example, the system may approach as a limiting case and for which the thermodynamic properties are readily derivable. Examples include the equation of state determinations based on the Thomas-Fermi theory (cf. Feynman, Metropolis, and Teller 1949); the cellular models, which include the ion-sphere approximation (cf. Salpeter 1961) and the Wigner-Seitz method for solids (cf. Seitz 1940); and the Monte-Carlo calculations (cf. Brush, Sahlin, and Teller 1966).

Within the stellar interior we deal with a gaseous configuration existing at temperatures from a few thousand degrees near the surface to a few million degrees at the center. The interior densities are sufficiently high that pressure ionization is complete near 5×10^4 °K. In addition the free electrons are partially degenerate in both regions of complete and partial ionization. In so far as the thermodynamic properties of the stellar interior are concerned, we may regard the interior as consisting of an equilibrium mixture of hydrogen and helium, that is, we may neglect the small abundance of the heavier elements. Specifically we consider helium to be present in all of its ionization states and hydrogen to be present in both ionization states as well as combined as molecular hydrogen. We neglect the less abundant ionic species H^- and H_2^+ . In this case we confront a physical situation for which none of the approximate theories for imperfect gases provides a completely satisfactory representation. As the basis for incorporating the interaction effects in the computation of the thermodynamic functions, however, we employ the DH theory together with the results of the Monte-Carlo (MC) calculations performed by Brush et al. (1966). At temperatures below 10^5 °K we introduce a rather artificial modification into the DH and MC treatments in order to prevent the occurrence of erroneously large electrostatic corrections. In proceeding in this manner we must

acknowledge that quantitatively our estimation of the interaction effects may be substantially in error. However, since we expect that we tend to overestimate these effects rather than underestimate them, our results should serve to indicate the magnitude of such effects on the overall structure and evolution of low mass stars.

We consider a gaseous mixture of hydrogen and helium at a temperature T and confined within a volume V . We suppose that the Helmholtz function, F , for the system, which may contain neutral atoms, molecules, ions, and free electrons, may be written as the sum of a perfect gas contribution, F_0 , and a correction term, F_C , arising from the effects of particle interactions. That is, we write

$$F = F_0 + F_C \quad (4.1)$$

Upon determining F , we may calculate the total gas pressure, P , and the entropy, S , from the thermodynamic relations

$$P = - \left(\frac{\partial F}{\partial V} \right)_{T, N_1, N_2, \dots} \quad (4.2)$$

and

$$S = - \left(\frac{\partial F}{\partial T} \right)_{V, N_1, N_2, \dots} \quad (4.3)$$

where N_1, N_2, \dots , denote the total numbers of the various species of particles present in the mixture. The total

thermodynamic internal energy, U , of the system is obtainable directly from the definition of the Helmholtz function, that is

$$U = F + TS \quad (4.4)$$

We note that we may regard each of these thermodynamic functions as consisting of the sum of a perfect gas term and a correction term to account for the interaction effects. Specifically we write $P = P_0 + P_C$, $S = S_0 + S_C$, and $U = U_0 + U_C$.

4.1.1 Debye-Hückel Region

In Appendix A we derive the correction to the Helmholtz function, F_C , for an ionized gas on the Debye-Hückel model modified to take into account the effects of electron degeneracy. The basic result is given by equation (A.40) and is

$$F_C = - \frac{kT V \kappa^3}{12\pi} \quad (4.5)$$

where k is the Boltzmann constant and κ is the inverse Debye length defined as

$$\kappa^2 = \frac{4\pi e^2}{kT} (z^2 n_i + n_e \theta_e) \quad (4.6)$$

Here e is the electronic charge, z is the mean charge number per ion (cf. equation A.17), and n_i and n_e are the mean ion and free electron number densities, respectively.

The quantity θ_e enters as a result of electron degeneracy and is defined in terms of the Fermi-Dirac integrals,

$F_\alpha(\eta)$, where

$$F_\alpha(\eta) = \int_0^\infty \frac{x^\alpha}{\exp(x-\eta) + 1} dx \quad (4.7)$$

The parameter η is defined such that in terms of the free electron number density and the temperature we have (Tolman 1938)

$$F_{1/2}(\eta) = \frac{1}{4} \sqrt{\pi} n_e \left(\frac{h^2}{2\pi m_e kT} \right)^{3/2} \quad (4.8)$$

where h is Planck's constant and m_e is the mass of an electron. In terms of these quantities we define (equation A.26)

$$\theta_e = F'_{1/2}(\eta)/F_{1/2}(\eta) \quad (4.9)$$

where the prime denotes differentiation with respect to η .

From equation (4.5) and equations (4.2)-(4.4) we determine the following corrections to the pressure, entropy, and internal energy:

$$P_C = -F_C \left(\frac{1}{V} + \frac{3}{\kappa} \frac{\partial \kappa}{\partial V} \right) \quad (4.10)$$

$$S_C = -F_C \left(\frac{1}{T} + \frac{3}{\kappa} \frac{\partial \kappa}{\partial T} \right) \quad (4.11)$$

and

$$U_C = \frac{kT^2 V}{4\pi} \kappa^2 \frac{\partial \kappa}{\partial T} \quad (4.12)$$

The quantities $\partial\kappa/\partial V$ and $\partial\kappa/\partial T$ are obtained by straightforward partial differentiation of equation (4.6) in which we note that n_i and n_e are defined such that if N_i and N_e are, respectively, the total numbers of ions and electrons in the gas, then $n_i = N_i/V$ and $n_e = N_e/V$. Thermodynamically κ is to be regarded as a function of V , T , N_i , and N_e . Thus the quantity $\partial\kappa/\partial V$ is evaluated holding T , N_i , and N_e fixed and, similarly, $\partial\kappa/\partial T$ is evaluated holding V , N_i , and N_e fixed.

Over that region of density and temperature for which the DH criterion, equation (A.11), is satisfied, we may add these formulae, equations (4.10)-(4.12) to the perfect gas expressions in order to obtain the total thermodynamic functions including the interaction effects. At higher densities, that is, beyond the DH limit, these results tend to overcorrect for the interaction effects and we must resort to other procedures.

4.1.2 Monte-Carlo Region

Following Brush et al. (1966) we define the parameter Γ such that

$$\Gamma = \frac{ze^2}{kT} (4/3\pi n_i)^{1/3} \quad (4.13)$$

In terms of this parameter the DH criterion, equation (A.11), may be written as

$$\Gamma \ll 0.1; \quad (4.14)$$

where this condition is satisfied we may apply the DH results. Over the region $0.05 \leq \Gamma \leq 0.1$ we fit the DH results to the results of the MC calculation of Brush et al. (1966) and above $\Gamma > 0.1$ we take over the MC results directly. The MC calculations were performed, however, for a one-component system consisting of positive point ions of charge number z immersed in a uniform negative charge background. Such a model corresponds, for example, to a physical system at sufficiently high densities that pressure ionization is complete and the free electrons are sufficiently degenerate that they are distributed nearly uniformly, independently of the ions. We regard this as being a reasonable approximation to the physical conditions existing within the interiors of low mass stars at temperatures above 10^5 °K. Below this temperature, at the densities we consider, this model is no longer adequate.

In essence a single Monte-Carlo chain consists of the determination of the equilibrium configuration of a system composed of a specified number of particles through consideration of the random motion of the constituent particles. Brush et al. (1966) construct 50 such chains on the model described above for systems containing from 32 to 500 particles. They calculate the total configurational potential energy as well as the pair distribution functions and from the former they obtain additionally the

overall thermodynamic properties of the system. These latter data are tabulated as functions of the parameter Γ over the range $0.05 \leq \Gamma \leq 125$. Near $\Gamma = 125$ they find the occurrence of a solid-fluid phase transition.

4.1.3 Ion-Pair Model

Below 10^5 °K we introduce an artifice into the DH and MC theories in order to extend their applicability beyond the DH limit. That the DH theory fails at high densities is a consequence of its representing the interaction effects through consideration of only two particle interactions. At low densities this suffices, but at high densities ternary and higher order interactions tend to yield more uniform particle distributions than predicted by the DH theory. These effects are the most serious at the lowest temperatures for which ionization is complete. Under these conditions we cannot disregard the ion-electron interactions; hence the above MC model is also inadequate. In order to compensate for these effects we adopt a procedure based on Bjerrum's (cf. Fowler 1936, p. 552) treatment of ion association.

We consider a volume V containing N_i and N_e free ions and electrons, respectively, and assume that the mean charge per ion is unity so that $N_i = N_e$. We consider an associated ion pair to be formed within the system when an electron is located within the radius a_p of an ion. For

the value of a_p we take that distance from the ion at which the maximum average relative kinetic energy between an ion and an electron (neglecting degeneracy) is equal in magnitude to the potential energy of the ion-electron pair, that is

$$\frac{e^2}{a_p} = 3kT \quad (4.15)$$

We let N_p be the total number of such pairs and let N_i and N_e be the total number of free ions and electrons, respectively, which are not associated as ion pairs. Letting Q_p , Q'_i , and Q'_e denote the respective partition functions we have

$$\frac{N_p}{N'_i N'_e} = \frac{Q_p}{Q'_i Q'_e} \quad (4.16)$$

We regard the partition functions as products of a translational term ℓ and a configurational term u . For the ion pairs we have $\ell_p = \ell_i \ell_e$. Regarding the ions as point particles and neglecting any interactions between them we have $u_i = V$, the total volume of the system. Letting $u_p = 4/3\pi a_p^3$, the spherical volume associated with the radial distance a_p about an ion, we have that u_e is just the volume available to the free, unassociated electrons regarded as classical particles, that is $u_e = V - N_e v_p$.

For the configurational partition function of the ion pairs we have

$$u_p = 2\pi V \int_0^{a_p} \exp\left[-\frac{\epsilon(r)}{kT}\right] r^2 dr \quad (4.17)$$

where $\epsilon(r)$ is the interaction energy between the ion and the electron composing an ion-pair at the separation r where $0 \leq r \leq a_p$. To expedite matters we set $\epsilon(r) = 0$ for all r and obtain $u_p = 1/2Vv_p$. We let β denote the ratio N'_e/N_e and write equation (4.16) as

$$\frac{1-\beta}{\beta^2 N_e} = \frac{\ell_p}{\ell_i \ell_e} \frac{u_p}{u_i u_e} = \frac{\frac{1}{2} v_p}{V - N_e v_p} \quad (4.18)$$

We define the ion-pairs equilibrium constant K_p such that

$$K_p = \frac{\frac{1}{2} v_p n_e}{1 - n_e v_p} = \frac{\frac{1}{2} q}{1 - q} \quad (4.19)$$

where n_e is the total mean free electron number density and $q = n_e v_p$. We then obtain the equilibrium relation

$$\beta^2 K_p + \beta - 1 = 0 \quad (4.20)$$

which may be solved explicitly for β given n_e and T . When $\beta = 1.0$ we have no ion-pairs existing within the system while $\beta = 0.0$ implies that all of the free electrons and ions are associated into ion-pairs. Physically we interpret ion-pair formation as a transient phenomenon whereby

an electron found within the radial distance a_p of an ion results in the momentary existence of a neutral particle. As such we assume that those free electrons and ions which are associated as ion-pairs make no contribution to the DH or MC corrections; hence we include only the unassociated free ions and electrons, thus employing the modified free electron number density $n'_e = \beta n_e$, in computing these corrections.

Although we can compute the parameter β for each n_e and T encountered, we find it more convenient to represent it by an analytic function of the parameter q . The function

$$\beta(q) = \frac{27(q-1)^2}{[1-2(q-1)]^3} \quad (4.21)$$

has the desired properties in as much as $\beta(0) = 1.0$ (no ion-pairs), $\beta(1.0) = 0.0$ (complete ion-pair formation), and $(d\beta/dq)_{q=0} = (d\beta/dq)_{q=1} = 0$.

In order to be thermodynamically consistent, the thermodynamic functions for the system should go smoothly over to those for the system of associated ion-pairs as $\beta \rightarrow 0$. However, for computational convenience, we assume that, with the exception of the pressure, all of the thermodynamic quantities go over to those values appropriate to a perfect gas mixture of ions and electrons as

$\beta \rightarrow 0.0$. For the total gas pressure we take

$$P_{\text{total}} = P_e + \beta P_i + P_C(\beta n_e, T) \quad (4.22)$$

where P_e and P_i are the ideal gas electron pressure (including degeneracy) and ion pressure, respectively, and P_C is the DH or MC correction term regarded as a function of the modified free electron number density βn_e and the temperature, T . We note that in the limit of complete ion-pair formation P_{total} becomes, in the absence of degeneracy, just half the total pressure that would obtain for an ideal gas mixture of free ions and electrons.

4.2 Pressure Ionization of Hydrogen and Helium

We wish to consider the ionization equilibrium in a gaseous mixture of hydrogen and helium which is at a temperature T and confined within a volume V . Thermodynamically ionization may be regarded as a special case of a chemical reaction of the type



where A_{r+1} and A_r denote the upper and lower stages of ionization, respectively, and e denotes an electron (cf. Landau and Lifschitz 1958). In order that a mixture of elements be in equilibrium at constant volume and temperature, we require that the Helmholtz function for the system, $F = F(T, V, N_1, N_2, \dots)$ be minimized with respect

to the concentrations, N_1, N_2, \dots , of the ionic species present. Let $N_{i,r}$ be the total number of particles of the i^{th} element in the r^{th} stage of ionization. We then require that

$$\begin{aligned} dF &= \sum_i \sum_r \left(\frac{\partial F}{\partial N_{i,r}} \right)_{T,V,N_{j,r},N_e} dN_{i,r} + \left(\frac{\partial F}{\partial N_e} \right)_{T,V,N_{i,r}} dN_e \\ &= \sum_i \sum_r \mu_{i,r} dN_{i,r} + \mu_e dN_e = 0 \end{aligned} \quad (4.24)$$

where $\mu_{i,r}$ are the respective chemical potentials and N_e and μ_e are the total number and the chemical potential, respectively, of the free electrons. Since the total number of particles of a particular element is fixed, we have, supposing the gas to be a mixture of m elements, the following m conditions of constraint

$$\sum_r N_{i,r} = N_i = \text{constant} \quad i = 1, \dots, m \quad (4.25)$$

which gives

$$\sum_r dN_{i,r} = 0 \quad i = 1, \dots, m. \quad (4.26)$$

Furthermore we require that the system be electrically neutral so that

$$N_e = \sum_{i,r} Z_r N_{i,r} \quad (4.27)$$

where Z_r is the charge number of an ion in the r^{th} stage of ionization. This leads to the condition that

$$dN_e = \sum_{i,r} Z_r dN_{i,r}. \quad (4.28)$$

Using equations (4.26) and (4.27) we may eliminate dN_e and m of the $dN_{i,r}$ in equation (4.24). Since the resulting equation must be true for arbitrary variation of the remaining $dN_{i,r}$, we must require that the coefficients of these $dN_{i,r}$ vanish. We are then left with the following set of equilibrium equations

$$\mu_{i,r+1} + \mu_e - \mu_{i,r} = 0 \quad (4.29)$$

for all elements i in all stages of ionization r . If we now assume that the ions may be treated as a classical, ideal Maxwell-Boltzmann gas we have (Mayer and Mayer 1940, p. 126)

$$\mu_{i,r} = kT \left\{ \ln n_{i,r} - \ln \left[\left(\frac{2\pi m_i kT}{h^2} \right)^{3/2} \right] - \ln Q_{i,r} \right\} \quad (4.30)$$

where $n_{i,r}$ is the number density and $Q_{i,r}$ the internal partition function for the i^{th} element in the r^{th} stage of ionization and m_i is the mass of the i^{th} element. In general the partition function is given by

$$Q = \sum_{s=1}^{\infty} g_s \exp\left(-\frac{\epsilon_s}{kT}\right) \quad (4.31)$$

where the summation is performed over all bound states s of energy ϵ_s and statistical weight g_s . It is conventional to measure the energies ϵ_s with respect to the ground state energy of the particular ion in question. In evaluating the partition functions, $Q_{i,r}$ and $Q_{i,r+1}$, for an element in two successive stages of ionization, we must refer the bound state energies to a common zero of energy. If we choose the ground state of the lower ionization stage as the zero point, then we must add to the energies of the upper stage the amount $X_{i,r}$, which is just the ionization energy of the lower stage. Letting $\eta = \mu_e/kT$ we obtain from equations (4.29) and (4.30)

$$\frac{n_{i,r+1}}{n_{i,r}} = \frac{Q_{i,r+1}}{Q_{i,r}} \exp \left(- \frac{X_{i,r}}{kT} - \eta \right). \quad (4.32)$$

If we further assume that the electrons may be treated as a Maxwell-Boltzmann gas and employ equation (4.30) to obtain μ_e , we find that equation (4.32) reduces to the usual form of the Saha equation. In general we are to be concerned with a gas in which the electrons may be degenerate in which case η must be evaluated from the Fermi-Dirac statistics.

That the summation involved in the evaluation of the partition function of the ions extends over an infinite number of bound states is a consequence of the Coulomb field in which the bound electrons move and the assumption

that a particular ion can be regarded as being isolated. In a real gas, however, no ion is completely isolated since it will be subject to the perturbing effects of neighboring particles. The electrostatic field about an ion will not be due to the Coulomb field of the ion alone but will be modified by the presence of the other particles, especially by other ions and the free electrons, such that it will vanish at some finite distance from the ion. Thus there will be in reality only a finite number of bound states, a consequence which provides a natural cutoff to the partition function summation. Furthermore the modified potential distribution about the ion will result in an upwards displacement of the bound state energies which will give rise to an effective lowering of the ionization energy. At a fixed temperature we then find that both the total number of bound states and the bound state energies become dependent on the density in such a manner as to shift the ionization equilibrium to higher stages of ionization with increasing density. This is the phenomenon of pressure ionization and is responsible for insuring that plasmas will tend towards complete ionization at very high densities. The effects of the particle interactions will also be to broaden the respective energy levels, an effect which we neglect in the present treatment.

In considering pressure ionization we are, of course, concerned with the time averaged effects of the

perturbations arising from the particle interactions. In principle one should treat these effects through statistical mechanical considerations but, because of the very complicated nature of the problem, it is more convenient to attempt to represent these effects by means of simple models. In a gas consisting of a mixture of charged and neutral particles we expect that the microfields established by the charged particles will provide the major perturbing influence on the bound states of any particular ion. Mayer (1947) and Armstrong et al. (1961) have utilized the ion-sphere model in order to estimate the lowering of the ionization energies in a plasma. In this model each ion is considered to be surrounded by a uniform spherical cloud of free electrons in which the number of electrons is equal to the charge number Z on the ion. The size of each ion sphere is chosen to be that of the mean volume per ion corresponding to the mean ion number density. It is assumed that the outermost bound electron moves in a potential field arising from the ion (including the screening effects of the inner bound electrons) and the outer free electrons composing the ion sphere. If Ze is the charge on the ion and a is the ion-sphere radius, where $a = (3/4\pi n)^{1/3}$ and n is the mean ion number density, then it is found that the ionization energy of the ion in question is lowered by the amount $3Ze^2/2a$. This model is, strictly speaking, applicable only to ions at high stages

of ionization and should be applied only under the condition that the ion-sphere radius is much greater than the radius associated with the orbit of the outermost bound electron.

Ecker and Kröll (1963) employ the simple Debye-Hückel model in order to estimate the lowering of the ionization energy of a given ion arising from the screening effects of neighboring ions and free electrons. They find that in the regions of density and temperature in which the Debye-Hückel approximation is valid, the lowering of the ionization energy in a classical plasma is given by $-\frac{1}{2}e^2\kappa(1 + Z_{r+1}^2 - Z_r^2)$, where κ is the inverse Debye length and Z_{r+1} and Z_r are the charge numbers of the upper and lower ionization stages, respectively, of the ion in question.

Stewart and Pyatt (1966) develop a theory for the lowering of the ionization energy in a plasma which yields the Debye-Hückel result in the low density, high temperature limit and the ion-sphere result in the limit of very high densities. They proceed by solving Poisson's equation for the time-averaged potential distribution about an ion arising from the assumed spherically symmetric distribution of ions and free electrons about the given ion. They assume that the bound electron distribution about the ion can be described by the Thomas-Fermi model and that, effectively, the distribution of ions and free electrons

can both be described by the Maxwell-Boltzmann distribution. The lowering of the ionization energy then appears as the work done in removing an electron from the origin to infinity against the potential field of the screening cloud of ions and free electrons.

While the procedure of Stewart and Pyatt yields an estimate of the lowering of the ionization potential over a wide range of density and temperature, it provides no information on the accompanying effect on the partition functions. To accomplish this, one would have to solve Schrödinger's equation for the array of bound states utilizing the total screened potential distribution about the ion. Once the associated energy eigenvalues were found, the partition functions can be computed from the summation indicated in equation (4.31). Harris and Trulio (1961) approximate the effect of particle interactions on the bound states in a pure hydrogen plasma by considering each atom to be confined within a box of dimensions equal to the mean volume per atom. The perturbed energy eigenvalues are obtained from the solution of Schrödinger's equation and it is found that this procedure leads to a qualitatively correct thermodynamic behavior of the gas.

A more realistic approach than this so-called box model is to consider the outermost bound electron to move in a Coulomb field which has been appropriately modified to account for the screening effects of neighboring charged

particles. In treating a pure hydrogen plasma, Harris (1962) adopts the Debye-Hückel potential distribution, which for a hydrogen-like atom of nuclear charge Z can be written as (cf. equation A.31)

$$\phi(r) = \frac{Ze}{r} \exp(-\kappa r) \quad (4.33)$$

where $\phi(r)$ is the potential at the distance r from the nucleus and κ is inverse Debye length. Approximate solutions to Schrödinger's equation,

$$\left[\frac{\hbar^2}{2m} \nabla^2 - \frac{Ze^2}{r} \exp(-\kappa r) \right] \psi_{n,\ell} = \epsilon_{n,\ell} \psi_{n,\ell}$$

are obtained using the variational technique in which unperturbed hydrogen atom wave functions are used as a basis set of functions for minimizing the energy. These calculations are made for the hydrogen atom ground state and 44 excited states up through $n = 9$ and $\ell = 8$. The resulting bound state energies are tabulated as functions of the parameter $\delta = \kappa a_0 / Z$ where a_0 is the radius of the first Bohr orbit. It is found that the bound state energies are shifted upwards towards the continuum with increasing δ with the consequence that at values of δ greater than $\delta = 1.15$ no more bound states exist and the atom is completely pressure ionized.

We shall utilize Harris' results in order to obtain the thermodynamic functions for a gaseous mixture of

hydrogen and helium. For the hydrogen-like species HI and HeII we can employ Harris' data directly although for ease in computation we shall introduce several simplifications. In computing the partition functions we shall not include the nine bound levels considered by Harris but shall sum explicitly only over all the states up through the $n = 4$ level. We consider all of the remaining upper states through the $n = 9$ level to lie at a common energy equal to that of the $n = 5$ level with which we associate the statistical weight $g = 510$. We further assume that all states of common n lie at the same energy; although use of the potential given in equation (4.33) removes the n - ℓ degeneracy peculiar to the pure Coulomb field. We assume that the states vanish sequentially with those of highest n and ℓ vanishing first. Below we tabulate the values of δ at which the various states we consider vanish and the statistical weight $g_{n\ell}$ associated with each state:

<u>State</u>	<u>δ</u>	<u>$g_{n\ell}$</u>
5s	0.05	510
4f	0.06	14
4d	0.06	10
4p	0.08	6
3d	0.09	10
3p	0.110	6
4s	0.120	2
3s	0.20	2
2p	0.21	6
2s	0.30	2
1s	1.15	2

In this model the partition function can be represented by

$$Q = \sum_{n=1}^{n'} \sum_{\ell=0}^{\ell'-1} g_{n,\ell} \exp\left(-\frac{\epsilon_{n,\ell}}{kT}\right) + g_{n',\ell'}(\delta) \exp\left(-\frac{\epsilon_{n',\ell'}}{kT}\right) \quad (4.34)$$

where n' and ℓ' are the quantum numbers associated with the uppermost state existing for a given value of δ and $\epsilon_{n,\ell}$ are the bound state energies. The partition function for the uppermost bound state is regarded as a function of δ and is computed such that it vanishes smoothly with δ as the excitation energy approaches zero, thereby insuring that the contribution of the uppermost state to the total partition function will, in fact, vanish. Specifically, taking the s^{th} level of unperturbed statistical weight g_s^0 to be the uppermost level existing at a value of δ such that $0 < \delta \leq \delta_s$, where δ_s is the value of δ at which the s^{th} level vanishes, we represent the δ dependent statistical weight, $g_s(\delta)$, by

$$g_s(\delta) = \frac{A_s (\delta - \delta_s)^2}{1 + B_s (\delta - \delta_s)^2} \quad (4.35)$$

The constants A_s and B_s are chosen such that $g_s \rightarrow g_s^0$ as $\delta \rightarrow 0$, $g_s \rightarrow 0$ as $\delta \rightarrow \delta_s$, and $g_s = 1/2 g_s^0$ when $\delta = \delta_{s+1}$, that is, we take the statistical weight of the s^{th} level to

have one-half its unperturbed value at that value of

$\delta = \delta_{s+1}$ at which the preceding level vanishes.

We note that in representing the partition function for the bound states in this way it becomes implicitly dependent upon the free electron number density and additionally dependent upon the temperature through the explicit dependence of the $\epsilon_{n,l}$ and the $g_{n,l}$ on the parameter $\delta = \delta(n_e, T)$. The dependence of the $g_{n,l}$ on δ has been introduced in a highly artificial way, however. Because of this, we neglect this implicit dependence of the partition function on n_e and T . Consequently, we continue to regard the subsystems containing bound electrons as constituting an assembly of ideal Boltzmann particles for which, however, the partition function vanishes with the disappearance of the bound states.

In applying Harris' data to neutral helium, we consider only one excited state whose dependence on δ we take to be the same as that of the 2s state of hydrogen. The partition function is computed in a manner completely analogous to equation (4.34) for HI and HeII. We assume that the dependence of the HeI ground state energy, and, thus, the ionization energy, is the same as that for a hydrogen-like atom having an effective nuclear charge number $Z = 1.344653$.

The total Helmholtz function for the system consists of the sum of the contributions arising from the

translational degrees of freedom of the ions and molecules and a correction term arising from the Coulomb interactions between the charged particles. If we let N_i be the total number of ions of the i^{th} ionic species (we herein regard neutral atoms as ions having an ionic charge number $Z_i = 0$) and let Q_i and m_i be the associated internal partition function and particle mass, respectively, then the contribution to the Helmholtz function due to the i^{th} species treated as a Maxwell-Boltzmann gas is

$$F_i = N_i kT \left[\ln N_i - \ln V - \ln \left(\frac{2\pi m_i kT}{h^2} \right)^{3/2} - \ln Q_i - 1 \right] \quad (4.36)$$

where h is Planck's constant and k is the Boltzmann constant. The total contribution from the ions, F_{ions} , is, of course,

$$F_{\text{ions}} = \sum F_i. \quad (4.37)$$

The contribution made by the free electrons, F_e , treated as an ideal Fermi-Dirac gas is

$$F_e = N_e kT \left[\eta - D(\eta) \right] \quad (4.38)$$

where N_e is the total number of electrons present and $\eta = \mu_{e0}/kT$ where μ_{e0} is the chemical potential of the free electrons corresponding to the mean free electron density $n_e = N_e/V$. The function $D(\eta)$ is defined in terms of the Fermi-Dirac integrals by $D(\eta) = 2/3 F_{3/2}(\eta)/F_{1/2}(\eta)$. The

contribution to the Helmholtz function, F_c , arising from the electrostatic interactions between the ions and the free electrons on the Debye-Hückel model is given by equation (4.5).

We now establish through the set of equilibrium conditions contained in equation (4.29) the equations governing the equilibrium concentrations of the various ionic species present. The chemical potential of the i^{th} ionic species, μ_i , is obtained from the thermodynamic relation

$$\mu_i = \left(\frac{\partial F}{\partial N_i} \right)_{T, V, N_j, N_e} \quad (4.39)$$

where the subscript N_j indicates that all of the ionic species other than the i^{th} are to be held constant in performing the differentiation. From equation (4.36) we have

$$\mu_i = kT \left[\ln n_i - \ln \left(\frac{2\pi m_i kT}{h^2} \right)^{3/2} - \ln Q_i \right] \quad (4.40)$$

where n_i is the mean number density of the i^{th} species.

The chemical potential of the free electrons, μ_e , is given by

$$\mu_e = \left(\frac{\partial F}{\partial N_e} \right)_{T, V, N_i} = \frac{\partial}{\partial N_e} (F_{\text{ions}} + F_e + F_c)_{T, V, N_i} \quad (4.41)$$

from which we obtain

$$\frac{\mu_e}{kT} = \eta + \eta_c \quad (4.42)$$

where

$$\eta_c = -\frac{1}{2} \frac{e^2 \kappa}{kT} \left[Z + \frac{F''_{1/2}(\eta)}{F'_{1/2}(\eta)} \right] \quad (4.43)$$

The primes denote differentiation with respect to the parameter η .

From these results and the discussion preceding equation (4.32), it follows that the ratio of the number densities, $n_{i,r}$ and $n_{i,r+1}$, of the i^{th} element in the successive stages of ionization, r and $r+1$, is given by

$$\frac{n_{i,r+1}}{n_{i,r}} = \frac{Q_{i,r+1}}{Q_{i,r}} \exp(-\phi_{i,r} - \eta - \eta_c) \quad (4.44)$$

where we let $\phi_{i,r} = X_{i,r}/kT$. In the treatment of pressure ionization which we employ here, both the ionization energy, $X_{i,r}$, and the partition functions, $Q_{i,r}$ and $Q_{i,r+1}$, are to be regarded as functions of the mean electron density and the temperature. Equation (4.44) represents the final form of the ionization equation which we shall utilize in computing the ionization equilibrium in the gas.

For the hydrogen-helium plasma which we consider here, we have the following equilibrium relations:

$$\frac{n_{H^+}}{n_{H^0}} = \frac{2}{Q_{H^0}} \exp(-\phi_{H^0} - \eta - \eta_C),$$

$$\frac{n_{He^+}}{n_{He^0}} = \frac{Q_{He^+}}{Q_{He^0}} \exp(-\phi_{He^0} - \eta - \eta_C) \quad (4.45a, c)$$

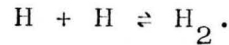
and

$$\frac{n_{He^{++}}}{n_{He^+}} = \frac{1}{Q_{He^+}} \exp(-\phi_{He^+} - \eta - \eta_C),$$

where the n_{H^0} , n_{H^+} , n_{He^0} , n_{He^+} , and $n_{He^{++}}$ are, respectively, the number densities of neutral and ionized hydrogen and neutral, singly and doubly ionized helium.

4.3 Pressure Dissociation of Molecular Hydrogen

In the low temperature regions of a star we must also allow for the presence of molecular hydrogen, which we consider to be in equilibrium with neutral atomic hydrogen through the reaction



In this case the equilibrium relation for molecular hydrogen is given by

$$\frac{n_{H_2}^2}{n_{H_2}} = \frac{Q_{H^0}^2}{Q_{H_2}} \left(\frac{\pi m_H kT}{h^2} \right)^{3/2} \exp(-D_e/kT) \quad (4.46)$$

where n_{H_2} is the number density, Q_{H_2} the partition function and D_e the dissociation energy for molecular hydrogen and

m_H the mass of a hydrogen atom. We neglect the possibility of electronic excitation and, assuming a normal mixture of the ortho and para modifications, write the H_2 partition function in the form

$$Q_{H_2} = \sum_v \sum_{J \text{ even}} (2J+1) \exp \left\{ -[\epsilon_v + \epsilon_J(v)]/kT \right\} \quad (4.47)$$

$$+ 3 \sum_v \sum_{J \text{ odd}} (2J+1) \exp \left\{ -[\epsilon_v + \epsilon_J(v)]/kT \right\}$$

where ϵ_v and ϵ_J are, respectively, the energies of the vibrational energy level with vibrational quantum number v and the rotational energy level with rotational quantum number J . From Herzberg (1950) we have

$$\frac{\epsilon_v}{hc} = (v + \frac{1}{2})\omega_e - (v + \frac{1}{2})^2 \omega_e x_e + (v + \frac{1}{2})^3 \omega_e y_e \quad (4.48)$$

and

$$\frac{\epsilon_J}{hc} = J(J+1)B_v - J^2(J+1)D_v + J^3(J+1)^3H. \quad (4.49)$$

where h is Planck's constant and c is the velocity of light. We take the following molecular constants from Herzberg (1950)

$$\omega_e = 4395.2$$

$$\omega_e x_e = 117$$

$$\omega_e y_e = 0.29$$

$$B_v = 60.8 - 2.993(v + \frac{1}{2}) - 0.025(v + \frac{1}{2})^2$$

$$D_v = 0.0465 - 0.00134(v + \frac{1}{2})$$

$$H_v = 0.0000518$$

The summation in equation (4.47) is terminated when

$$\epsilon_v + \epsilon_J(v) = D_e.$$

We provide for the effects of pressure dissociation following Vardya (1965) who estimates the lowering of the dissociation energy of a hydrogen molecule arising from its interaction with the nearest neutral hydrogen atom. He finds that the dissociation energy is depressed by an amount ΔD given by

$$\Delta D = \left| \left[1.2u\left(\frac{r}{2}\right) - 0.6u(r) \right] \right| \quad (4.50)$$

where

$$u(\xi) = - 7.605 \times 10^{-12} (1.0 + 2.04\xi) \exp(-2.04\xi) \quad (4.51)$$

and $\xi = r/r_e - 1$. Here $r_e = 0.7414$ Å and is the equilibrium separation of the two protons in the nucleus of a hydrogen molecule. For r we choose the mean volume per particle in the gas rather than the mean volume per neutral hydrogen atom as was originally done by Vardya (1965).

In performing the partition function summation of equation (4.47) as well as in evaluating equation (4.46) we take the effective dissociation energy $D_e = D_o - \Delta D$, where we denote by D_o the unperturbed value. It is this partition function and dissociation energy which we employ in the subsequent evaluation of the thermodynamic functions of molecular hydrogen.

4.4 Interior Opacity

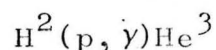
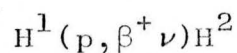
The computation of Rosseland mean opacities appropriate to stellar matter requires a knowledge of the total monochromatic opacity κ_ν at every frequency ν . In general the monochromatic opacity at a particular frequency is the sum of contributions arising from a large number of absorption processes involving many elements in various stages of ionization. We shall employ the extensive opacity data compiled by Cox and Stewart (1965) who have computed tables of opacities, including the effects of electron conduction, in a number of different chemical compositions. In computing the Rosseland mean they have included both discrete and continuous absorbing processes and have computed the contribution to the total opacity made by conduction on the basis of the Mestel (1950) treatment of electron conduction. The data are presented as tables of the logarithm of the total opacity versus the logarithms of the temperature and mass density.

In particular we shall utilize the opacity tables for the composition which Cox and Stewart designate as the Cameron Mixture I. We shall find, however, that in applying these tables we shall require data at densities greater than those included in the tabulated data. To extend these tables to higher densities we resort to the following expediency: In this range of density and temperature the effective opacity is principally determined by electron conduction. We therefore assume that the radiative contribution to the opacity remains constant with increasing density and equal to the last tabular entry, and we compute the conductive contribution from the Mestel theory following Cox (1965). It should be noted, however, that in this region of density and temperature, the conductivity as computed from the Mestel theory may be in error by as much as an order of magnitude (Hubbard, 1966).

4.5 Nuclear Energy Generation Rate

In the region of density and temperature appropriate to the deep interior regions of low mass stars the proton-proton chain is the principal source of nuclear energy generation. At temperatures less than about 6×10^6 °K the proton-proton chain will terminate with the production of He^3 . At higher temperatures the reactions proceed at sufficiently high rates that He^3 will obtain an equilibrium abundance, and the proton-proton chain will

terminate with the production of He^4 . We anticipate that the central temperatures of the stars under investigation here will, in fact, be less than 6×10^6 °K in which case the proton-proton chain will involve only the following two reactions:



We obtain the reaction rates and, hence, the rate of energy generation from the data given by Parker, Bahcall, and Fowler (1964). For temperatures greater than about 5×10^5 °K we can assume that the rates of production and destruction of H^2 are equal. In this case the rate of energy generation per gram for the proton-proton chain, $\epsilon_{\text{p-p}}$ can be written as

$$\epsilon_{\text{p-p}} = (2.803931 \times 10^{24}) \rho X^2 f S r^2 e^{-\tau} \text{ erg/gm} \quad (4.52)$$

where ρ is the mass density and X is the fractional abundance by mass of hydrogen. Letting T_6 be the temperature in units of 10^6 °K, the cross-section factor S is given by

$$S(T_6) = S_o \left\{ 1 + \frac{5}{12\tau} + \frac{1}{S_o} \left(\frac{dS}{dE} \right)_o \left[E_o(T_6) + \frac{35}{36} k T_6 \right] \dots \right\}$$

where

$$S_o = 3.36 \times 10^{-22}$$

$$\frac{1}{S_o} \left(\frac{dS}{dE} \right)_o = 8.036 \times 10^{-3}$$

$$E_o(T_6) = 0.968315 T_6^{3/2}$$

and k is the Boltzmann constant. The factor r is given by

$$r = \frac{33.7164}{T_6^{1/3}}$$

The screening factor f is computed according to the treatment of Salpeter (1954). We find, however, that we will be concerned with a region of density and temperature intermediate between Salpeter's cases of weak and strong screening. To obtain an estimate of the appropriate screening factor in this region we compute a weighted mean of f such that f reduces to the factor for weak screening at low densities and to the factor for strong screening at high densities.

4.6 Constitutive Data Table

In the preceding sections we have established the formulae by which the constitutive data are to be computed. Because of the rather complicated numerical procedure involved in evaluating the thermodynamic quantities, we find it most convenient to provide these data in tabular form over the range of temperature and pressure encountered

within the stellar interior. In constructing such a table we consider specifically the problem of computing the total mass density, ρ , the internal energy per gram, u , the adiabatic gradient, ∇_{ad} , as well as the opacity and the nuclear energy generation rate for a fixed chemical composition specified by the values of X , Y , Z , and for given values of the temperature, T , and the total pressure, P . We choose the Population I composition $X = 0.739$, $Y = 0.240$, and $Z = 0.021$. We now reformulate and summarize the results of Sections 4.1 and 4.2 so as to render them more suitable for use in the numerical procedures.

4.6.1 $T > 5000$ °K

At temperatures above 5000 °K we consider a plasma undergoing ionization or in which ionization is complete. We let n denote the mean free electron number density and let n_0 and n_i be the mean number densities of atomic nuclei and ions, respectively. We let α be the fractional abundance by number of helium nuclei where $\alpha = (1-X)/(1+3X)$. We define the mean charge number per ion, z such that $n = zn_i$. Because z does not vary sensibly from 1.0 even under the condition of complete ionization for the assumed hydrogen-helium abundance, we expediently set $z = \text{constant} = 1.0$ for all P and T considered.

We define the following quantities:

$$\alpha = \pi^{1/2} n^{1/2} e^3 / (kT)^{3/2}, \quad (4.53)$$

$$H = \Theta_e = F'_{y_2} / F_{y_2}, \quad (4.54)$$

$$C = F''_{y_2} / F'_{y_2}, \quad (4.55)$$

and

$$G = C - H \quad (4.56)$$

where the primes denote differentiation with respect to the degeneracy parameter, η , which is defined in terms of the mean free electron number density, n . The inverse Debye length, κ , may be expressed in terms of the above quantities as

$$\kappa^3 = 8\pi n \gamma (1+H)^{3/2} \quad (4.57)$$

Defining $w = n_0/n$ and letting n_k ($k = 1,6$) be the number densities of H^0 , He^0 , He^+ , H_2 , H^+ , and He^{++} , respectively, we define the ionization parameters, x_k ($k = 1,4$), and the abundance parameters, y_k ($k = 1,6$), as follows:

$$\begin{aligned} x_1 &= \frac{n_1}{(1-\alpha)n_0} & x_3 &= \frac{n_3}{\alpha n_0} \\ x_2 &= \frac{n_5}{(1-\alpha)n_0} & x_4 &= \frac{n_6}{\alpha n_0} \end{aligned} \quad (4.58a,d)$$

and

$$\begin{aligned} y_1 &= (1-\alpha)x_1 & y_4 &= \frac{1}{2}(1-\alpha)(1-x_1-x_2) \\ y_2 &= \alpha(1-x_3-x_4) & y_5 &= (1-\alpha)x_2 \\ y_3 &= \alpha x_3 & y_6 &= \alpha x_4 \end{aligned} \quad (4.59a,f)$$

We let Q_k ($k = 1, 4$) and X_k ($k = 1, 4$) be, respectively, the internal partition functions and the ionization and dissociation energies for H^0 , He^0 , He^+ , and H_2 , computed in accordance with the results of Section 4.2. We define φ_k ($k = 1, 4$) such that $\varphi_k = X_k/kT$. We may now write the ionization-dissociation equilibrium relations, equations (4.45a,c) and equation (4.46), so as to define the respective equilibrium constants K_k ($k = 1, 4$) as follows:

$$\frac{x_2}{x_1} = \frac{Q_2}{Q_1} \exp(-\varphi_1 - \eta^*) = K_1$$

$$\frac{x_3}{1-x_3-x_4} = \frac{Q_3}{Q_2} \exp(-\varphi_2 - \eta^*) = K_2$$

(4.60a,d)

$$\frac{x_4}{x_3} = \frac{1}{Q_3} \exp(-\varphi_3 - \eta^*) = K_3$$

$$\frac{2x_1^2}{1-x_1-x_2} = \frac{Q_1^2}{Q_4} \frac{AT^{3/2}}{wn} \exp(-\varphi_4) = \frac{K_4}{wn}$$

where we have set $\eta^* = \eta - \eta_c$. The pressure ionization parameter, η_c , is, from equation (4.43),

$$\eta_c = -Y(1+C)(1+H)^{1/2} \quad (4.61)$$

The quantity A appearing in equation (4.60d) is

$$A = \left(\frac{\pi m_H^k}{h^2} \right)^{3/2} \frac{1}{1-\alpha}$$

We may solve equations (4.60a,d) directly for the respective x_k :

$$\begin{aligned} x_1 &= \frac{1}{4} \left[K_0^{1/2} - K_4(1+K_1) \right] \\ x_2 &= K_1 x_1 \\ x_3 &= K_2 / \left[1 + K_2(1+K_3) \right] \\ x_4 &= K_3 x_3 \end{aligned} \tag{4.62a,d}$$

where

$$K_0 = K_4^2(1+K_1)^2 + 8K_4$$

Noting that the parameter w defined above and appearing in equation (4.60d) is given by

$$w = \left[(1-\alpha)x_2 + \alpha(x_3 + 2x_4) \right]^{-1}, \tag{4.63}$$

we may evaluate equations (4.62a,d) directly. In the absence of H_2 (that is, under the conditions of complete pressure dissociation), we have $x_1 = 1 - x_2$ and $x_2 = K_1(1 - K_1)$ in which case these relations assume a particularly simple form. We note that, in the instance of complete ionization and dissociation of all particle species, we have $x_1 = x_2 = 0$ and $x_3 = x_4 = 1.0$.

We may now write down explicit expressions for the total pressure, P (we neglect radiation pressure), the internal energy per gram, u , and the dimensionless entropy

per gram $\sigma = \mu_o m_H s/k$, where μ_o is the mean molecular weight per nucleon, $\mu_o = 1 + 3\alpha$, m_H is the mass of a hydrogen atom, s is the total entropy per gram, and k is Boltzmann's constant. We regard these quantities as consisting of the sum of an ideal gas contribution plus a correction term to account for the electrostatic interactions; that is, we write

$$P = P_o + P_C,$$

$$u = u_o + u_C \quad (4.64a,c)$$

$$\sigma = \sigma_o + \sigma_C$$

In the notation of the present section we have

$$P_o = (\beta w \sum_{k=1}^6 y_k + D) nkT,$$

$$u_o = \left[\sum_{k=1}^6 y_k \left(\frac{3}{2} + \frac{\partial \ln Q_k}{\partial \ln T} \right) + \frac{3}{2} \frac{D}{w} \right] \frac{kT}{\mu_o m_H} \quad (4.65a,c)$$

$$\begin{aligned} \sigma_o = \sum_{k=1}^6 y_k & \left[\frac{5}{2} + \frac{3}{2} \ln T - \ln(y_k w n) + \ln C_k \right. \\ & \left. + \ln Q_k + \frac{\partial \ln Q_k}{\partial \ln T} \right] + \frac{1}{w} (2.5D - \eta) \end{aligned}$$

where β is the ion-pair abundance parameter given in equation (4.21), D is as defined previously, $D = 2/3 F_{3/2} / F_{1/2}$,

and the constants C_k ($k = 1, 6$) appearing in equation (4.65c) are given by .

$$C_k = \left(\frac{2\pi m_k k}{h^2} \right)^{3/2} \quad (4.66)$$

where the m_k are the masses of the respective particles, k is Boltzmann's constant, and h is Planck's constant.

Where the Monte-Carlo corrections are applicable, we compute the parameter $\Gamma = (e^2/kT)(4/3\pi n)^{1/3}$ and interpolate directly in the tabular data of Brush et al. (1966). In the DH region the respective correction terms, including the additional correction for ion-pair formation, are determined from equations (4.10), (4.11), (4.12), and (4.57)

$$\begin{aligned} p_c &= -\beta^{3/2} \gamma (1+H)^{1/2} \left[\frac{1}{3}(1+H) + G \right] nkT \\ u_c &= -\beta^{3/2} \gamma (1+H)^{1/2} (1+H+G) \frac{kT}{\mu_o m_H w} \\ \sigma_c &= - \frac{\gamma \beta^{3/2}}{w} (1+H)^{1/2} \left[\frac{1}{3}(1+H) + \frac{3}{2}G \right] \end{aligned} \quad (4.67a,c)$$

The total mass density is given by

$$\rho = \mu_o m_H w n \quad (4.68)$$

and the adiabatic gradient is given by

$$\begin{aligned}
V_{ad} &= \left(\frac{\partial \log P}{\partial \log T} \right)_{\sigma} \\
&= \frac{T}{P} \left[\left(\frac{\partial P}{\partial T} \right)_n - \left(\frac{\partial P}{\partial n} \right)_T \frac{(\partial \sigma / \partial T)_n}{(\partial \sigma / \partial n)_T} \right] \quad (4.69)
\end{aligned}$$

In the above formulation the thermodynamic quantities, including the DH and MC corrections, as well as the ionization-dissociation equilibrium relations have been regarded explicitly as functions of n and T . Upon specification of a P and T , we compute these quantities by first computing the corresponding value of n . We employ a Newton-Raphson iterative procedure whereby corrections, Δn , to trial values, n^* , of the electron density are computed from

$$\Delta n = \frac{P - P^*}{(\partial P / \partial n)_{n=n^*}} \quad (4.70)$$

where $P^* = P(n^*, T)$. The iteration on n is continued until the electron density converges to within a specified tolerance.

The prescription proceeds as follows: For a trial value of n and the given T we compute the degeneracy parameter $F_{1/2}$ from equation (4.8) and obtain the other degeneracy parameters η , $2/3 F_{3/2}$, and the derivatives of $F_{1/2}$ either by direct interpolation in the tables of McDougall and Stoner (1938) or by using the appropriate

extrapolation formulae for values of $F_{1/2}$ outside the range of these tables. We compute κ and, thus, $\delta = \kappa a_0$ and evaluate the atomic partition functions and ionization energies. For the trial n , we know the total particle number density from which we evaluate the dissociation energy and the partition function for molecular hydrogen. We then compute the respective x 's from equations (4.62a,d) and the y 's from equations (4.59a-f). We then compute P^* from equations (4.65a) and (4.67a) and determine Δn from equation (4.70). Once the convergence of n has been obtained, the remaining thermodynamic quantities may be evaluated directly. The derivatives required in the iteration procedure as well as in the computation of V_{ad} are obtained through straightforward differentiation of the respective quantities $P(n,T)$ and $\sigma(n,T)$. In keeping with the discussion of Section 4.2 we neglect any implicit dependence of the atomic partition functions and ionization energies on n and T .

4.6.2 $T < 5000$ °K

At temperatures below 5000 °K both hydrogen and helium remain neutral at all relevant pressures so that we need only consider a mixture of neutral atomic helium and neutral atomic hydrogen in equilibrium with molecular hydrogen. We let the subscripts $k = 1, 2, 3$ denote those quantities pertaining to H , H_2 , and He , respectively. The

respective partial pressures are P_k ($k = 1, 3$) and the total pressure is $\sum_{k=1}^3 P_k$. The $H-H_2$ dissociation equilibrium relation is

$$P_1^2 / P_2 = K \quad (4.71)$$

where

$$K = \frac{Q_1^2}{Q_2} \left(\frac{\pi m_H kT}{h^2} \right)^{3/2} kT$$

Here the Q 's denote the respective partition functions. If we let x be the ratio of the number of atomic hydrogen nuclei to the total number of H nuclei present and introduce the abundance parameter α as defined previously, equation (4.71) may be rewritten in the form

$$(1-\alpha)(K^*+4)x^2 + 2\alpha K^*x - (1-\alpha)K^* = 0 \quad (4.72)$$

where $K^* = K/P$. Upon specification of P and T , this equation may be solved for x in terms of which we calculate the partial pressures of atomic and molecular hydrogen, that is,

$$P_1 = x(1-\alpha)P_0 \quad (4.73)$$

and

$$P_2 = \frac{1}{2}(1-x)(1-\alpha)P_0. \quad (4.74)$$

In terms of α the partial pressure of helium is

$$P_3 = \alpha P_0 \quad (4.75)$$

where

$$P_0 = P_1 + 2P_2 + P_3 = 2P / \left[(1-\alpha)x + (1+\alpha) \right].$$

From the perfect gas law we obtain the total mass density, ρ ,

$$\rho = \frac{\mu m_H}{k} \frac{P}{T} \quad (4.76)$$

where the mean molecular weight per particle, μ , is

$$\mu = (P_1 + 2P_2 + 4P_3) / P \quad (4.77)$$

The dimensionless entropy per gram, which we now define as $\sigma = m_H s/k$, where s is the total entropy per gram, is given by

$$\sigma = \sum_{k=1}^3 \sigma_k \quad (4.78)$$

where

$$\sigma_k = \frac{P_k}{P_\mu} \left[\frac{5}{2}(1 + \ln T) + \ln(C_k Q_k / P_k) + \frac{\partial \ln Q_k}{\partial \ln T} \right] \quad (4.79)$$

The C_k are as defined in equation (4.66) and the Q_k are the respective partition functions (we note that $\partial \ln Q_1 / \partial \ln T = \partial \ln Q_3 / \partial \ln T = 0$). The adiabatic gradient is given by

$$\begin{aligned}
 \nabla_{\text{ad}} &= \left(\frac{\partial \log P}{\partial \log T} \right)_{\sigma} \\
 &= - \frac{T}{P} \frac{(\partial \sigma / \partial T)_P}{(\partial \sigma / \partial P)_T}
 \end{aligned}
 \tag{4.80}$$

the derivatives of σ with respect to T and P are evaluated by differentiation of equation (4.78). Finally, the expression for the internal energy per gram, u , is given by

$$u = \frac{3}{2} \frac{P}{\rho} \tag{4.81}$$

Having determined the thermodynamic quantities for a given P and T , we may now compute the opacity, κ , and the nuclear energy generation rate, ϵ , both of which, according to the developments of Sections 4.4 and 4.5, are functions of the density and the temperature. Below 10^5 °K we set $\epsilon = 0$, and below 10^4 °K we fit the Cox and Stewart opacities to the atmospheric opacity table constructed as described in Section 5.1.

We construct a table (the "constitutive data table") of the constitutive data with $\log T$ and $\log P$ as arguments over the temperature range $3.1 \leq \log t \leq 7.0$ with a spacing in $\log T$ of $\Delta \log T = 0.1$. For each temperature entry, we compute the constitutive quantities, ρ , u , ∇_{ad} , ϵ , and κ , for 56 values of $\log P$ such that the total span in $\log P$ is equal to 5.0. The low pressure boundary of the table at a given value of $\log T$ is defined by the relation

$$(\log P)_{\text{low}} = 2.94118 \cdot \log T - 4.58825 \quad (4.82)$$

By defining the constitutive data table in this way, we intend to encompass the entire range of temperature and pressure that we expect to encounter in the interior structure of low mass stars, at least over that segment of their evolution with which we are to be concerned. It is these data which we later utilize in the construction of what we designate the "detailed" stellar models.

In Figures 8 and 9 we summarize some of the quantitative results we find relating to the thermodynamic properties of the actual hydrogen-helium mixture we consider in constructing the constitutive data table. In Figure 8 we plot the loci in the $\log \rho$, $\log T$ plane of several relevant boundary lines. The shaded boundary delimits the region above $\log T = 4.0$ within which the constitutive data table is defined. The lines labeled I_1 and I_2 demarcate the regions of complete pressure ionization of hydrogen and helium. To the left of I_1 both hydrogen and helium are partially ionized; between I_1 and I_2 hydrogen is completely, but helium partially, ionized; and to the right of I_2 both hydrogen and helium are completely ionized. Below $\log T = 4.3$ the pressure ionization effects we consider cease to be important and the gas remains inappreciably ionized over the entire range of densities encountered in constructing the constitutive data

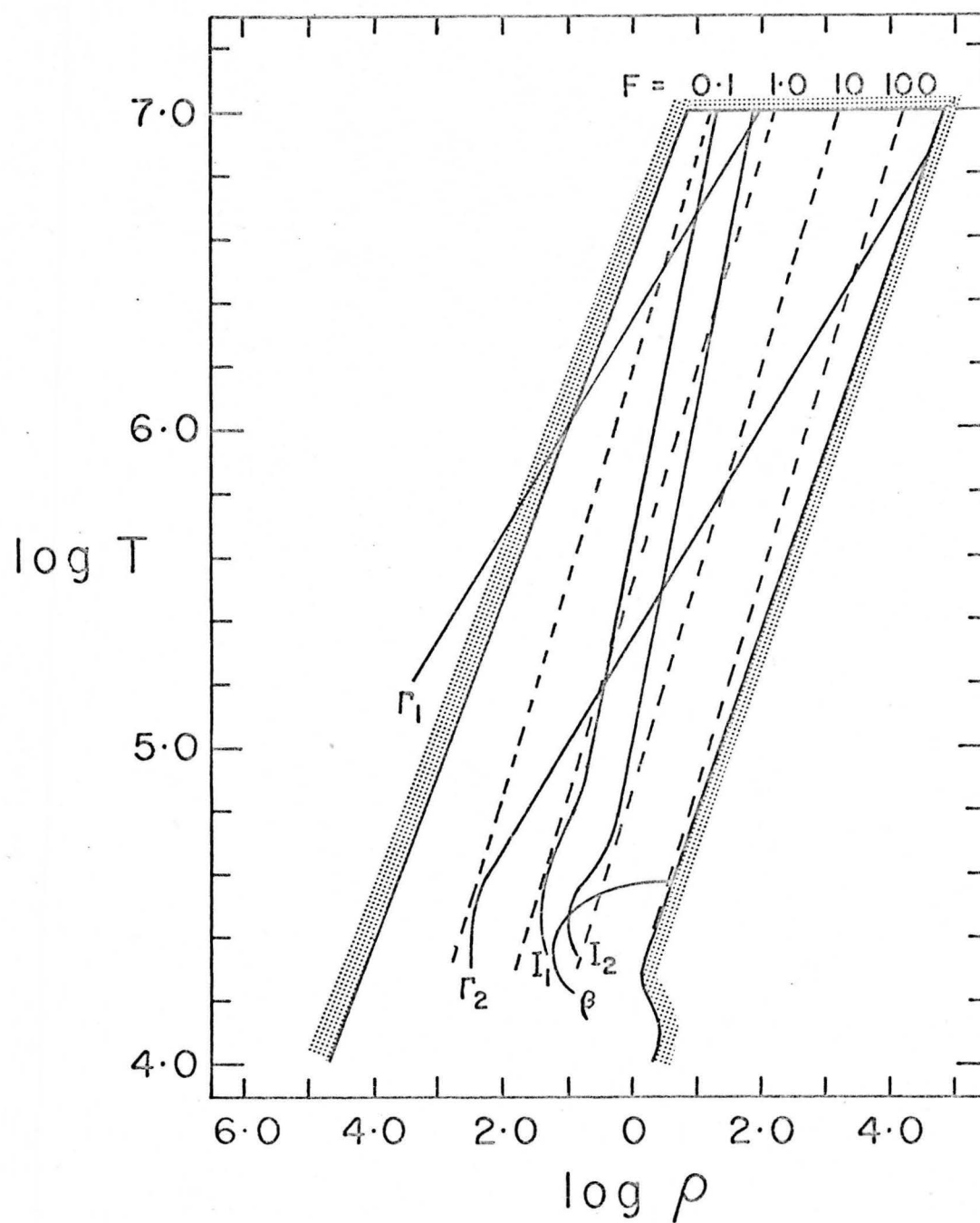


Fig. 8. Domain of the constitutive data table in the $\log \rho$, $\log T$ plane.

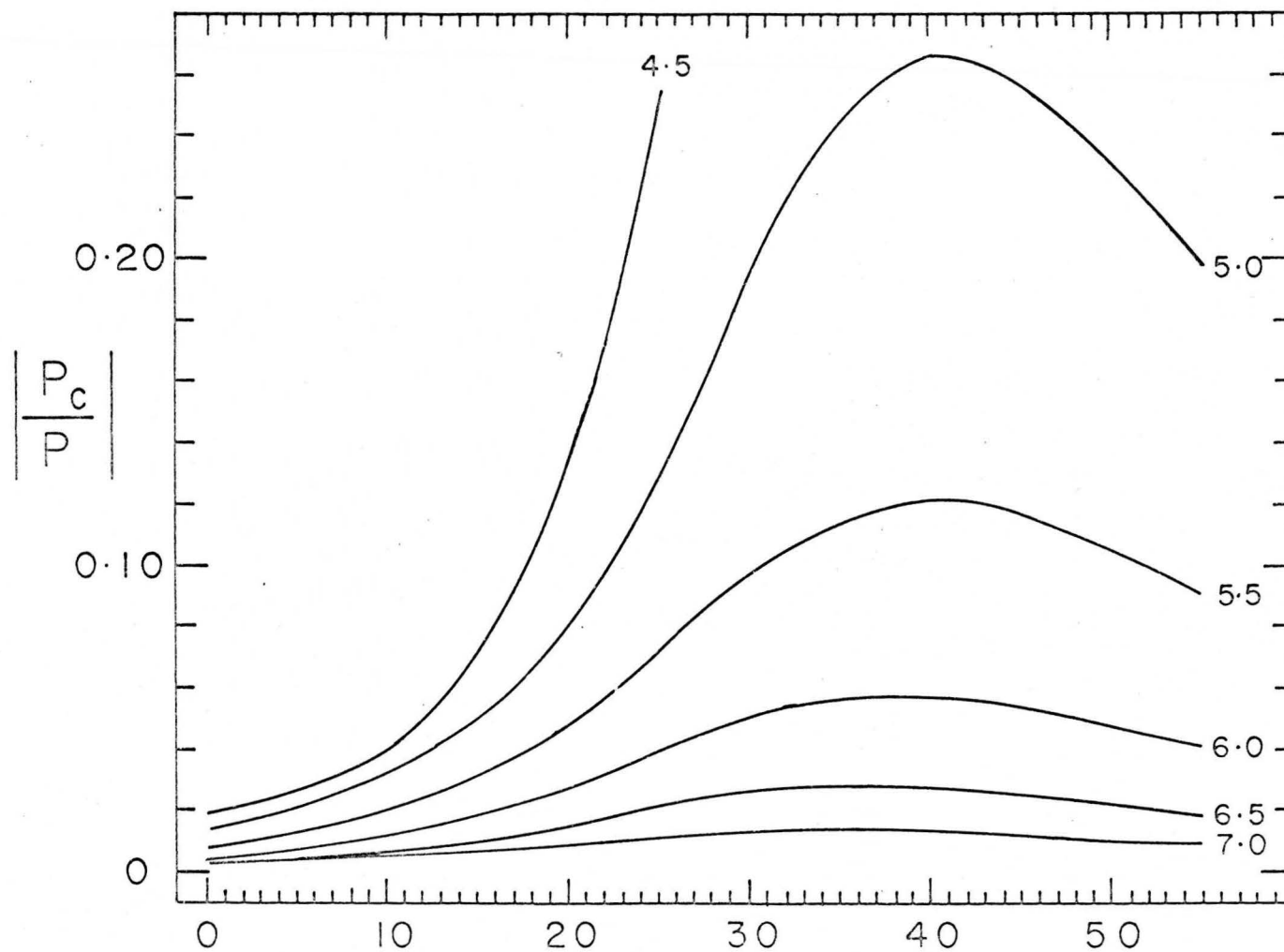


Fig. 9. The magnitude of the pressure correction as a function of the pressure and temperature in a hydrogen-helium plasma.

table. We therefore take $\log T = 4.3$ to be the low temperature limit in Figure 8 at which we terminate the plotted loci of those quantities dependent upon the degree of ionization.

The line Γ_1 in Figure 8 is defined by the condition $\Gamma = 0.1$, where Γ is as defined in equation (4.13). This line is just the DH criterion, equation (4.14); consequently to the left of this line we apply the DH results while to the right we employ the MC results. We observe that the MC data are used almost exclusively in estimating the thermodynamic corrections due to the interaction effects. The line Γ_2 is defined by the condition $\Gamma = 1.0$ and serves to indicate the degree to which we penetrate the MC region. At temperatures below 10^5 °K we employ the ion-pair artifice and in the region below and to the right of the line labeled β we find on this model that all of the charged particles are associated as ion-pairs. The dashed lines labeled by values of the parameter F indicate the degree of electron degeneracy encountered. In terms of the Fermi-Dirac integral $F_{1/2}(\eta)$ we have from equation (4.8) that the degeneracy criterion, equation (A.3), may be expressed as

$$F_{1/2}(\eta) << \frac{1}{4}\sqrt{\pi}$$

We define $F = \frac{1}{4}\sqrt{\pi}/F_{1/2}(\eta)$ and plot the resulting lines for $F = 0.1, 1.0, 10, \text{ and } 100$ appropriate, however, to the condition of complete ionization. We observe that the electrons are to be regarded as being partially degenerate throughout the region within the constitutive data table in which the gas is appreciably ionized.

In Figure 9 we plot for several temperatures the ratio of the magnitude of the pressure correction term, $|P_C|$, to the total gas pressure, P , against the total pressure. Instead of the actual values of the pressure (or $\log P$), however, we employ as abscissa in Figure 9 the running numbers 0-55 with which we label the pressure grid points at a fixed $\log T$ in the constitutive data table. The grid spacing in $\log P$ is 0.090909 and the pressure at a given temperature corresponding to the point 0 is determined from equation (4.82). In Figure 9 we plot data for $\log T = 4.5, 5.0, 5.5, 6.0, 6.5, \text{ and } 7.0$.

We see from Figure 9, as we should expect, that the magnitude of the pressure correction decreases with increasing temperature; that is, the gas becomes increasingly ideal with increasing temperature. In addition we see that at a fixed temperature $|P_C|/P$ is an increasing function of the pressure at low pressures but at a sufficiently high pressure it reaches a maximum and thereafter decreases with increasing pressure. Although $|P_C|$ is a monotonically increasing function of the pressure (at fixed

T), we find that at high pressures it increases much less rapidly than the (perfect gas) contribution to the total pressure due to the degenerate electrons. Consequently when the degree of degeneracy becomes sufficiently high the gas is driven towards perfection. This accounts for the behavior of $|P_C|/P$ shown in Figure 9 for $\log T \geq 5.0$. At $\log T = 4.5$ we are well within the region within which none of our approximate treatments of gas imperfection are adequate. Here we resort to the ion-pair artifice and we find, but do not show in Figure 9, that $|P_C|/P$ approaches a constant value of nearly 0.50.

Our approach to the computation of the thermodynamic quantities has been at best very approximate and at worst very crude. We have neglected entirely the effects of interactions between neutral atoms and molecules and, in ignoring the presence of H_2^+ and H^- , have certainly not considered all of the possible particle species. We have made provision for pressure ionization and dissociation, but our approach has caused us to ascribe rather artificial properties to the partition functions in order to insure that the Saha equation will yield completely ionized species at high pressures. In this approach we have incorporated, in the form of the modified Coloumb potential of equation (4.33), the effects of interactions on the atomic bound states, but have ignored these interactions inasmuch as we have employed the usual ideal gas

expressions for the thermodynamic functions. Furthermore, the physical significance of ion-pair formation and its consequences are highly suspect. What is required is a theory allowing for interactions of any order occurring between both neutral and charged particles. At low densities such a theory must yield the usual ideal gas relations; while at very high densities it must encounter a fluid-solid phase transition. While we may not feel secure that our results accurately represent the physical state of the stellar interior, we, nevertheless, gain some insight into the complications introduced by extending thermodynamic theory beyond the ideal gas approximation.

CHAPTER 5

ATMOSPHERIC MODELS FOR LOW MASS STARS

The overall structure of stars which are either wholly in convective equilibrium or which possess deep outer convection zones is very sensitive to the surface boundary conditions (cf. Henyey, Vardya, and Bodenheimer 1965). Consequently it is necessary to have a knowledge of the structure of the outer atmospheric layers of such stars. For the purposes of this investigation we consider the atmospheric layers to consist of two distinct regions, an outermost region which is in strict radiative equilibrium and an underlying transition zone which is convectively unstable and in which convection and radiation act simultaneously to transport energy outward. We shall treat the radiative region by means of the gray atmosphere approximation and the transition zone by means of a simple version of the mixing length theory. We acknowledge that the approximate treatments accorded these regions may well constitute the greatest source of uncertainty in the model calculations. For example, preliminary calculations by Gingerich et al. (1967) indicate considerable departures from grayness in a stellar atmosphere having an effective temperature $T_e = 2500$ °K. It is well known (Henyey et al.

1965) that the mixing length theory is, at best, a rather rough approximation for treating the convective transition zone. Because of the current lack of a completely rigorous theory by which we may treat these regions, we adopt these very approximate methods of treatment with the hopeful expectation that such will suffice for providing physically realistic boundary conditions for the interior models.

5.1 Equation of State, Adiabatic Gradient, and Radiative Opacity

Although each of the two atmospheric regions requires a considerably different method of attack, the equation of state, adiabatic gradient, and radiative opacity are treated in the same way in both regions. In computing the equation of state and the adiabatic gradient we follow the procedures described by Weymann and Moore (1963). We consider hydrogen in four states, H_2 , H , H^- , and H^+ , and helium in all of its ionization states. In computing the electron pressure we include the first ionization of the metals K, Na, Mg, Si, C, and (Ca+Al) with the abundances adjusted so as to account for the presence of the other metals of low ionization energies which are not specifically included. The partial pressure of atomic hydrogen and the electron pressure are computed as functions of the total pressure and the temperature by a procedure based on the Newton-Raphson method. The adiabatic gradient is computed in a manner similar to that employed by Vardya (1960) in

which the thermodynamic functions for molecular hydrogen are computed so as to account for the effects of pressure dissociation following Vardya (1965).

We have computed a table of Rosseland mean opacities for use in the region of temperature and pressure appropriate to the atmospheres of M dwarf stars. The sources of opacity considered in these calculations include the continuous absorption due to the photoionization of neutral hydrogen, bound-free and free-free absorption by H^- , free-free absorption by H_2^- as well as Rayleigh scattering by atomic and molecular hydrogen. We also include the effects of the band absorption by water vapor in an approximate way.

For the absorption coefficient due to the photoionization of neutral hydrogen, we employ the expression quoted by Allen (1963),

$$\alpha_\nu = (1.045 \times 10^{-14}) \frac{\lambda^3}{n^5} g \quad (\text{cm}^2)$$

where α_ν is the ionization cross-section at the frequency ν , λ is the wavelength in microns, n is the principal quantum number, and g is the Gaunt factor which we set equal to unity. We specifically include the absorption arising from the states up through $n = 3$.

We use Chandrasekhar's (1958) values of the absorption coefficient for the bound-free H^- absorption.

Following Gaustad (1963), we multiply the tabulated values by the factor

$$\phi = 4.158 \times 10^{-10} \theta^{5/2} \exp(1.726 \theta)$$

where $\theta = 5040.39/T$ and T is the temperature, to obtain the cross-section per neutral hydrogen atom and unit electron pressure. We employ Geltman's (1965) tabulations for the H^- free-free absorption coefficient. For temperatures below and wavelengths longer than those considered by Geltman, we use Gingerich's (1961) polynomial approximations. More recently John (1966) has extended the calculation of H^- free-free absorption coefficients into the far infrared but, since his calculations do not extend beyond $\theta = 2.0$, we have, for the sake of expediency, continued to use the polynomial approximation for all regions outside of Geltman's data. We follow Vardya (1966) and take the H_2^- free-free absorption coefficient to be twice that due to H^- free-free. The Rayleigh scattering cross-sections are taken from Vardya (1962) who gives

$$\sigma_H = 7.3693 \times 10^{-29} \lambda(\mu)^{-4} \quad (\text{cm}^2)$$

for the cross-section per neutral H atom and

$$\sigma_{H_2} = 8.4909 \times 10^{-29} \lambda(\mu)^{-4} \quad (\text{cm}^2)$$

for that per H_2 molecule.

It is now rather firmly established that water vapor will be an important source of opacity in the atmospheres of cool stars. Strong absorption features due to water vapor have been found in the spectra of M type giants by several investigators (Kuiper 1963; Woolf, Schwarzschild, and Rose 1964; Danielson, Woolf, and Gaustad 1965; Spinrad and Newburn 1965; Spinrad et al. 1966; McCammon, Münch, and Neugebauer 1966). From detailed calculations of water vapor opacities, Auman (1966) has found that water vapor is expected to be an important source of opacity at temperatures less than 3400 °K and the dominant source at temperatures less than 2500 °K. We include the effects of water vapor absorption by employing the experimentally based absorption coefficients for the vibration-rotation bands and the pure rotation band of water vapor obtained by Ferriso, Ludwig, and Thomson (1966). These data were obtained from the measurement of water vapor emissivity over the temperature range from 300 °K to 3000 °K and at one atmosphere pressure. The monochromatic absorption coefficient is obtained from the emissivity data through an averaging process over finite wavenumber intervals. In proceeding in this manner we smear out the intrinsic line absorption and replace it by a pseudo-continuous absorption. Such a procedure is justified if the mean line spacing in the bands is less than the mean widths of the individual lines. We find that in the temperature range

from 1500 °K to 3000 °K and at pressures greater than one atmosphere the combined effects of thermal smearing, arising from the increased number of lines at elevated temperatures, and pressure broadening are sufficient to satisfy the above requirement. At lower pressures this procedure becomes somewhat questionable and may result in an over estimation of the contribution made by water vapor to the total opacity, since it neglects the possibility of radiation leaking out through the spaces between the lines. We have neglected this latter effect in applying the data of Ferriso et al. (1966), and have used their data as presented over the entire range of pressures encountered in the atmospheric models.

Having obtained the absorption cross-section, $\alpha_i(\nu)$, due to the i^{th} absorbing species at the frequency ν , we may obtain the total monochromatic opacity per gram, κ_ν , from the relation

$$\kappa_\nu = \frac{1}{\mu m_H} \sum_i \alpha_i(\nu) \frac{P_i}{P}$$

where μ is the mean molecular weight, m_H is the mass of the hydrogen atom and P_i/P is the ratio of the partial pressure of the i^{th} absorbing species, P_i , to the total pressure P . We calculate the Rosseland mean, $\bar{\kappa}_R$, from

$$\frac{1}{\kappa_R} = \frac{\int_0^\infty \frac{1}{\kappa_\nu} \frac{\partial B_\nu(T)}{\partial T} d\nu}{\int_0^\infty \frac{\partial B_\nu(T)}{\partial T} d\nu}$$

where $B_\nu(T)$ is the Planck function evaluated at the temperature T and frequency ν . In Table 3 we present the calculated Rosseland mean opacities as functions of the temperature and the total pressure over the range $3.0 \leq \log T \leq 4.0$ and $1.0 \leq \log P \leq 10.0$. At temperatures greater than 10,000 °K we use the opacity tables of Cox and Stewart (1965).

In computing the partial pressure of water vapor we resort to the expediency of assuming that all of the carbon present is in the form of CO. We then assume that water vapor will be in equilibrium with OH with the initial oxygen abundance being reduced in amount by that of carbon. From Vardya's (1966) calculations of the run of molecular abundances in the atmospheres of late-type stars, it appears that this is a quite reasonable procedure; although one should, perhaps, also account for the presence of SiO.

5.2 Radiative Region

In the outermost radiative region of the atmosphere we shall adopt the temperature distribution appropriate to the Eddington approximation for a gray atmosphere. If we let T be the temperature at optical depth τ in a star

Table 3. Rosseland Mean Atmospheric Opacities
($\text{Log } \bar{\kappa}_R$)

Log T	Log P									
	1.0	2.0	3.0	4.0	5.0	6.0	7.0	8.0	9.0	10.0
3.00	-2.978	-2.978	-2.978	-2.978	-2.978	-2.978	-2.978	-2.978	-2.978	-2.977
3.10	-3.519	-3.519	-3.519	-3.519	-3.519	-3.518	-3.516	-3.510	-3.492	-3.441
3.20	-3.869	-3.870	-3.869	-3.866	-3.856	-3.827	-3.749	-3.580	-3.302	-2.937
3.30	-3.797	-3.757	-3.710	-3.627	-3.501	-3.298	-2.993	-2.606	-2.176	-1.738
3.40	-3.986	-2.997	-2.410	-2.174	-2.075	-1.982	-1.835	-1.592	-1.247	-0.840
3.50	-4.541	-3.987	-3.339	-2.577	-1.825	-1.293	-0.964	-0.690	-0.385	-0.039
3.60	-4.178	-3.409	-2.633	-1.919	-1.248	-0.626	-0.104	0.229	0.459	0.684
3.70	-3.236	-2.792	-2.273	-1.607	-0.830	-0.103	0.497	0.898	1.156	1.334
3.80	-2.035	-1.616	-1.154	-0.681	-0.190	0.350	0.943	1.482	1.788	1.932
3.90	-1.136	-0.476	-0.052	0.373	0.816	1.271	1.737	2.207	2.533	2.605
4.00	-2.412	-0.552	0.732	1.333	1.755	2.176	2.601	3.038	3.430	3.550

having an effective temperature T_e , we have

$$T^4 = \frac{3}{4} T_e^4 \left(\tau + \frac{2}{3} \right). \quad (5.1)$$

The optical depth at the radial distance r from the center of the star is defined such that

$$\tau = \int_r^\infty \kappa \rho dr \quad (5.2)$$

where κ is the opacity per gram and ρ is the mass density. The condition of hydrostatic equilibrium in this region can be written as $dP/dr = -g_r \rho$ which, with $d\tau = -\kappa \rho dr$, gives

$$\frac{dP}{d\tau} = \frac{g_r}{\kappa} \quad (5.3)$$

where P is the total pressure. Here g_r is the acceleration due to gravity, $g_r = GM_r/r^2$ where G is the constant of gravitation and M_r is the total mass interior to a sphere of radius r . Combining equations (5.1) and (5.3) we obtain

$$\frac{d \log T}{d \log P} = \frac{3}{16} \frac{\kappa T_e^4}{g_r} \frac{P}{T^4}. \quad (5.4)$$

Let us now define the quantities x and q such that $x = r/R$ and $q = M_r/M$ where R and M are, respectively, the radius and total mass of the star. From equation (5.3) and the condition for the conservation of mass, $dM_r = 4\pi r^2 \rho dr$, we obtain

$$\frac{d \log x}{d \log P} = - \frac{1}{R} \frac{P}{\rho} \frac{1}{x g_r} \quad (5.5)$$

and

$$\frac{d \log q}{d \log P} = \frac{R^3}{M} \frac{4\pi x^3}{q} \rho \frac{d \log x}{d \log P} \quad (5.6)$$

We must now numerically integrate equations (5.4), (5.5), and (5.6) in order to obtain the structure of the radiative zone. To obtain starting values of P , T , x , and q , we estimate the pressure at a very shallow optical depth, say, $\tau_0 = 0.005$. We assume that the total pressure at this point can be approximated by the sum of the partial pressures of atomic and molecular hydrogen and that the total opacity is due to H^- and H_2^- alone. We obtain the temperature at this optical depth from equation (5.1) and use the approximate expression for the H^- opacity, κ_{H^-} , given by Demarque (1960),

$$\kappa_{H^-} = X \frac{P_H P_e}{P} (8.87 \times 10^{-3}) \theta^{5/2} 10^{0.747\theta}$$

where X is the fractional abundance of hydrogen by mass and P_H , P_e , and P are the partial pressure of atomic hydrogen, the electron pressure, and the total pressure, respectively. For this calculation we assume that $P_e = 10^{-5}P$. For $\kappa_{H_2^-}$ we take

$$\kappa_{H_2^-} = 2\kappa_{H^-} \left(\frac{P_H/P}{2 - P_H/P} \right).$$

Writing equation (5.3) as a difference equation and eliminating ρ through the ideal gas law, we can write at

$$\tau = \tau_o$$

$$P_o = \left[\frac{2g_{\text{surf}}}{f(T_o, P_o)} \tau_o \right]^{1/2}$$

where g_{surf} is the surface gravity and $f(T_o, P_o)$ is a function of the temperature, T_o , and pressure, P_o , at $\tau = \tau_o$. We solve for P_o through an iterative procedure and use the resultant values of T_o and P_o for initializing the numerical integration of equations (5.4) through (5.6), assuming that $q_o = 1.0$ and $x_o = \tau_o / \rho_o \kappa_o$. The actual numerical integration is performed using the Heun method and we continue the integration through the radiative region until the point is reached at which the local adiabatic gradient is less steep than the prevailing radiative gradient given by the inverse of equation (5.4). At this point convective motions will break out and we encounter the transition zone.

We must emphasize the very approximate nature of this treatment of the radiative region. A more thorough treatment would involve the construction of non-gray atmospheric models which would take into account the effects of molecular line blanketing in a more adequate way than that attempted here. It is not yet clear that all of the possible important sources of opacity present

in very cool stars are known. Vardya and Böhm (1965) have investigated the possible existence of unknown sources of opacity in the atmosphere of the M2V star Lal 21185 by comparing the total pressure obtained from a model atmosphere calculation with the observed pressure broadening of the λ 4227 line of CaI. They find that for an effective temperature of 3400 °K, which is in good agreement with the value (3500 °K) given by Johnson (1965) for this star, the pressures as determined from the model and the observations are in quite reasonable agreement. We cannot, however, be assured that this will be the case in much cooler atmospheres. In cool atmospheres we would expect that the band absorption due to molecular species other than water vapor, such as CO, for example, will also contribute to the infrared opacity. Free-free transitions of electrons in the fields of atomic and molecular species other than neutral and molecular hydrogen will also contribute to the opacity in the infrared (Dalgarno and Lane 1966). Since the opacities used in this work were computed, extensive data on the absorption coefficient due to free-free transitions by neutral helium have become available (Somerville 1965; McDowell, Williamson, and Myerscough 1966). Furthermore, Linsky and Gingerich (Linsky 1966) have found that the pseudo-continuous absorption arising from pressure induced dipole transitions in molecular hydrogen may contribute to the opacity in the infrared at temperatures

less than 2500 °K. It should be borne in mind, however, that at these low temperatures, water vapor will be overwhelmingly the dominant source of opacity in atmospheres having a normal oxygen abundance.

5.3 Convective Transition Region

To continue the integration of equations (5.4) through (5.6) through the convective transition region we employ the simple form of the mixing length theory described by Schwarzschild (1958, p. 44). In this region the prevailing temperature gradient will be superadiabatic but will be less steep than the local radiative gradient. Both radiation and convection will be responsible for the outward transport of energy and the total outward flux F can be written as the sum of a radiative contribution, F_{rad} , and a convective contribution, F_{conv} . The radiative flux is given by

$$F_{\text{rad}} = \frac{16\sigma}{3} \frac{g_r}{\kappa} \frac{T^4}{P} \frac{d \log T}{d \log P}. \quad (5.7)$$

According to the mixing length theory, the convective flux can be approximated by

$$F_{\text{conv}} = c_p \rho \frac{g_r^{1/2}}{T^{1/2}} \frac{\ell^2}{4} (\Delta \nabla T)^{3/2} \quad (5.8)$$

where c_p is the ratio of specific heats of the material at constant pressure, ρ is the mass density, ℓ is the mixing

length, which is essentially a measure of the distance over which an individual convective element exists, and $\Delta \nabla T$ denotes the difference between the prevailing ("True") and the local adiabatic gradient, that is,

$$\Delta \nabla T = g_r \rho \frac{T}{P} \left[\left(\frac{d \log T}{d \log P} \right)_{\text{True}} - \left(\frac{d \log T}{d \log P} \right)_{\text{ad}} \right]. \quad (5.9)$$

Letting $\xi = (d \log T / d \log P)_{\text{True}}$ and $\zeta = (d \log T / d \log P)_{\text{ad}}$ and employing the perfect gas law to eliminate ρ , we obtain from equation (5.9)

$$\Delta \nabla T = \frac{\mu_{mH}}{k} g_r (\xi - \zeta). \quad (5.10)$$

Let us now set $\ell = a H_P$ where a is a constant and H_P is the pressure scale height defined by

$$\frac{1}{H_P} = \frac{1}{P} \frac{dP}{dr} = - \frac{g_r \rho}{P}. \quad (5.11)$$

The total flux can then be written as

$$F = \alpha \xi + \beta^{-1} (\xi - \zeta)^{3/2} \quad (5.12)$$

where we let

$$\alpha = \frac{16\sigma}{3} \frac{g_r}{\kappa} \frac{T^4}{P} \quad \beta = \frac{4}{c_P} \left(\frac{k}{\mu_{mH}} \right)^{1/2} \frac{1}{a^{2PT^{1/2}}}$$

Solving for the true gradient ξ we obtain a cubic equation of the form

$$\xi^3 + A\xi^2 + B\xi + C = 0 \quad (5.13)$$

where the coefficients are given by

$$A = - (3\zeta + \alpha^2\beta^2)$$

$$B = (3\zeta^2 + 2\alpha\beta^2F)$$

and

$$C = - (\zeta^3 + \beta^2F^2).$$

For a star having an effective temperature T_e the flux at any radial distance r from the center (assuming r to be above the region in which energy generation occurs) is given by

$$F(r) = \frac{\sigma T_e^4 R^2}{r^2} \quad (5.14)$$

where R is the total radius. We can compute F at any point r and solve equation (5.13) for the superadiabatic gradient. Knowing the gradient we can continue the numerical integration of equations (5.4) through (5.6) through the convective transition region. A point will be reached at which the prevailing temperature gradient becomes effectively equal to the adiabatic gradient and energy may be assumed to be wholly transported by convection. It is the values of the pressure and temperature at this point, the base of the mixing length region, that we employ as a boundary condition for the integration of the interior model.

In order to employ the mixing length theory we must specify the appropriate value of the mixing length, ℓ . Considerable attention has been paid to obtaining physically realistic values for ℓ using constant values of the parameter a as well as values which vary with depth (see Henyey et al. 1965). We simply adopt the value of unity for a and, thus, take ℓ to be equal to the pressure scale height. In M dwarf stars near the main sequence we expect that the atmospheric densities will be sufficiently high that convection will rapidly become an efficient mode of energy transport as one proceeds inward from the radiative zone. In such cases the convective transition region will be relatively shallow and the values of the pressure and temperature at the base of the mixing length region will be rather insensitive to the precise value of ℓ .

5.4 Computation of Atmospheric Data Table

Because of the excessive computer time that would be involved in directly computing the atmospheric structure for each stellar model, we find it most convenient to provide the atmospheric data required for the solution of the equations of stellar structure in tabular form. These data include the fractional radius, x_{mxl} ; the pressure, P_{mxl} ; and the temperature, T_{mxl} , evaluated at the base of the mixing length region. We find from the atmospheric models that for the low mass stars the atmospheric region is

sufficiently shallow that we may neglect its mass compared to the total mass of the star. Consequently we find it convenient to provide the atmospheric data as functions of the effective temperature, T_e , and the logarithm of the surface gravity, g_{srf} . In terms of the total mass, M , and radius, R , we have

$$g_{\text{srf}} = \frac{GM}{R^2}$$

We have constructed a grid of model atmospheres over the range $1500 \text{ }^\circ\text{K} \leq T_e \leq 3500 \text{ }^\circ\text{K}$ and $3.0 \leq \log g_{\text{srf}} \leq 6.0$ with a spacing $\Delta T_e = 200 \text{ }^\circ\text{K}$ and $\Delta \log g_{\text{srf}} = 0.2$. Interpolation in this table of 176 model atmosphere integrations provides the outer boundary condition for the stellar model calculations. In Figures 10 and 11 we show the resulting relations between $\log T_{\text{mxl}}$ and $\log P_{\text{mxl}}$, respectively, and $\log g_{\text{srf}}$ with T_e as parameter. At low T_e and high g_{srf} the convective transition region disappears and the star becomes adiabatic immediately below the radiative region. This accounts for the distinctly linear portions of the relations shown in Figures 10 and 11 and especially noticeable in Figure 11. Over the entire grid of atmospheres we find that x_{mxl} remains sufficiently close to unity that we may, to very good approximation, completely neglect the geometric thickness of the atmosphere.

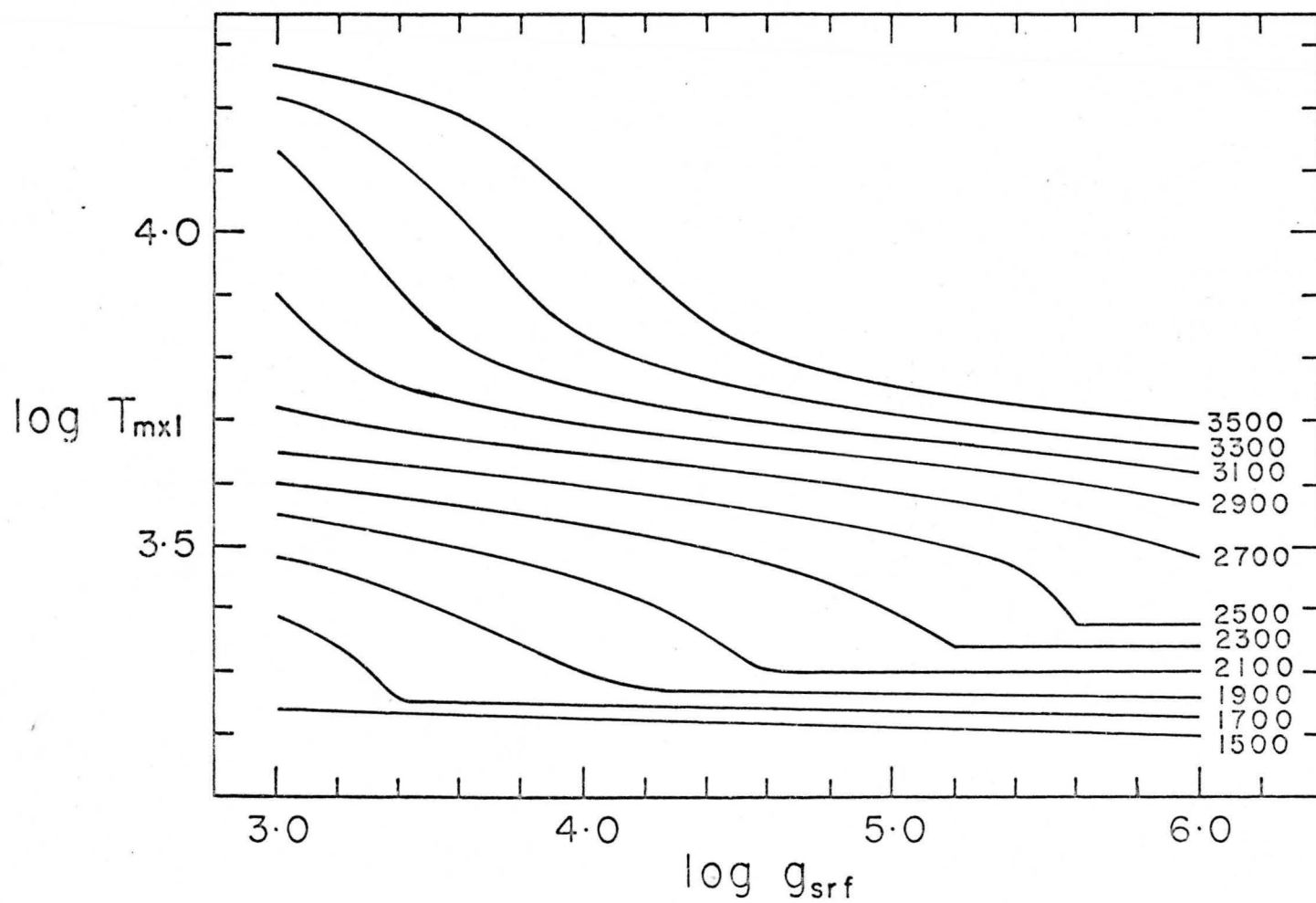


Fig. 10. $\log T_{\text{mxl}}$ as a function of g_{srf} with T_e as parameter.

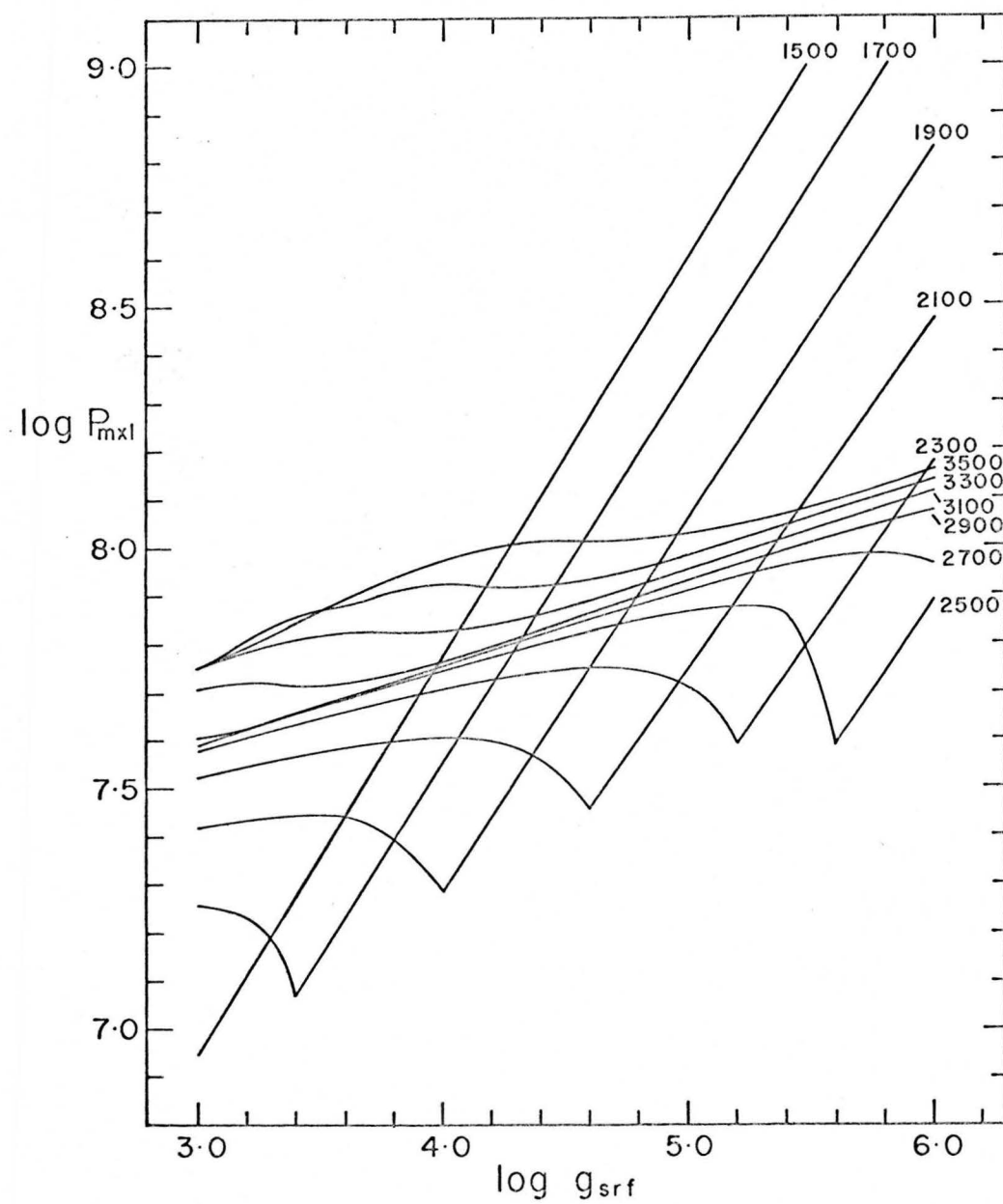


Fig. 11. $\log P_{\text{mxl}}$ as a function of g_{srf} with T_e as parameter.

In addition to these data we have also constructed a table of the entropy at the base of the mixing length region, which we designate s_{mxl} , over the grid of atmospheres. The entropy values were computed under the assumption that all of the particle species present, including the free electrons, at the given value of T_{mxl} and P_{mxl} behaved as ideal Boltzmann particles. In this case the entropy may be computed in a very straightforward manner from equation (4.65c). These data provide the outer boundary condition for the determination of the simple polytrope evolutionary sequences which we construct in Section 6.1.

CHAPTER 6

CONSTRUCTION OF THE THEORETICAL EVOLUTIONARY STELLAR MODELS

We assume at the outset that we may neglect the effects of rotation, magnetic fields, and pulsation in so far as they affect overall stellar structure and evolution. In neglecting these effects we may additionally assume that stars are spherically symmetric. We assume that the objects we consider are chemically homogeneous, a condition which is rigorously true as long as the interior is in a state of convective equilibrium throughout. Lastly, we assume that at any point in time a star may be regarded as existing in a state of essentially strict mechanical and thermal equilibrium. That this is a reasonable assumption is borne out by noting that the time scale over which dynamical readjustment of the interior structure would occur following a perturbation from equilibrium is very much shorter than that associated with the usually slow evolutionary changes (Schwarzschild 1958, p. 32).

It is from the conditions of mechanical and thermal equilibrium that we derive the equations of stellar structure (see Schwarzschild 1958, Chapter 2). The condition of hydrostatic equilibrium requires that the inward directed gravitational force acting on an element of matter

at any radial distance r from the center must be exactly balanced by the outward directed pressure force to give

$$\frac{\partial P}{\partial r} = - \frac{G m_r}{r^2} \rho \quad (6.1)$$

where P and ρ are, respectively, the total pressure and the mass density at r , m_r is the total mass interior to the spherical volume of radius r , and G is the constant of gravitation. The conservation of mass requires

$$\frac{\partial m_r}{\partial r} = 4\pi r^2 \rho \quad (6.2)$$

The condition of thermal equilibrium requires that the net outward flux of energy per gram from an element of matter be equal to the rate of nuclear energy generation per gram within the element, ϵ , minus the time rate of change of internal energy per gram within the element, u , plus the work done on the element due to contraction. In terms of the luminosity at r , L_r , we have

$$\frac{\partial L_r}{\partial r} = 4\pi r^2 \rho \left(\epsilon - \frac{\partial u}{\partial t} + \frac{P}{\rho} \frac{\partial \rho}{\partial t} \right) \quad (6.3)$$

Finally we have that the temperature gradient is given by, in the case of convective transport of energy,

$$\frac{\partial T}{\partial r} = \frac{1}{V_{ad}} \frac{T}{P} \frac{\partial P}{\partial r} \quad (6.4a)$$

where ∇_{ad} is the adiabatic gradient defined as $\nabla_{\text{ad}} = (d \log P / d \log T)_{\text{ad}}$, or in the case of radiative transport

$$\frac{\partial T}{\partial r} = - \frac{3}{16\sigma} \frac{\kappa \rho}{T^3} \frac{L_r}{4\pi r^2} \quad (6.4b)$$

where κ is the opacity per gram of material and σ is the Stefan-Boltzmann constant. The condition that a region be unstable against convection is that the adiabatic gradient be less steep than the radiative gradient, both being evaluated at the same point, thus

$$\left(\frac{\partial T}{\partial r}\right)_{\text{ad}} < \left(\frac{\partial T}{\partial r}\right)_{r_{\text{ad}}} \quad (6.5)$$

These four first order non-linear differential equations together with the appropriate boundary conditions at the center and at the surface of the star determine the equilibrium structure. At the center we have $L_r \rightarrow 0$, $m_r \rightarrow 0$ as $r \rightarrow 0$; while at the surface we have $P \rightarrow 0$ as $r \rightarrow R$, the total radius. In addition we must specify the dependence of the temperature on, for example, the pressure as the surface is approached. We express this dependence through the values of the radius, temperature, and pressure at the base of the mixing length region which we provide as described in Chapter 5. Upon providing the required constitutive data, that is the values of ρ , u , ∇_{ad} , ϵ , and κ , these equations may be solved numerically to give the

run of mass, temperature, pressure, and luminosity with radius. In addition we obtain the total radius and luminosity appropriate to the equilibrium structure. By further including the dependence upon the time, we may construct a succession of equilibrium models to represent the evolutionary course of the object.

In the following two sections we describe the techniques by which we calculate the structure and evolution of stars having masses in the vicinity of $0.1 M_{\odot}$. In Section 6.1 we perform a reconnaissance of the problem by considering the simplifications resulting from the assumption that the interior structure may be represented by a polytrope of index $n = 1.5$. In Section 6.2 we construct evolutionary sequences of models for objects of $0.1 M_{\odot}$ and $0.07 M_{\odot}$ using the tables of the constitutive data computed as described in Chapter 4. In Section 6.3 we analyze the results of these model calculations and compare them with the observational data presented in Chapter 3.

6.1 Polytropic Evolutionary Models

It has been shown by Hayashi and Nakano (1963) and Ezer and Cameron (1966) that objects less massive than $0.26 M_{\odot}$ remain in convective equilibrium throughout the Hayashi phase of pre-main sequence contraction. By assuming that the thermodynamic properties of the interiors of such objects can be represented by a completely ionized,

partially degenerate ideal gas, we may, following Limber (1958b), represent the interior structure over the region of complete ionization by a polytrope of index $n = 1.5$. Under these assumptions the calculation of the evolutionary behavior, as we shall now show, assumes an especially simple form.

We assume that the thermodynamic properties within the deep interior may be adequately represented by those of a completely ionized, partially degenerate hydrogen-helium plasma. We let n_i be the number density of ions and define the parameter α such that the number densities of H^+ and He^{++} ions are given by $(1 - \alpha) n_i$ and αn_i , respectively. The free electron number density n_e is, then, $n_e = (1 + \alpha) n_i$. We let μ_i be the mean molecular weight per ion such that in terms of the mass density ρ

$$n_i = \frac{\rho}{\mu_i m_H} \quad (6.7)$$

in which case, $\mu_i = 1 + 3\alpha$. Here m_H is the mass of the hydrogen atom. In terms of the fractional abundance by mass of hydrogen, X , we have

$$\alpha = (1 - X)/(1 + 3X) \quad (6.8)$$

We write the equation of state, including the effects of electron degeneracy, in the form

$$P = \frac{k}{\mu m_H} \rho \theta \quad (6.9)$$

where μ is the mean molecular weight per particle,

$$\mu = \frac{4}{3 + 5X} \quad (6.10)$$

P is the pressure, k is Boltzmann's constant, and θ is defined in terms of the temperature T as $\theta = \Lambda T$. The parameter Λ is introduced to account for degeneracy and is given by

$$\Lambda = \frac{n_i + n_e D}{n_i + n_e} = \frac{1 + (1 + \alpha) D}{2 + \alpha} \quad (6.11)$$

where $D = 2/3 F_{3/2}/F_{1/2}$ and the F 's are defined by equation (4.27). We note that Λ is a constant with respect to the radius r (cf. Limber 1958b).

Assuming the interior structure to be represented by an $n = 1.5$ polytrope, we obtain (Chandrasekhar 1939, pp. 95-100) the following expressions relating the total radius, R , the central pressure, P_C , and the central density, ρ_C , to the mass of the object, M , and the value of θ at the center, $\theta_C = \Lambda T_C$:

$$R = K_1 \frac{M}{\theta_C} \quad (6.12)$$

$$P_C = K_2 \frac{\theta_C^4}{M^2} \quad (6.13)$$

and

$$\rho_C = K_3 \frac{\theta_C^3}{M^2} \quad (6.14)$$

The constants K_1 , K_2 , and K_3 are given by

$$K_1 = (4\pi\mu_{\text{m}_H}GW_n)/(3ka),$$

$$K_2 = GW_n/K_1^4$$

and

$$K_3 = 3a/(4\pi K_1^3)$$

where we have from Chandrasekhar (1939, p. 96) that

$$W_n = 0.77014 \text{ and } a = \rho_C/\bar{\rho} = 5.99071.$$

Since from these results it is apparent that the interior structure for an object of given mass and chemical composition is determined upon specification of θ_C , it follows that the evolutionary behavior is obtainable from a determination of the time dependence of θ_C . Using equation (6.2), we may rewrite equation (6.3) in the following form:

$$\frac{\partial u}{\partial t} = \frac{P}{\rho^2} \frac{\partial \rho}{\partial t} - \frac{\partial L_r}{\partial m} + \epsilon \quad (6.15)$$

The internal energy per gram at any point is

$$u = \frac{3}{2} \frac{P}{\rho} = \frac{3}{2} \frac{k}{\mu_{\text{m}_H}} \sigma \theta_C$$

where we have employed equation (6.9) and defined the time independent quantity $\sigma = \theta/\theta_C$. Whereas $\theta = \theta(r, t)$, we have that $\theta_C = \theta_C(t)$ only, where t denotes the time. The quantity $\sigma = \sigma(r)$ is obtainable directly from the polytrope solution. For the nuclear energy generation rate we

employ the interpolation formula of Hayashi and Nakano (1963), which is based on the energy release for the He^3 terminated proton-proton chain,

$$\epsilon = \epsilon_o \rho T^\nu \quad (6.16)$$

where $\epsilon_o = (2.5515 \times 10^{-8}) X^2$ and $\nu = 6.6$. We may now write equation (6.15) as

$$\frac{3}{2} \frac{k}{\mu m_H} \sigma \dot{\theta}_C = \frac{\partial L_r}{\partial m} + \frac{\epsilon_o K_3}{M^2} T_C^\nu \sigma^\nu + 3/2$$

where we have used equation (6.14) for ρ_C and to find

$\dot{\rho}_C / \rho_C = 3 \dot{\theta}_C / \theta_C$. Here we simplify our notation by using dots to denote differentiation with respect to the time. We integrate this result over the total mass of the star to obtain

$$\dot{\theta}_C = C_1(M)L - C_2(M)T_C^\nu \theta_C^3 \quad (6.17)$$

where L is the total luminosity and

$$C_1(M) = \frac{2}{3} \frac{1}{M k_1}$$

and

$$C_2(M) = \frac{2}{3} \frac{\epsilon_o K_3}{M^2} \frac{k_2}{k_1}$$

Here the constant k_1 is obtained from the relation

$$\frac{k\theta_C}{\mu m_H} \int_0^M \sigma dm = -\frac{1}{3} \Omega = \frac{2}{7} \frac{GM^2}{R},$$

where Ω is the total gravitational potential energy (cf. Chandrasekhar 1939, p. 100). Using equation (6.12) we obtain $k_1 = 2/7 G/K_1$. We define the constant k_2 to be

$$k_2 = \int_0^M \sigma^{\nu + 3/2} dm$$

which, with $\nu = 6.6$, has been evaluated using Simpson's rule and tables of the $n = 1.5$ polytrope solution to give $k_2 = 0.58927$.

We may solve equation (6.17) numerically for a specified mass and chemical composition provided that we can determine T_C and L for given θ_C . Using equation (4.31), noting that $n_e = 1/2(1 + X) \rho_C/m_H$ and using equation (6.14), we obtain the relation

$$F_{1/2} - K \theta_C^{3/2} = 0, \quad (6.18)$$

where the constant K is

$$K = (9.1752 \times 10^{-15}) \frac{(1 + X)K_3}{m_H M^2}.$$

For a given value of θ_C , we regard equation (6.18) as a transcendental equation in $F_{1/2}$ which we solve by means of a Newton-Raphson iterative technique using the tables of

$F_{1/2}$ and $2/3 F_{3/2}$ compiled by McDougall and Stoner (1938) together with the definition of the parameter D and equation (6.11) for Λ . Obtaining the value of Λ corresponding to a given value of θ_C , we calculate T_C from the defining relation for θ_C that is, $T_C = \theta_C / \Lambda$.

We obtain the total luminosity L corresponding to given θ_C from the atmospheric data of Chapter 5. From the assumption that the interior be in complete convective equilibrium, and, hence, adiabatic, it follows that the entropy per gram of material must be constant with radius out to the base of the mixing length region. We regard the atmospheric solution appropriate to a model of given mass and θ_C to be that for which the entropy per gram computed at the base of the mixing length region be equal to the entropy per gram computed at the center of the object. Employing the notation and results of Section 4.1, the dimensionless entropy per gram, Σ , for an ideal gas mixture of hydrogen and helium nuclei, regarded as Boltzmann particles, and partially degenerate electrons at a pressure, P , and temperature, T , is (cf. equation 4.65c)

$$\begin{aligned} \mu_i \Sigma = & \frac{5}{2} \ln T - \ln P + (1+\alpha) \left(\frac{5}{2} D - \eta \right) \\ & + \ln \left[1 + (1+\alpha) D \right] + C \end{aligned} \quad (6.19)$$

where μ_i is as defined in equation (6.7), the degeneracy parameters D and η are computed using the free electron

density corresponding to the given P and T and the constant C is

$$C = \frac{5}{2} + (1-\alpha)C_H + \alpha C_{He} - (1-\alpha)\ln(1-\alpha) - \alpha\ln\alpha \quad (6.20)$$

where C_H and C_{He} are computed from

$$C_j = \ln \left[\frac{(2\pi m_j)^{3/2} k^{5/2}}{h^3} \right] + \ln Q_j$$

where m_j and Q_j are the respective masses and partition functions. For the assumed polytrope configuration, we may utilize the adiabatic relation between the pressure and the parameter θ , that is, $P = K_{int} \theta^{5/2}$ (with $K_{int} = \text{constant}$), and equation (6.13) to give at the center of an object

$$P_C = K_{int} \theta_C^{5/2} \quad (6.21)$$

with

$$K_{int} = \frac{K_2 \theta_C^{3/2}}{M^2} \quad (6.22)$$

Substituting for P_C in equation (6.19) and using equation (6.11), we obtain for Σ_C , at the center of the object,

$$\begin{aligned} \Sigma_C = \frac{1}{\mu_i} \left\{ \Sigma_o - \ln K_{int} - \frac{3}{2} \ln [1 + (1+\alpha)D] \right. \\ \left. + (1+\alpha) \left(\frac{5}{2} D - \eta \right) \right\} \end{aligned} \quad (6.23)$$

where $\Sigma_o = \frac{5}{2} \ln(2+\alpha) + C$.

The prescription which we now employ to obtain L for a given M , θ_C combination is as follows: We calculate K_{int} from equation (6.22) and, using the values of Λ and D obtained from the auxiliary solution for T_C from equation (6.18), we compute Σ_C . From equation (6.12) we calculate the polytrope radius R and, hence, the surface gravity $g_{\text{srf}} = GM/R^2$. By requiring that $\Sigma_C = \Sigma_{\text{mxl}}$, the entropy at the base of the mixing length region, we interpolate within the table of effective temperature versus $\log g_{\text{srf}}$ and Σ_{mxl} (constructed as described in Section 5.4) to obtain the effective temperature corresponding to the calculated Σ_C and g_{srf} . We then compute L from the relation $L = 4\pi\sigma R^2 T_e^4$, where here, of course, σ denotes the Stefan-Boltzmann constant. In this procedure, we should note, we have neglected the thickness of the relatively shallow zone near the surface within which hydrogen and helium are incompletely ionized.

Using the Runge-Kutta technique, we have integrated equation (6.17) numerically to obtain the evolutionary behavior during the Hayashi contraction phase for a number of masses. We present the results for objects of 0.1, 0.08, 0.06, 0.04, and 0.02 M_\odot in Figure 12 in which we show the resulting tracks in the H-R diagram. In performing these calculations we have chosen, quite arbitrarily, the starting time to be 10^4 years and, for each mass, picked a sufficiently low value for the initial value of the central

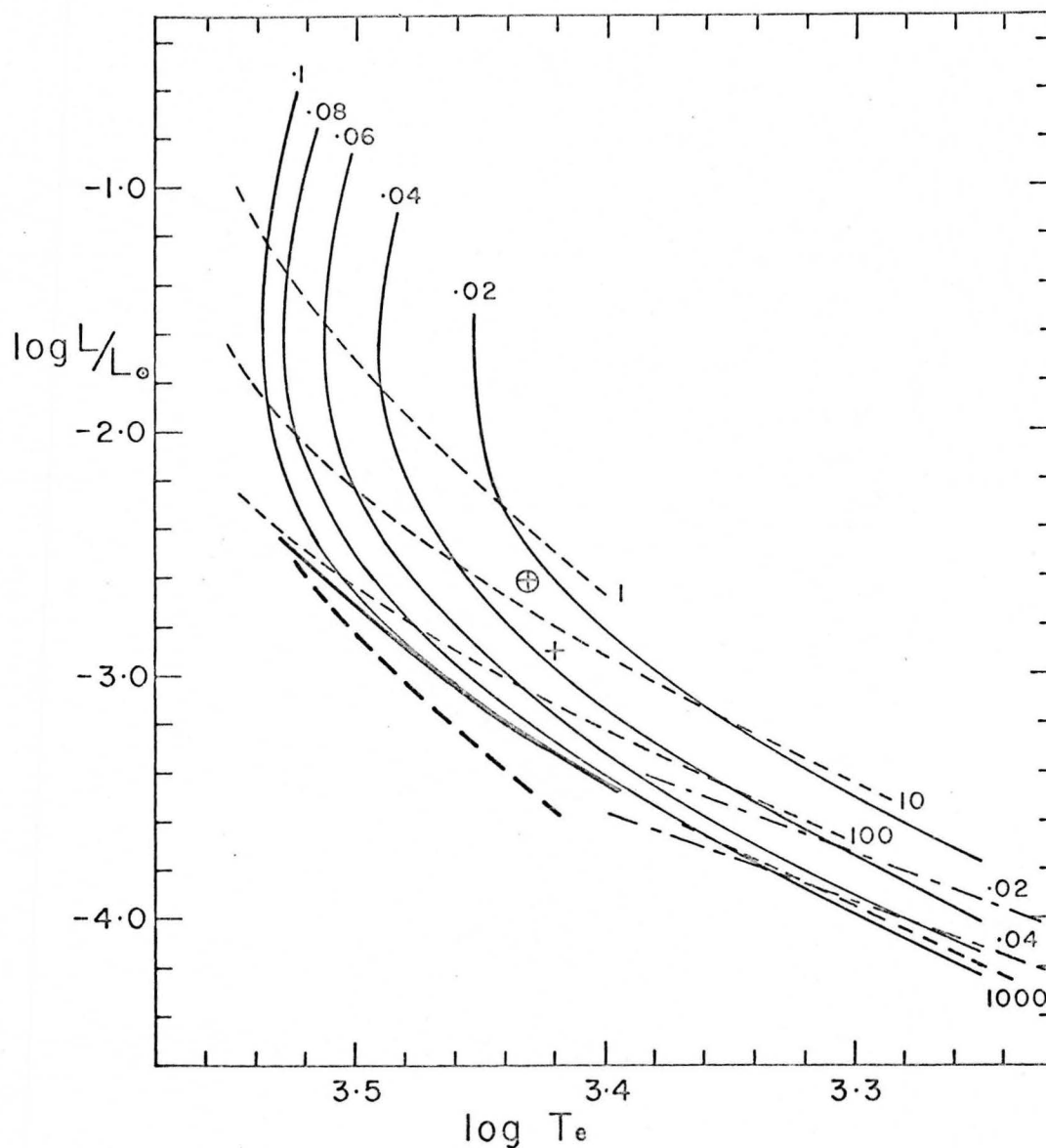


Fig. 12. Polytropic evolution in the H-R diagram.

Evolutionary tracks labeled by mass in M_{\odot} (solid line), main sequence locus (heavy solid line), main sequence locus of Hayashi and Nakano (1963) (heavy dashed line), lines of constant time (light dashed lines labeled by time in millions of years), loci of completely degenerate configurations of .02 and .04 M_{\odot} (dot-dash lines labeled by mass), and observed positions of Ross 614B (cross) and UV Ceti (circled cross).

temperature such that we can be sure that the object is initially well up on the Hayashi track. We observe that of the masses considered only the $0.1 M_{\odot}$ object stabilizes on the main sequence, while the less massive objects remain in a state of continued slow contraction toward completely degenerate configurations. In Figure 12 we show by the straight lines labeled $.04 M_{\odot}$ and $.02 M_{\odot}$, respectively, the lines of constant radius which correspond to the limiting radii appropriate to completely degenerate configurations of 0.04 and $0.02 M_{\odot}$. We also show the lines of constant time in Figure 12 corresponding to the evolutionary ages of 10^6 , 10^7 , 10^8 , and 10^9 years. Because of the arbitrary specification of the initial time at which the integration of equation (6.17) is begun, the absolute values of the time indicated in Figure 12 are not physically meaningful. However we can attach meaning to the time differences between different points in the evolutionary track at a specific mass.

Upon setting $\dot{\theta}_C = 0$ in equation (6.17) we may solve the resulting transcendental equation for θ_C , given the mass, and obtain thereby the corresponding main sequence configurations as a function of stellar mass. In Table 4 we present the resulting main sequence configurations for objects having masses in the range 0.14 to $0.085 M_{\odot}$. In Figure 12 we show by the heavy solid line the resulting main sequence line in the H-R diagram. The filled circles

Table 4. Theoretical Main Sequence Properties of
the Polytropic Models

M/M_{\odot}	$\text{Log } T_c$	$\text{Log } P_c$	$\text{Log } \rho_c$	$F_{1/2}$	$\text{Log } R/R_{\odot}$	$\text{Log } L/L_{\odot}$	$\text{Log } T_e$	M_{bol}
0.085	6.482	17.777	2.841	12.502	-0.995	-3.431	3.403	13.42
0.09	6.547	17.584	2.684	6.966	-0.934	-3.138	3.446	12.68
0.10	6.598	17.441	2.554	4.325	-0.876	-2.883	3.480	12.04
0.11	6.630	17.356	2.469	3.184	-0.834	-2.714	3.502	11.62
0.12	6.654	17.291	2.402	2.509	-0.799	-2.585	3.516	11.30
0.13	6.674	17.238	2.345	2.059	-0.768	-2.479	3.528	11.04
0.14	6.690	17.193	2.295	1.736	-0.741	-2.390	3.536	10.81

along this line indicate, from left to right, the main sequence positions of objects having masses of 0.14, 0.12, 0.10, 0.09, and $0.085 M_{\odot}$, respectively. For masses below $0.085 M_{\odot}$ we find that equation (6.17) (with $\dot{\theta}_C = 0$) has no solution and we conclude that, to the extent that these essentially polytropic models represent real stars, $0.085 M_{\odot}$ is the lower limiting mass for main sequence objects of solar composition.

In Figure 13 we plot $\log T_C$ versus $\log \rho_C$ for these objects. In this diagram we see that the central temperature does in fact pass through a maximum value and begin to decrease for those objects insufficiently massive to reach the main sequence. This turn-over in the central temperature will actually occur for a contracting object of any mass once the interior density, and hence the degree of electron degeneracy, becomes sufficiently high. For objects more massive than the limiting mass, however, a combination of T_C and ρ_C will be encountered on the rising limb of the $\log T_C - \log \rho_C$ curve such that the nuclear energy generation rate will be sufficiently high to halt the contraction and, thus, stabilize the object on the main sequence. For these objects, however, we hypothesize that there exists two combinations of T_C and ρ_C , one on the rising side and one which would occur on the falling side of the $\log T_C - \log \rho_C$ curve, for which we may achieve stable configurations. Only the first will actually be

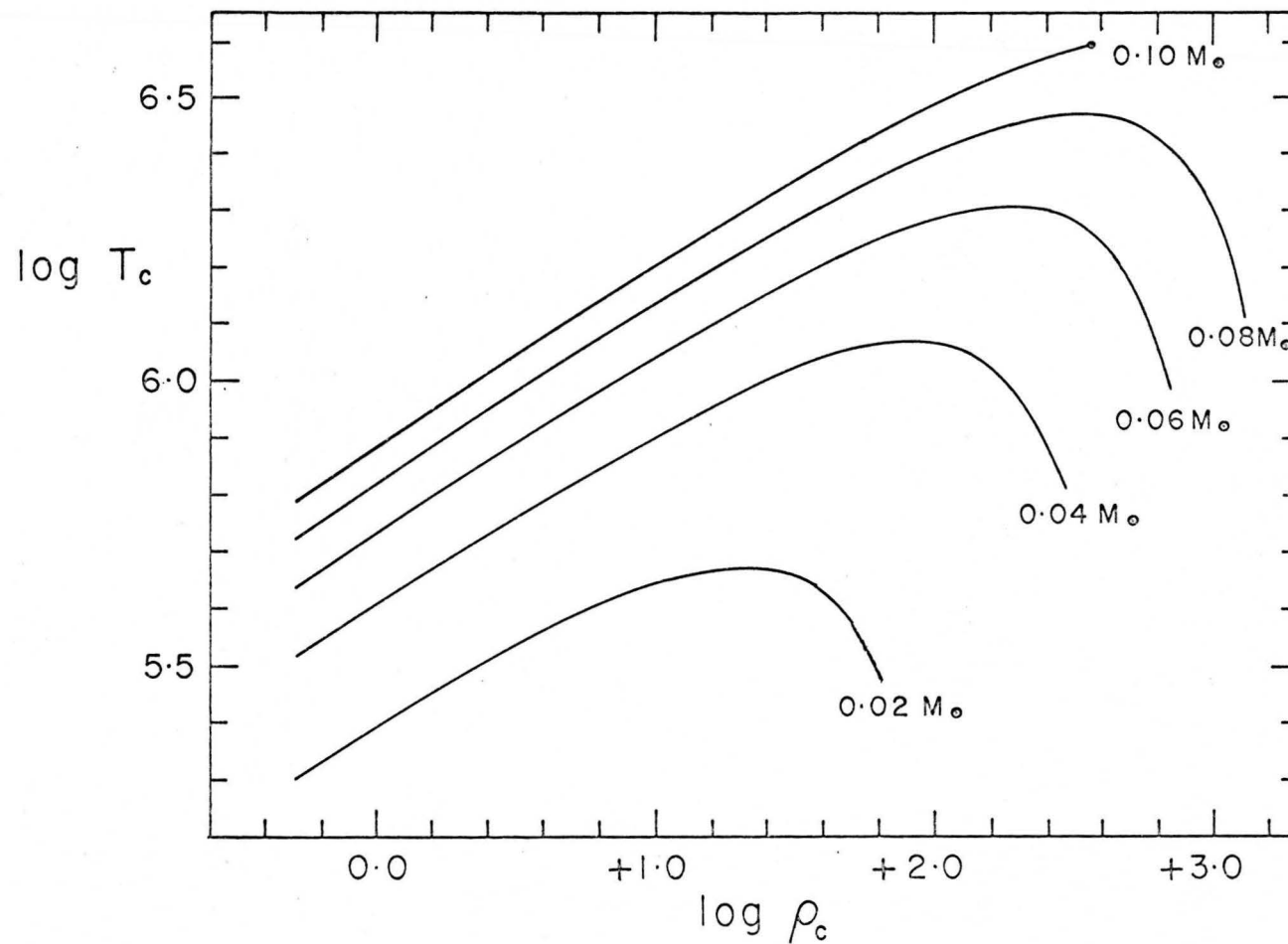


Fig. 13. Behavior of central values of the temperature and the density for the polytropic evolutionary models.

encountered in nature but such a result implies, at least theoretically, the existence of two main sequence solutions at any mass above the limiting mass. Presumably, the locus of the second set of solutions in the H-R diagram will fall below the usual zero-age main sequence with the two solutions becoming coincident at the limiting mass. Of course, the second set of main sequence solutions is only of academic interest but its existence does pose an interesting counter example to the uniqueness of the solution of the stellar structure problem implied by the Russell-Vogt theorem. We have made no attempt to obtain these solutions explicitly, however.

In addition to the present results we also show in Figure 12 by a dashed line the theoretical main sequence solution obtained by Hayashi and Nakano (1963). The filled circles along this line, again from left to right, indicate the main sequence positions Hayashi and Nakano determine for objects of 0.14 , 0.12 , 0.10 , 0.09 , and $0.08 M_{\odot}$, respectively (they find the main sequence limiting mass to be at $0.08 M_{\odot}$). We observe that their results are in quite reasonably good agreement with those we have obtained. The small discrepancy is readily explained in terms of the different composition used by Hayashi and Nakano (they take $X = 0.61$, $Y = 0.37$) and, more significantly, the difference by which the outer atmospheric boundary condition was obtained. Hayashi and Nakano approximate the atmosphere as

an isothermal region extending above the photosphere which was defined to lie at an optical depth of $2/3$. We, on the other hand, have utilized complete, albeit crude, atmospheric models which include an explicit treatment of the convective transition region. Since we have assumed in these models that the interior structure may be represented by a polytrope with $n = 1.5$, as did Hayashi and Nakano, our treatment of the atmospheric regions is the major improvement over their work as well as that of Kumar (1963) whose original investigation of the limiting mass problem included no treatment of the atmospheric boundary condition whatsoever.

In an attempt to further improve the theory we now consider the problem of constructing detailed evolutionary models at 0.10 and $0.07 M_{\odot}$ utilizing the computations of the thermodynamic data described in Chapter 4 as well as including the effect of the hydrogen-helium ionization zone on the structure.

6.2 Calculation of the Detailed Evolutionary Models

In order to construct the detailed stellar models for low mass stars, that is models utilizing the constitutive data computations of Chapter 4 and constructed without benefit of the simplifications introduced in the preceding section, we employ the so-called "fitting method" of model construction as described by Schwarzschild (1958),

Haselgrove and Hoyle (1956), and Sears and Brownlee (1965). In this procedure we separate the evolutionary calculation into a "space part" and a "time part." In the space part of the problem we are concerned with the explicit solution of the equations of stellar structure to obtain a single stellar model at a specific point in time. The time part considers the evolutionary time change resulting from, for example, the work done through gravitational contraction and provides the input data by which a new (static) stellar model is computed at some forward step in time. By proceeding in this way we treat the time dependence implicitly in order to construct a time ordered sequence of static, equilibrium stellar models. The use of this "fitting method," rather than the implicit difference method developed by Henyey and his co-workers (cf. Henyey, Forbes, and Gould 1964) for stellar evolution problems, was necessitated by the severe storage limitations of the IBM 7072 computer used in the initial stages of this work. The final calculations were performed on a CDC 6400 computer, however.

Regarding m , which we now designate to be the mass interior to r , as the independent variable, we rewrite the equations of structure, equations (6.1) through (6.4), as follows:

$$\frac{\partial P}{\partial m} = - \frac{G}{4\pi} \frac{m}{r^4} \quad (6.24)$$

$$\frac{\partial r}{\partial m} = \frac{1}{4\pi} \frac{1}{r^2 \rho} \quad (6.25)$$

$$\frac{\partial T}{\partial m} = \frac{1}{V_{ad}} \frac{T}{P} \frac{\partial P}{\partial m} \quad (\text{convective}) \quad (6.26a)$$

or

$$\frac{\partial T}{\partial m} = - \frac{3}{256\pi^2 \sigma} \frac{L_r \kappa}{T^3 r^4} \quad (\text{radiative}) \quad (6.26b)$$

and

$$\frac{\partial L_r}{\partial m} = \epsilon - \frac{\partial u}{\partial t} - P \frac{\partial}{\partial t} \left(\frac{1}{\rho} \right) \quad (6.27)$$

In the actual numerical calculations we replace the time derivatives in equation (6.27) by the difference relation

$$- \frac{1}{\Delta t} \left[(u_2 - u_1) + P_2 \left(\frac{1}{\rho_2} - \frac{1}{\rho_1} \right) \right]$$

where the subscripts 2 and 1 designate those quantities appropriate to the present and previous models, respectively, and Δt is the time step separating these two models. At any point within a model we choose between equations (6.26a) and (6.26b) by means of the criterion expressed through equation (6.6). It is the solution of these equations which constitutes the space part of the problem.

Because of the presence of singularities at the center and surface, we cannot solve these equations directly from either the center to the surface or from the

surface to the center. We choose therefore a convenient point within the star, which we designate the fitting point, and develop solutions outward from the center and inward from the surface. For an object of total mass M , we regard the outward solution to be a function of the central temperature, T_C , and the central pressure, P_C , and the inward solution to be a function of the total radius, R , and the luminosity, L . The equilibrium structure of a specific model, as well as the corresponding values of T_C , P_C , R , and L , are determined by that pair of solutions which join smoothly at the fitting point with all of the physical variables, r , T , P , and L being continuous across the fitting point boundary. In the present application we have chosen the fitting point to be at that mass, m_f , for which $m_f/M = 0.6$.

Because of the complicating effects arising from the release of gravitational and internal thermal energy, we must modify, to some extent, the usual numerical methods by which this problem is treated (a review of the usual methods is given by Sears and Brownlee 1965). As input data to begin the construction of a specific model we require initial trial values for T_C , P_C , R , and L . These may be obtained, for example, by extrapolation from preceding models in the evolutionary sequence or, in the case of the first model, from the properties of the corresponding polytrope solution. Holding the trial value

of T_C fixed, we first determine through variation of the parameters P_C , R , and L that configuration for which r , P , and T are continuous across the fitting point. We accomplish this iteratively through the usual Newton-Raphson technique (cf. Sears and Brownlee 1965). We then employ an auxiliary iterative procedure, again based on the Newton-Raphson technique, in order to determine that value of T_C for which the luminosity, L_r , as well as the other physical variables, are continuous across the fitting point. For each iteration on T_C we must perform the subsidiary iteration on the parameters P_C , R , and L to determine that structure for which r , P , and T are continuous across the fitting point.

Upon specification of M , L , and R the starting values of r , T , and P for the inward solution were obtained by direct interpolation within the atmosphere data table constructed as described in Chapter 5. The starting values for the outward integration were obtained from the simple expansions given by Schwarzschild (1958, p. 114). The constitutive data, ρ , u , ∇_{ad} , ϵ , and κ , for each value of T and P encountered in the numerical solutions were obtained from a four-point Lagrangian interpolation scheme within the constitutive data table. Both the atmospheric and the constitutive data tables were stored on magnetic tape and read into the computer prior to execution of the evolutionary program. Because of its size, the

constitutive data table was divided into two equal parts, only one of which was stored in the computer's central memory at a time. The numerical integrations of equations (6.24) through (6.27) were performed using the Heun method of numerical integration.

In Tables 5 and 6 we present the results of the detailed evolutionary calculations for objects of 0.1 and $0.07 M_{\odot}$, respectively. In Figure 14 we show the corresponding tracks in the H-R diagram along with those computed according to the simple scheme of Section 6.1. As was found for the simple polytrope models, the $0.1 M_{\odot}$ object stabilizes on the main sequence while the $0.07 M_{\odot}$ object does not. A more significant conclusion to be drawn from Figure 14, however, is that the complications introduced into the computation of the interior thermodynamic properties for the detailed models appear to have little effect on the evolutionary behavior in the H-R diagram. Quantitatively, however, we find that the main sequence values of the radius, luminosity, central temperature, and central density of the detailed model differ by -9% , -27% , $+11\%$, and $+6.5\%$, respectively, over the corresponding values for the polytropic model. The physical differences between the models include the corrections for non-ideal gas effects, a revised form of the energy generation law, and the inclusion of the hydrogen-helium ionization zone. To the extent that the non-ideal gas

Table 5. Detailed Evolution at $0.1 M_{\odot}$

Log t (yrs)	Log T_C	Log P_C	Log ρ_C	Log R/R_{\odot}	Log L/L_{\odot}	Log T_e
4.324	5.958	14.258	0.164	-0.091	-1.102	3.533
5.344	5.985	14.372	0.249	-0.119	-1.154	3.534
5.624	6.009	14.470	0.324	-0.144	-1.200	3.535
5.793	6.029	14.558	0.389	-0.166	-1.241	3.536
5.898	6.046	14.626	0.441	-0.183	-1.272	3.537
5.994	6.062	14.697	0.494	-0.200	-1.316	3.537
6.173	6.093	14.827	0.592	-0.233	-1.367	3.538
6.496	6.150	15.065	0.771	-0.291	-1.482	3.539
6.607	6.181	15.200	0.872	-0.325	-1.548	3.539
6.903	6.196	15.263	0.919	-0.340	-1.580	3.538
7.153	6.309	15.757	1.290	-0.463	-1.841	3.535
7.403	6.368	16.027	1.495	-0.531	-1.994	3.530
7.653	6.428	16.310	1.705	-0.601	-2.143	3.528
7.903	6.486	16.599	1.922	-0.673	-2.306	3.523
8.153	6.539	16.887	2.138	-0.745	-2.482	3.515
8.403	6.582	17.163	2.345	-0.812	-2.663	3.504
8.778	6.621	17.520	2.612	-0.903	-2.924	3.484
8.828	6.624	17.565	2.646	-0.914	-2.961	3.480
8.878	6.625	17.599	2.671	-0.923	-2.988	3.478

Table 6. Detailed Evolution at $0.07 M_{\odot}$

Log t (yrs)	Log T_c	Log P_c	Log ρ_c	Log R/R_{\odot}	Log L/L_{\odot}	Log T_e
4.206	5.849	14.130	0.145	-0.141	-1.258	3.519
5.335	5.881	15.265	0.246	-0.174	-1.319	3.520
5.619	5.908	14.380	0.333	-0.202	-1.372	3.521
5.790	5.931	14.480	0.409	-0.227	-1.430	3.522
5.895	5.950	14.558	0.467	-0.246	-1.457	3.522
5.998	5.969	14.641	0.529	-0.267	-1.496	3.522
6.248	6.012	14.827	0.669	-0.312	-1.589	3.522
6.498	6.062	15.042	0.830	-0.366	-1.701	3.521
6.748	6.115	15.280	1.009	-0.425	-1.830	3.518
6.998	6.171	15.534	1.200	-0.488	-1.975	3.514
7.248	6.229	15.807	1.404	-0.556	-2.116	3.512
7.498	6.285	16.088	1.616	-0.625	-2.275	3.508
7.748	6.337	16.373	1.829	-0.697	-2.448	3.500
7.998	6.382	16.655	2.040	-0.767	-2.633	3.488
8.248	6.414	16.928	2.245	-0.836	-2.829	3.474
8.253	6.418	16.994	2.295	-0.861	-2.874	3.475
8.268	6.422	17.119	2.388	-0.914	-2.992	3.472
8.342	6.417	17.284	2.512	-0.973	-3.153	3.462
8.394	6.412	17.345	2.558	-0.991	-3.221	3.454

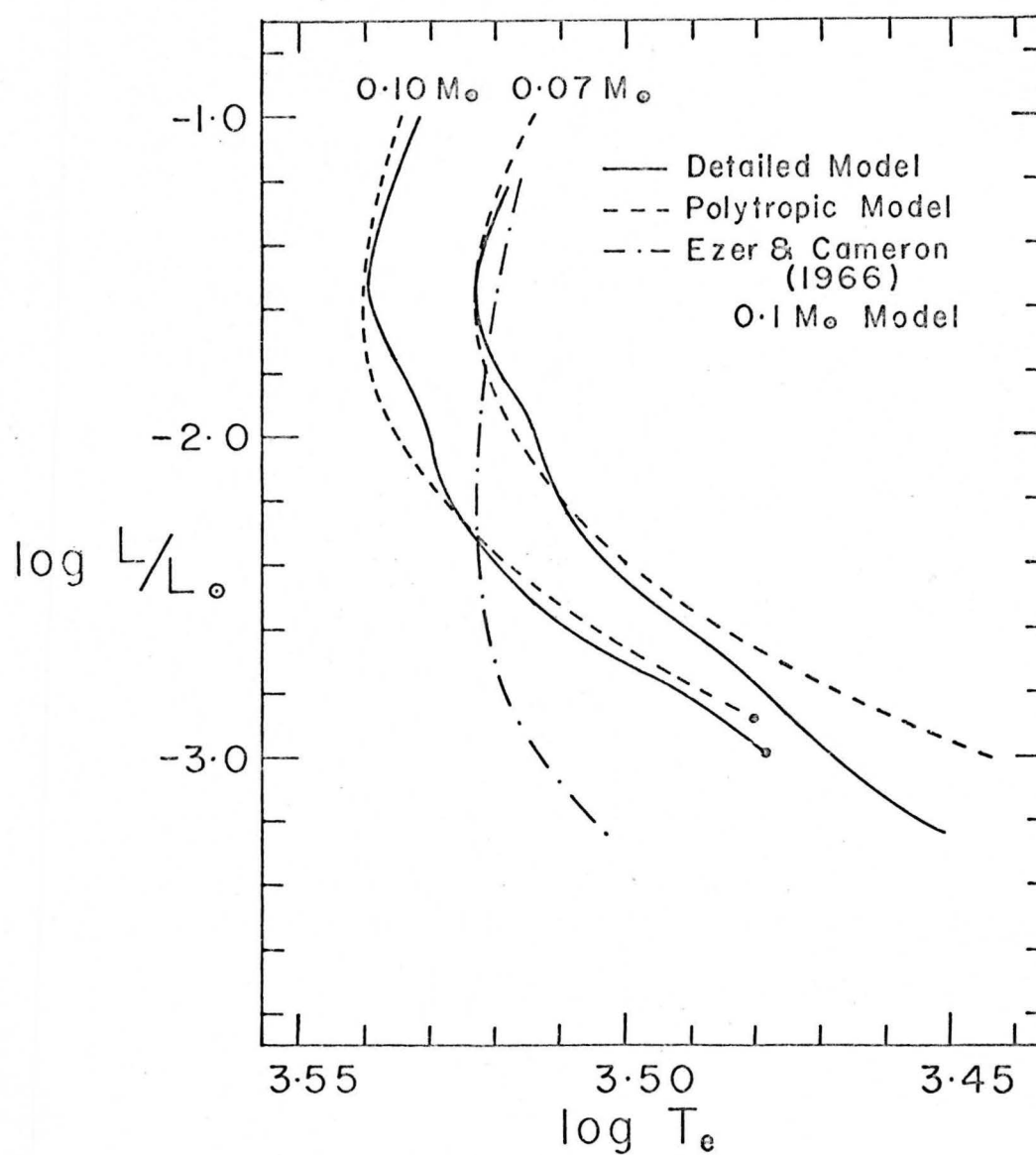


Fig. 14. Evolution of the detailed 0.1 and $0.07 M_{\odot}$ models in the H-R diagram.

Filled circles indicate main sequence termination points.

behavior of the interior is represented by the developments of Chapter 4, we conclude that we may feel relatively secure in neglecting these effects in considering the structure of main sequence objects.

For the $0.07 M_{\odot}$ object we find that the departure of the detailed track in Figure 14 from that corresponding to the polytrope models increases as evolution proceeds. This is to be expected inasmuch as the non-ideal gas effects will become more important once the central temperature passes through its maximum value and the interior begins to cool. At the point where the central temperature reaches its maximum value the differences between the central temperature, radius, luminosity, and central density of the detailed model over the polytrope model amount to +4%, -6%, +18%, and -10%.

In Figure 14 we also show the evolutionary track computed for a $0.1 M_{\odot}$ star by Ezer and Cameron (1966). Using the same composition as that employed in the present work, they find that this object fails to produce enough nuclear burning to stabilize on the main sequence. In Figure 15 we compare our results (shown by a solid line) for the radius, luminosity, and central density regarded as functions of the central temperature with theirs (shown by dashed lines). The turn-overs in Ezer and Cameron's results occur because of the passage of their central temperature through a maximum. That our results, other

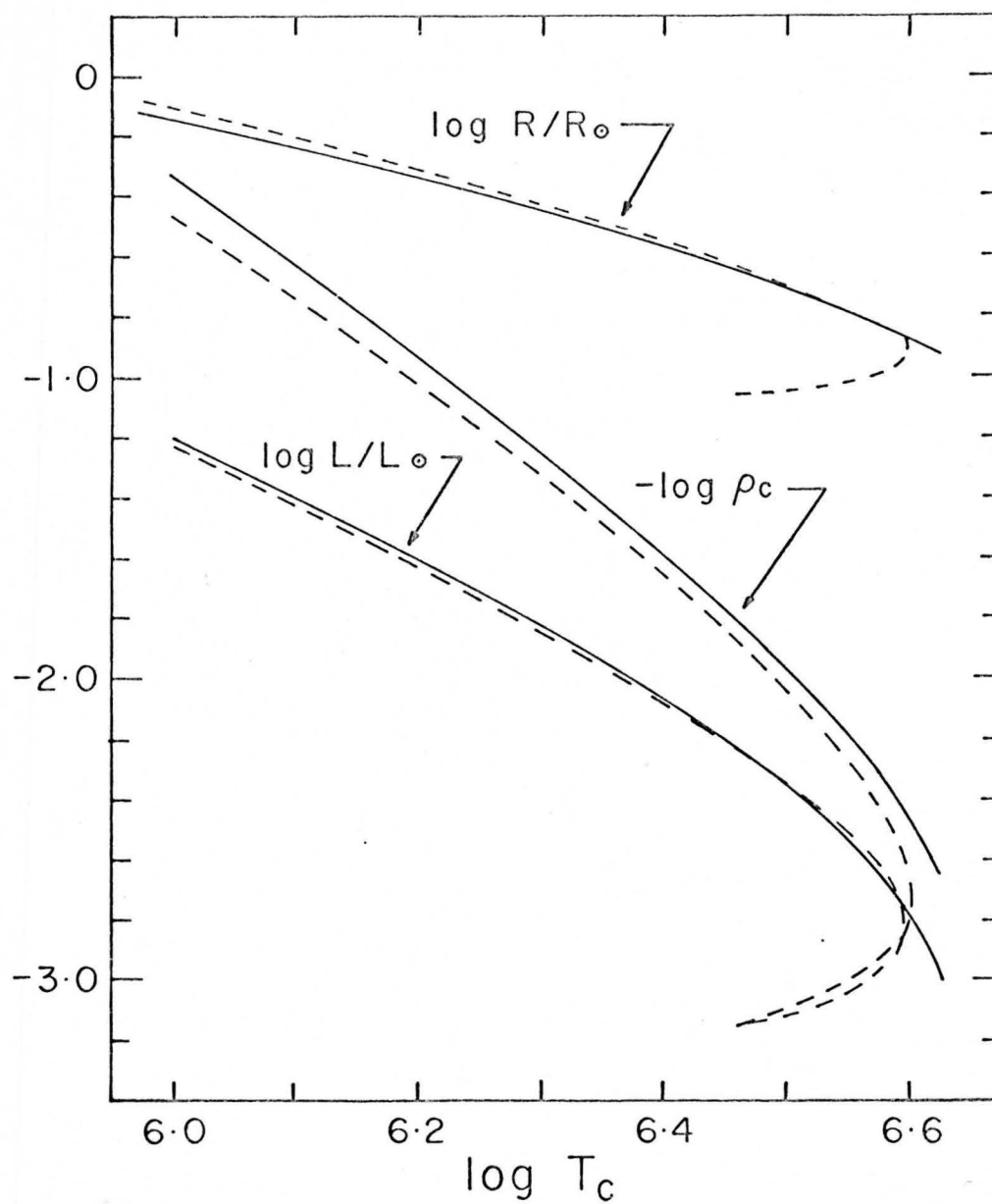


Fig. 15. Comparison of the evolutionary behavior of detailed $0.1 M_\odot$ model with that calculated by Ezer and Cameron (1966).

than for the behavior of the central temperature, agree so well with theirs suggests that the basic difference lies in the calculated energy generation rate. Apparently they find that the He^3 terminated proton-proton chain produces less energy than do we. The only apparent difference between the two formulations of the energy generation rate lies in the use of different methods of treating the screening function. For these stars we deal with a situation lying between Salpeter's (1954) cases of weak and strong screening. We have used a mean screening function taken between these two extremes while Ezer and Cameron have employed whichever approximation, weak or strong, gives the larger value. The principal source for the difference between the tracks in the H-R diagram can readily be explained by the difference in the way which the outer atmospheric boundary condition has been treated. Our boundary condition is based on model atmosphere integrations; while they employ a somewhat more approximate procedure (Ezer and Cameron 1963). The difference between our results for the central density regarded as a function of the central temperature and those of Ezer and Cameron is an indication of the magnitude of the effects of including particle interactions in the equation of state.

6.3 Comparison and Discussion of the Theoretical and Empirical Main Sequence Properties

In Figures 16 through 18 we summarize graphically the theoretical results obtained in the preceding sections for main sequence objects and compare them with the adopted mean empirical data for the main sequence given in Table 2. In Figures 16 and 17 we compare the theoretical and empirical mass-luminosity and mass-radius relations, respectively. In these diagrams we show by solid lines labeled MS and ZAMS, respectively, the polytropic main sequence from Table 4 and the empirical relations from Table 2. For comparison we show the theoretical results of Hayashi and Nakano (1963) and Ezer and Cameron (1966) by dashed lines labeled HN and EC, respectively. In addition we show the main sequence position of the detailed $0.1 M_{\odot}$ object from Table 5 by a circled cross, the position of YY Gem by a cross and that of the sun by the symbol \odot .

Examination of these figures reveals that while the theoretical and empirical mass-luminosity relations appear to be in quite reasonable agreement, there is an appreciable lack of agreement between the theoretical and empirical mass-radius relations. This discrepancy between theory and observation is also apparent in the H-R diagram as may be seen in Figure 18. Here, using the same notation as in Figures 16 and 17, we plot the main sequence loci in the H-R diagram, that is, the plot of M_{bol} versus the effective

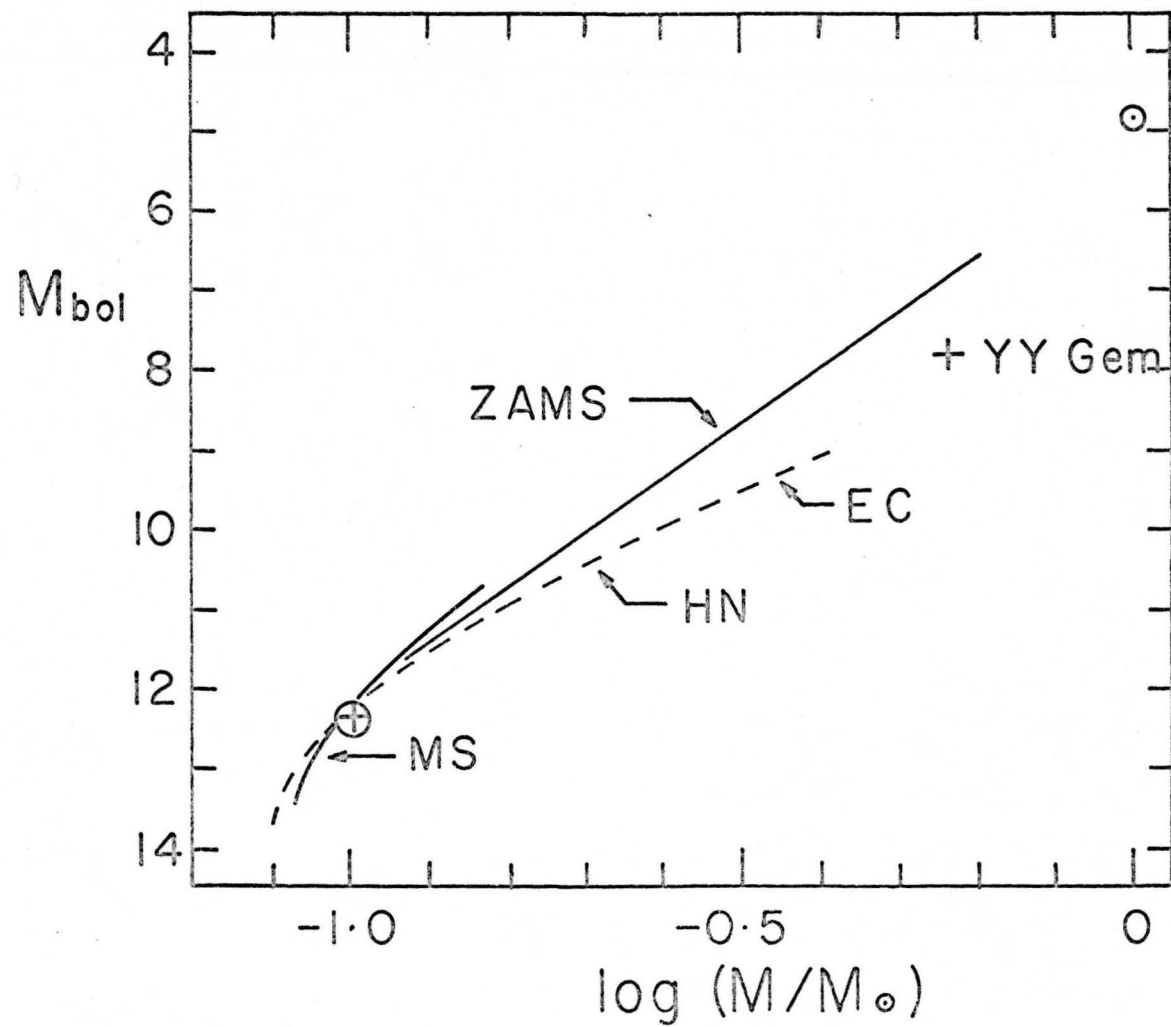


Fig. 16. Comparison of theoretical and empirical mass-luminosity relations.

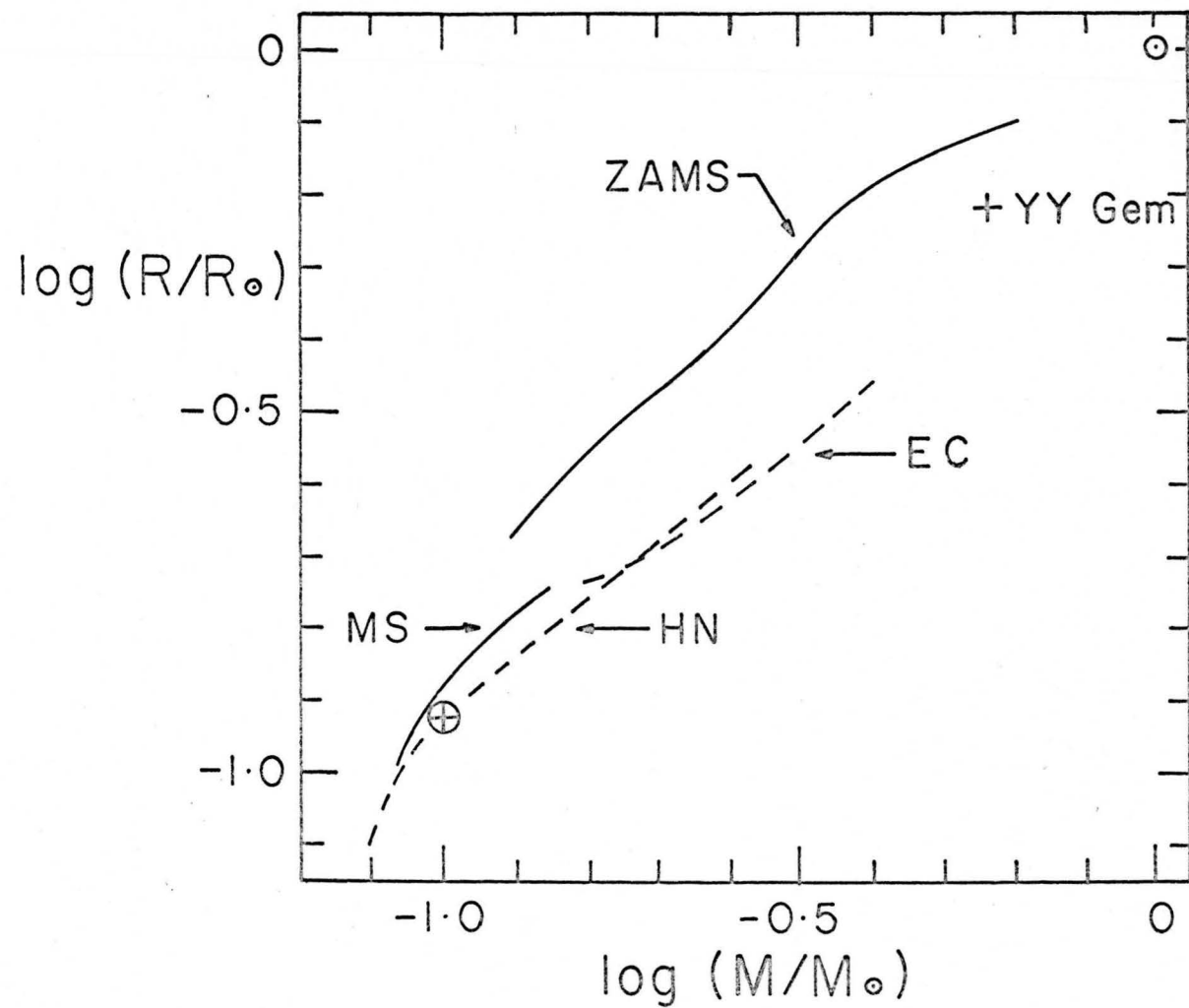


Fig. 17. Comparison of theoretical and empirical mass-radius relations.

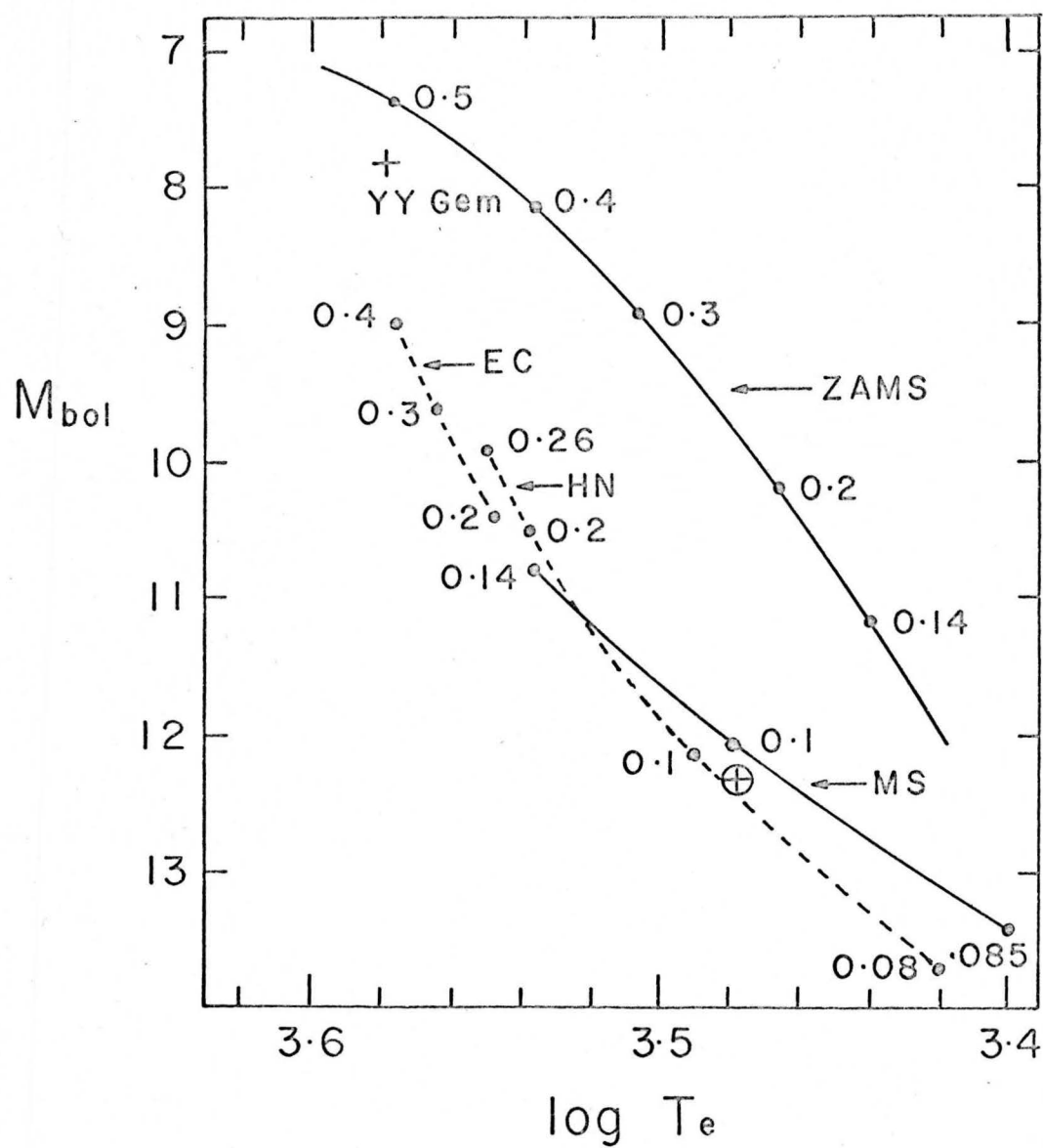


Fig. 18. Comparison of the theoretical and empirical main sequence loci in the H-R diagram.

temperature. Along each of these loci we show the positions of objects of various masses by filled circles which we label by the corresponding value of the mass in M_{\odot} . We see that not only are the theoretical and empirical main sequences displaced by as much as 700° in effective temperature but they also exhibit quite different slopes as well.

The difficulties presented by Figures 17 and 18, that is, the lack of agreement between the main sequence mass-radius relations and the loci in the H-R diagram, are significant and oblige us to re-examine the adequacy of the theoretical models as well as the adopted mean empirical relations. Although we must acknowledge the possibility that the apparent good agreement between the theoretical and empirical mass-luminosity relations indicated in Figure 16 may be fortuitous, we assume for the moment that our theoretical models do in fact provide a satisfactory representation of the low mass, main sequence mass-luminosity relation for stars of solar composition. It is within the context of this assumption that we now undertake a reassessment of the assumptions and approximations entering into the model calculations and the derivation of the mean empirical relations.

6.3.1 Theoretical Models

In deriving the theoretical main sequence properties for the very low mass objects listed in Table 4, we have assumed that the internal structure of these objects may be represented by polytropes of index $n = 1.5$. For this to be the case, as discussed in Section 6.1, objects must be in complete convective equilibrium throughout, composed of an ideal, completely ionized gas and the thickness of the outer layers in which hydrogen and helium are incompletely ionized must be very small compared to the total radius. This in fact appears to be the case along the very low mass main sequence. Hayashi and Nakano (1963) and Ezer and Cameron (1966) find that below about $0.25 M_{\odot}$ stars arrive and remain on the main sequence as wholly convective objects. From the results of the detailed $0.1 M_{\odot}$ model considered in Section 6.2, we find that not only is it wholly convective on the main sequence but also that the atmospheric regions as well as the hydrogen-helium ionization-dissociation zone involve only a few per cent of the total radius. We also explored in this detailed model the effect on the overall structure of electrostatic particle interactions within the ionized interior. We find that, at least on the main sequence, these effects may be ignored and that the bulk of the interior may be safely regarded as composed of a completely ionized ideal gas. Thus a polytropic representation of very low mass main

sequence objects should be quite adequate; although we did find that the radius of the detailed $0.1 M_{\odot}$ main sequence model to be 9% smaller than that of the corresponding simple polytropic model (cf. Tables 4 and 5), which worsens the existing discrepancy between the theoretical and empirical mass-radius relations.

The primary effect of the stellar atmosphere on the completely convective models is to determine the luminosity. Although the main sequence position in the H-R diagram, as well as that of the pre-main sequence evolutionary tracks, will be sensitive to the atmospheric opacity, we expect the main sequence radii to be little affected by changes in the opacity. Consequently, we expect that the errors to be associated with the computed values of the atmospheric opacity, Table 3, will not greatly affect the existing discrepancy between the theoretical and empirical mass-radius relations. Similar remarks apply to the determination of the outer boundary condition for the interior structure through the calculation of detailed non-gray atmospheric models which is, perhaps, the major improvement to be made on the present low mass models. Because these regions are so extremely shallow, it seems unlikely that improvements on the simple mixing length theory employed in Section 5.3 or on our treatment of pressure ionization and dissociation in the hydrogen-helium

ionization-dissociation zone will greatly affect the theoretical results.

The pre-main sequence contraction of a star is halted when the rate of nuclear energy release becomes sufficient to supply completely the total luminosity. We therefore consider the possibility that we have underestimated the nuclear energy generation rate in the present models to the extent that, for a given mass, gravitational contraction actually will be halted at that radius appropriate to the adopted empirical mass-radius relation. For a $0.14 M_{\odot}$ object we find, roughly, that this would increase the main sequence luminosity by nearly one magnitude in M_{bol} and would require the energy generation rate to be increased by a factor of about 25. Not only does it seem unlikely that our nuclear energy formulae could admit of so large an error, but we would also then be faced with having to account for the resulting discrepancy between the theoretical and empirical mass-luminosity relations.

We conclude from the above discussion that neither the approximations nor the obvious improvements to be made in the models can be expected to explain the discrepancy between theory and observation. If this discrepancy is due to inherent inadequacy of the models, we suggest that it is due to the omission of some major physical effect which results in large scale departures from polytropic structure.

Before pursuing such possibilities, however, we should first be certain that we possess a completely adequate set of empirical data with which to compare the theoretical models and, thus, that the discrepancy exhibited in Figures 17 and 18 really exists.

6.3.2 Empirical Data

In Chapter 3 we derived on the basis of the currently available observational data a set of mean relations between the masses, radii, luminosities, and effective temperatures for the M dwarf stars. We summarize these adopted relations in Table 2 and take them to define the mean empirical properties of low mass stars of solar composition. The adopted mass-luminosity relation is based on the data taken from Eggen (1965, 1967) for the masses, m , and the absolute visual magnitudes, M_V , of the visual binary pairs listed in Table 1a and plotted in Figure 4. Disregarding the objects ADS 7114BC, 8048BC, 8166AB, 10158AB, and UV Ceti, we represented the correlation between $\log m$ and M_V for these stars by the linear relation given in equation (3.2). From Figure 4, we suggested that equation (3.2) adequately represents the available data for masses above $0.5 M_\odot$ and, perhaps, to masses as low as $0.3 M_\odot$. (The rather large departures, indicated in Figure 4, of Ross 614 AB from the adopted mass luminosity relation may be due to the fact that these are young objects which

have not yet reached the main sequence, a point to which we return in Section 6.4.)

The bolometric corrections given by Johnson (1966) for the M dwarfs were obtained essentially by integrating under the spectral energy distributions derived from the results of broad band infrared photometry of a selected sample of M dwarf stars (Johnson 1965, 1966). We take these bolometric corrections to be quite reliable. Thus except for having to use equation (3.2) to extrapolate to masses below $0.3 M_{\odot}$, we derive our adopted mass-luminosity relation, that is the $\log m, M_{\text{bol}}$ relation, directly from observation. Below $0.3 M_{\odot}$ we lack sufficient data to determine empirically the mass-luminosity relation with any confidence. However from Figure 16 we observe that the theoretical results of Ezer and Cameron (1966) and Hayashi and Nakano (1963) over the range of mass 0.1 to $0.4 M_{\odot}$ show no abrupt change of slope in the $\log m, M_{\text{bol}}$ plane. This suggests that there is some validity for the linear extrapolation based on equation (3.2) of the adopted mass-luminosity relation down to masses of about $0.1 M_{\odot}$.

We cannot determine the empirical mass-radius relation for the M dwarf stars directly by observation, however. It has thus far been possible to determine directly the mass and radius of only a single M dwarf, the MO.5 components of the eclipsing system YY Gem. To determine our adopted empirical mass-radius relation we have

resorted to the indirect procedure of using our adopted mass-luminosity relation together with equation (3.1) and the effective temperature, R-I calibration of Johnson (1966). In Figure 19 we compare the mass-radius relation obtained in this way with the data given by Popper (1967) for the masses and radii of those eclipsing binary systems consisting of main sequence components. We plot the data for the individual objects as filled circles and show by a dashed line our adopted empirical relation. In addition we show the theoretical mass-radius relation from Table 4 by a solid line, the position of YY Gem by a cross, and that of the sun by the symbol \odot . From this diagram we see that the eclipsing systems define a distinct mass-radius relation but only for masses above one solar mass.

It is to be emphasized that our adopted mass-radius relation below $0.6 M_{\odot}$ rests entirely on Johnson's (1966) calibration between the R-I index and the effective temperature and the adopted mass-luminosity relation. For stars later than solar type and with the exception of YY Gem, this calibration rests ultimately on the interferometric measures of the angular diameters of seven stars, all of which are giants or supergiants. The fact that there appears to be fair agreement between the effective temperature and the color temperatures derived from the I-L index for these objects was utilized by Johnson (1966) to extend the original effective temperature, I-L calibration to

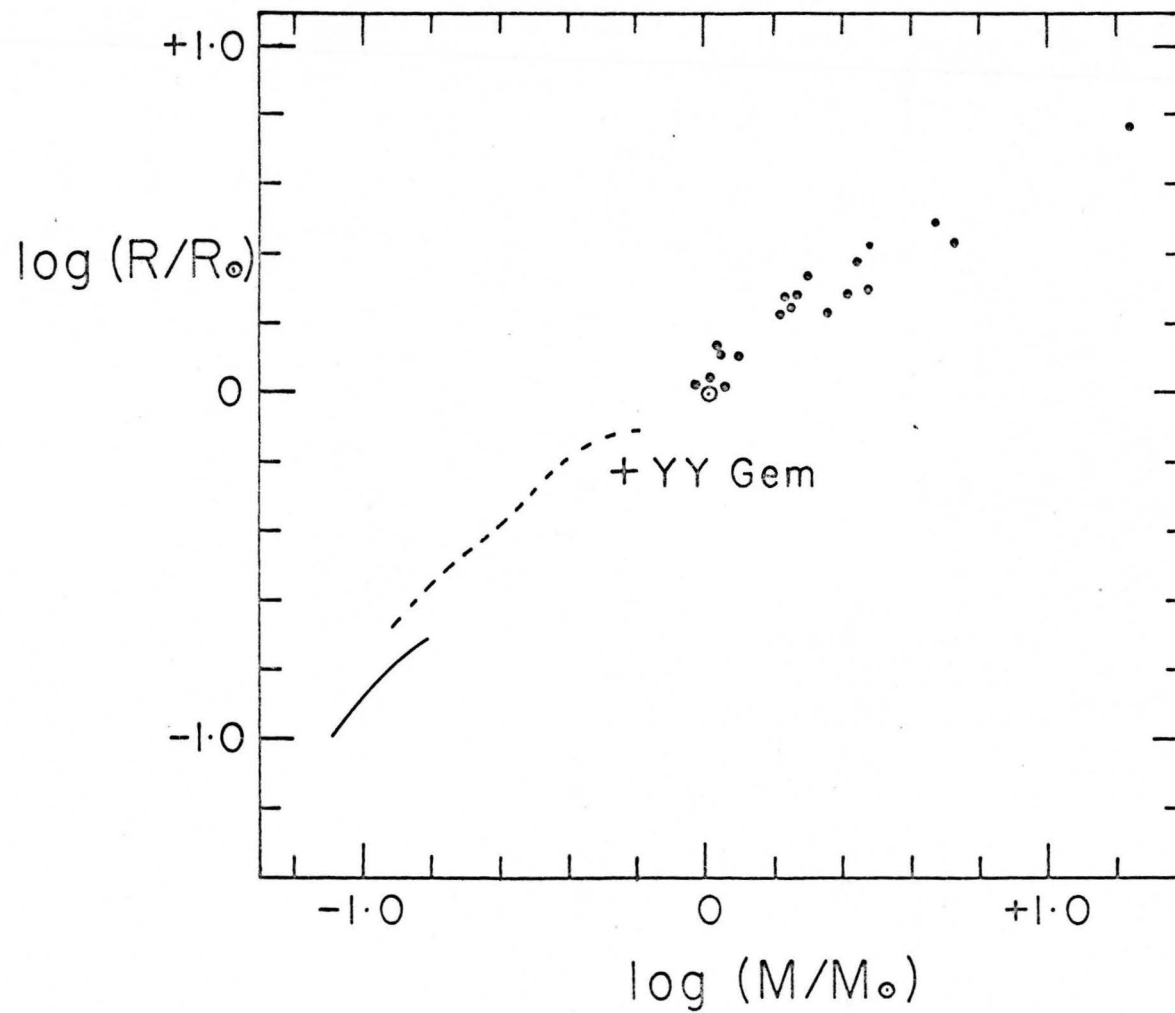


Fig. 19. Comparison of the empirical and theoretical mass-radius relations with the data for the eclipsing binary systems.

objects of spectral type later than M0. The validity of the extension of the effective temperature, R-I relation to the dwarfs, however, rests on the assumption that this same relation applies equally well to dwarfs as to giants. The only direct evidence for this assumption is that the observed data for YY Gem fits Johnson's (1966) original relation rather well. Nevertheless, since the value of the surface gravity ranges over perhaps four or even five orders of magnitude between the supergiants and dwarfs of late spectral types, one must be somewhat cautious about the validity of this assumption for dwarfs appreciably cooler than YY Gem. Not only might the dominant sources of opacity and the resultant nature of the departure from grayness be quite different in the dwarf atmospheres, but also the role of sub-photospheric convection will be quite different and may influence the spectral energy distribution. In order to bring the theoretical models into agreement with the mean empirical data, the value of the effective temperature for a $0.14 M_{\odot}$ object of spectral type M7 and $R-I = +2.08$ would have to be increased by 700 degrees. Whether or not we can reasonably expect this large a difference between the effective temperature of the very late M dwarfs and giants is open to question. Unless low mass eclipsing systems are discovered which yield reliable radii, the only way to attack this problem would

seem to be to construct detailed theoretical non-gray model atmospheres for both giants and dwarfs.

Since at the present time YY Gem plays a critical role in establishing the effective temperature scale for the late type dwarfs, it is interesting to note that YY Gem falls distinctly off the mean empirical mass-radius relation as well as the mean empirical mass-luminosity relation. These discrepancies seem significantly larger than can be accounted for by the probable errors in the determination of the mass, radius, and luminosity of this object. This need not necessarily invalidate the use of YY Gem as a means of calibrating the effective temperature with the R-I index, since there is no indication that YY Gem is photometrically anomalous. Nevertheless, this anomaly (and the curious fact that the values of the mass and radius of YY Gem do place it on what appears to be a simple extension of the mass-radius relation defined by the more massive eclipsing systems, cf. Figure 19) suggests that considerably more work, both observational and theoretical, needs to be done before we can claim a good understanding of the structure of the very low mass stars.

6.4 Stars Below the Main Sequence Limiting Mass

There are two stars, Ross 614B and the components of UV Ceti, whose masses of 0.08 and 0.03 M_{\odot} , respectively, lie below the main sequence limiting mass as determined in

Section 6.1. We have shown by a cross and a circled cross, respectively, the observed positions of these stars in the theoretical H-R diagram shown in Figure 12. It is difficult to reach many conclusions regarding the evolutionary state of these objects. UV Ceti is a member of the Hyades common motion group (Eggen 1963) and, since it presumably shares any abundance differences that may exist between the Hyades stars and the sun, we cannot necessarily expect our $0.03 M_{\odot}$ evolutionary track to represent this object. Ross 614B, however, seemingly falls along Eggen's sun-Sirius mass-luminosity relation (cf. Figure 4) and we conclude that it is likely to be a solar composition object. We note from Figure 12, however, that Ross 614B is discrepant relative to our computed evolutionary track for a $0.08 M_{\odot}$ object. This simply reflects the discrepancy between the theoretical and empirical main sequence properties discussed in the preceding section.

Because its observed mass is so near to the main sequence limiting mass and its observed luminosity places it so near to the theoretical main sequence line, we may speculate that Ross 614B is in fact on the main sequence. Should this be the case, it would seemingly indicate a lower value for the main sequence limiting mass than the value of $0.1 M_{\odot}$ determined by Ezer and Cameron (1966). Our value of $0.085 M_{\odot}$ may be more nearly correct; however we cannot attach much significance to any theoretical

determination of a main sequence limiting mass until we satisfactorily remove the discrepancy between the theoretical and empirical main sequence mass-radius relations.

In connection with the discussion of Figure 4 in the previous section, we pointed out that the objects Ross 614AB depart appreciably from our adopted empirical mass-luminosity relation. Should it be that Ross 614B is insufficiently massive to reach the main sequence, the displacement of both components may be intrinsic, since we could not expect the B component to obey a main sequence mass-luminosity relation and the A component, while massive enough ($0.14 M_{\odot}$) to reach the main sequence, may be sufficiently young as not yet to have completely contracted to its main sequence configuration. If this is the case, then the A component should appear overly luminous for its mass which is, in fact, consistent with its plotted position in Figure 4.

6.5 The Shape of the Mass Function

From the luminosity function data of Luyten (1968) and the sun-Sirius mass-luminosity relation of Eggen (1965) we have obtained the mass function for the solar neighborhood shown in Figure 7. This curve indicates the occurrence of a sharp peak in the mass function at about $0.16 M_{\odot}$ with a rapid decline in the numbers of observed stars as we proceed to lower masses. Assuming the

observational data pertaining to the luminosity function to be complete at least through the maximum of the mass function, we find the mass at which the maximum occurs to be somewhat greater than that which we find for the main sequence limiting mass. Nevertheless it is tempting to associate the observed behavior of the mass function with the existence of the limiting mass. For example, should it be the case that as a consequence of star formation, the initial mass function increases monotonically with decreasing stellar mass down to masses below the limiting mass, then we would expect to observe a form for the mass function shown in Figure 7. There would be a piling up of stars on the main sequence with the maximum number occurring at the limiting mass. Below the limiting mass there would be a paucity of observable objects, since all that could be seen would be those stars young enough to be observably high on the Hayashi contraction tracks. This would have the interesting consequence that the galaxy may contain a large component of very low mass, dark objects.

Gaustad (1963) suggests, however, that if fragmentation in massive clouds of gas and dust determines the initial mass function, we might well expect the majority of stellar objects formed to have masses of a few tenths of a solar mass. This too would lead to a mass function having the shape shown in Figure 7 and would have nothing at all to do with the existence of a main sequence limiting mass.

This interpretation of the mass function would be favored should it be that the maximum in the mass function occurs at an appreciably higher mass than the limiting mass. We must, therefore, be convinced that both the mass function and the limiting mass are determined sufficiently accurately. Again, we cannot trust our value for the limiting mass so long as there remains a discrepancy between our theoretical models and the empirical data.

APPENDIX A

DEBYE-HÜCKEL THEORY FOR AN IONIZED, PARTIALLY DEGENERATE PLASMA

We consider a fully ionized plasma at a temperature T and confined within a volume V . We regard the ions and electrons as point charges and consider each charged particle in the gas to be surrounded by an inhomogeneously charged but spherically symmetric distribution of ions and electrons. We assume that the total potential energy of the system, W , may be written as the sum of two-particle electrostatic interactions, that is

$$W = \sum_{a,b} \frac{z_a z_b e^2}{r_{ab}}$$

where the summation is performed over all pairs of particles a, b of charges $z_a e$ and $z_b e$, respectively, and separation r_{ab} (cf. Fowler and Guggenheim 1956, pp. 283-393). Let us choose a particular charged particle, say particle a , to be at the origin of a system of spherical coordinates. At any instant the electrostatic potential $\phi_a(r)$ at a distance r from particle a is related to the charge density $\rho_a(r)$ at r through Poisson's equation,

$$\nabla^2 \phi_a(r) = -4\pi \rho_a(r). \quad (\text{A.1})$$

We shall be concerned with time averages of the potential and charge density which we assume to be equivalent to averages taken over all possible spatial configurations of the particles. We then assert that the average potential at r is related to the average charge density at r through

$$\nabla^2 \langle \varphi_a(r) \rangle_a = -4\pi \langle \rho_a(r) \rangle_a \quad (\text{A.2})$$

where $\langle \varphi_a(r) \rangle_a$ and $\langle \rho_a(r) \rangle_a$ are the potential and charge density, respectively, at r averaged over all possible spatial distributions of the other charged particles in the gas with particle a held fixed.

Let us now assume that all of the particles in the gas, both the ions and the electrons, obey the Maxwell-Boltzmann statistics. While this is always a good approximation for the ions, it is valid for the electrons only if the electron number density n_e satisfies the condition

$$n_e \ll \frac{(2\pi m_e kT)^{3/2}}{h^3} \quad (\text{A.3})$$

where h is Planck's constant, m_e is the mass of an electron and k is Boltzmann's constant. Upon assuming this condition to be satisfied, we may write down the probability, $\Psi_{ab}(r_{ab})$, that any particle b of charge $z_b e$, where e is the charge of the electron, be found at a distance r_{ab} from particle a of charge $z_a e$, that is

$$\Psi_{ab}(r_{ab}) = A \exp[-\beta \epsilon_{ab}(r_{ab})]$$

where A is a constant, $\beta = (kT)^{-1}$, and $\epsilon_{ab}(r_{ab})$ is the interaction energy between particles a and b in the presence of all the other particles in the gas. The average probability that particle b be found at a distance r_{ab} from a is

$$\langle \Psi_{ab} \rangle_{ab} = A \langle \exp[-\beta \epsilon_{ab}(r_{ab})] \rangle_{ab} \quad (A.4)$$

where the average is taken over all configurations of particles holding particles a and b fixed. In their study of the effects of ionic interactions in solutions of strong electrolytes, Debye and Hückel (1923) (see also Fowler and Guggenheim 1956) introduced the following approximations, which we label the DH approximations,

$$\langle \exp[-\beta \epsilon_{ab}(r_{ab})] \rangle_{ab} = \exp[-\beta \langle \epsilon_{ab}(r_{ab}) \rangle_{ab}] \quad (A.5)$$

and

$$\langle \epsilon_{ab}(r_{ab}) \rangle_{ab} = z_b e \langle \phi_a(r_{ab}) \rangle_a. \quad (A.6)$$

As in equation (A.2), $\langle \phi_a(r_{ab}) \rangle_a$ is the electrostatic potential at the distance r_{ab} from particle a averaged over all configurations of particles with a held fixed. We see that the first DH approximation can be strictly valid only if

$$\langle \epsilon_{ab}^2(r_{ab}) \rangle_{ab} = \langle \epsilon_{ab}(r_{ab}) \rangle_{ab}^2$$

$$\langle \epsilon_{ab}^3(r_{ab}) \rangle_{ab} = \langle \epsilon_{ab}(r_{ab}) \rangle_{ab}^3$$

$$\begin{array}{ccc} \cdot & & \cdot \\ \cdot & & \cdot \\ \cdot & & \cdot \end{array}$$

$$\langle \epsilon_{ab}^n(r_{ab}) \rangle_{ab} = \langle \epsilon_{ab}(r_{ab}) \rangle_{ab}^n.$$

The averaging to obtain $\langle \epsilon_{ab}(r_{ab}) \rangle_{ab}$ is performed over all particles except a and b, which are held fixed, while the averaging to obtain $\langle \phi_a(r_{ab}) \rangle_a$ is performed over all particles except a, which is held fixed, but including particle b. We see that the second DH approximation will be best when particle b does not contribute appreciably to $\langle \phi_a(r_{ab}) \rangle_a$. This condition will be met if z_b is small and if the density of the other charged particles is high.

The quantity $\langle \epsilon_{ab}(r_{ab}) \rangle_{ab}$ can be interpreted as the work necessary to bring particle b from infinity to the distance r_{ab} from particle a averaged over all possible configurations of the other particles. By symmetry we must have that $\langle \epsilon_{ab}(r_{ab}) \rangle_{ab} = \langle \epsilon_{ba}(r_{ba}) \rangle_{ba}$ which, with the second DH approximation leads to the condition

$$\frac{\langle \phi_a(r) \rangle_a}{z_a} = \frac{\langle \phi_b(r) \rangle_b}{z_b} \quad (\text{A.7})$$

for all pairs of charged particles within the system. It can also be shown from general principles (Fowler and Guggenheim 1956) that the instantaneous electrostatic potentials at particles a and b, say $\phi_a(0)$ and $\phi_b(0)$, due only to the presence of the other charged particles in the system, that is, excluding the self-potentials of the two particles, must obey the relation

$$\frac{\partial \phi_a(0)}{\partial z_b} = \frac{\partial \phi_b(0)}{\partial z_a}. \quad (\text{A.8})$$

Equations (A.7) and (A.8) can be used to test the self-consistency of any approximate solutions to the problem.

Employing the second DH approximation we may write equation (A.4) as

$$\langle \Psi_{ab} \rangle_{ab} = A \exp \left[z_b e \langle \phi_a(r_{ab}) \rangle_a \right]. \quad (\text{A.9})$$

For simplicity of notation let $\phi_a(r)$ now denote the potential at the distance r from particle a averaged over all particles excluding a. If we now let n_{so} denote the mean number density of the s^{th} species of charged particle in the absence of any electrostatic interactions, it follows from equation (A.9) that we may approximate the distribution of the s^{th} species of particles about particle a by

$$n_{as}(r) = n_{so} \exp \left[- z_s e \phi_a(r) \right]. \quad (\text{A.10})$$

In what follows we shall assume that the gas deviates only slightly from a perfect gas which implies that the Coulomb interaction between the particles must be small compared to the mean thermal energy per particle. If we let ze be the mean charge per particle and r_o be the mean particle separation, we require that

$$\frac{z^2 e^2}{r_o} \ll kT$$

which gives the condition on the mean charged particle number density n that

$$n \ll \frac{3}{4\pi} \left(\frac{kT}{z^2 e^2} \right)^3. \quad (A.11)$$

This is equivalent to assuming that $z_s e \phi_a(r) \ll kT$ which allows us to expand the exponential in equation (A.10) to give, retaining only the first order term in ϕ ,

$$n_{as}(r) = n_{so} \left[1 - z_s e \beta \phi_a(r) \right]. \quad (A.12)$$

At this point we have introduced the further approximation of considering a linearized treatment of the DH problem. In so doing we shall see that the conditions contained in equations (A.7) and (A.8) will be automatically satisfied. In general any attempt to improve the results through the retention of higher order terms in the expansion of equation (A.10) will not be consistent with respect to these symmetry conditions. The criterion on the density and

temperature contained in equation (A.11) defines the region over which these considerations will remain valid. At the lowest densities we have a perfect gas while at sufficiently high densities that equation (A.11) is not satisfied, we shall find it necessary to introduce a new model by which we may estimate the non-ideal behavior of the system.

In arriving at equation (A.10) we have assumed that all of the particles in the gas may be treated by the Maxwell-Boltzmann statistics. We now wish to generalize to the case in which we explicitly consider the electrons to obey the Fermi-Dirac statistics. To accomplish this we employ what is essentially the Thomas-Fermi approximation and assume that any given electron moving in the vicinity of any particular charged particle moves in a potential field arising from the superposition of that of the given particle and that of all of the other charged particles in the gas such that the fractional change in the potential is negligibly small over a distance corresponding to the mean thermal de Broglie wavelength of an electron. This is equivalent to treating the electron as if it were moving in the presence of a static, uniform external field. Let $\mu_a(r)$ be the chemical potential of the electrons at a distance r from particle a . We may express $\mu_a(r)$ as

$$\mu_a(r) = \mu_{ae}(r) + \epsilon_{ae}(r) \quad (\text{A.13})$$

where μ_{ae} is the chemical potential appropriate to the electron density at r and ϵ_{ae} is the interaction energy between particle a and an electron at r . We employ the second DH approximation and assume that

$$\langle \epsilon_{ae}(r) \rangle_{ae} = -e\phi_a(r) \quad (\text{A.14})$$

where $\langle \epsilon_{ae} \rangle_{ae}$ is the electrostatic interaction energy between particle a and an electron at r averaged over all configurations of particles with particle a and the electron held fixed. Under the conditions of equilibrium the chemical potential of the electrons must be constant with r otherwise the electrons would migrate to those regions of space in which the chemical potential were minimum. Hence we may write equation (A.13) in the form

$$\mu_{ae}(r) - e\phi_a(r) = \mu_a = \text{constant}. \quad (\text{A.15})$$

We now consider a gaseous mixture of ions and electrons. Let z_k and n_{ko} be the charge number and the mean number density of the k^{th} species of ion, respectively. We can define a total mean ion number density, n_{io} , and a mean ionic charge number z such that

$$n_{io} = \sum_k n_{ko} \quad (\text{A.16})$$

and

$$z = \frac{1}{n_{io}} \sum_k z_k n_{ko}. \quad (\text{A.17})$$

We may thus treat the gas as consisting of a mixture of $N_i = Vn_{io}$ ions of charge ze and $N_e = Vn_{eo}$ electrons of charge $-e$. Requiring that the system be electrically neutral as a whole gives

$$n_{eo} = zn_{io}. \quad (\text{A.18})$$

The mean charge density $\rho_i(r)$ at a distance r from the i^{th} ion can be written as

$$\rho_i(r) = en_{ii}(r) - en_{ie}(r) \quad (\text{A.19})$$

where $n_{ii}(r)$ and $n_{ie}(r)$ are, respectively, the mean ion and electron number densities at the distance r from the i^{th} ion. We may use the Boltzmann formula, equation (A.10), for $n_{ii}(r)$,

$$n_{ii}(r) = n_{io} \exp \left[-\beta e\phi_i(r) \right] \quad (\text{A.20})$$

where $\phi_i(r)$ is the mean potential at the distance r from the i^{th} ion. From the Fermi-Dirac distribution (see Tolman 1938) we may write

$$n_{ie}(r) = \frac{4\pi}{h^3} (2m_e kT)^{3/2} F_{1/2}(\eta_i) \quad (\text{A.21})$$

where from equation (A.15) we have

$$\eta_i = \beta\mu_i = \beta \left[\mu_{ie}(r) - e\phi_i(r) \right] \quad (\text{A.22})$$

and the Fermi-Dirac integrals are defined by

$$F_{\alpha}(\eta) = \int_0^{\infty} \frac{x^{\alpha}}{\exp(x-\eta)+1} dx. \quad (\text{A.23})$$

Expanding the exponential in equation (A.20) we have to first order

$$n_{ii}(r) = n_{io} \left[1 - ze^{\beta\phi_i(r)} \right] \quad (\text{A.24})$$

while expanding $n_{ie}(r)$ in a Taylor's series about μ_o , the chemical potential of the electrons in the absence of particle interactions, we obtain to first order in $\phi_i(r)$

$$n_{ie}(r) = n_{eo} \left[1 + e^{\beta\phi_i(r)} \theta_e \right] \quad (\text{A.25})$$

where θ_e is defined by

$$\theta_e = \frac{4\pi}{n_{eo} h^3} (2\pi m_e kT)^{3/2} F'_{1/2}(\eta_o) = \frac{F'_{1/2}(\eta_o)}{F_{1/2}(\eta_o)} \quad (\text{A.26})$$

since from Tolman (1938) it may be shown that

$$F_{1/2}(\eta_o) = \frac{n_{eo}}{4\pi} \left(\frac{h^2}{2m_e kT} \right)^{3/2}. \quad (\text{A.27})$$

In equations (A.21) and (A.22) we have let $\eta_o = \beta\mu_o$, and the prime denotes differentiation with respect to η_o .

We may now write down Poisson's equation for the potential field about the i^{th} ion, that is

$$\nabla^2 \phi_i(r) = -4\pi \rho_i(r) \quad (\text{A.28})$$

which upon substituting equations (A.24) and (A.25) for $\rho_i(r)$ gives, approximately,

$$\nabla^2 \varphi_i(r) = 4\pi e^2 \beta (z^2 n_{i0} + n_{e0} \theta_e) \varphi_i(r). \quad (\text{A.29})$$

Letting κ be the inverse Debye length, where

$$\kappa^2 = 4\pi e^2 \beta (z^2 n_{i0} + n_{e0} \theta_e) \quad (\text{A.30})$$

and noting that $\varphi_i(r)$ must satisfy the following two boundary conditions

$$\lim_{r \rightarrow \infty} [\varphi_i(r)] = 0$$

and

$$\lim_{r \rightarrow 0} [r\varphi_i(r)] = ze$$

we obtain the solution

$$\varphi_i(r) = \frac{ze}{r} \exp(-\kappa r). \quad (\text{A.31})$$

We proceed in a completely analogous manner to obtain the potential distribution about a particular electron in the gas. We write down Poisson's equation

$$\nabla^2 \varphi_e(r) = -4\pi \rho_e(r)$$

where $\varphi_e(r)$ and $\rho_e(r)$ are the mean potential and charge densities, respectively, about the given electron, and $\rho_e(r)$ can be written as

$$\rho_e(r) = zn_{ei}(r) - en_{ee}(r) \quad (\text{A.32})$$

where $n_{ei}(r)$ and $n_{ee}(r)$ denote, respectively, the mean ion and electron number density distributions about the given electron. To obtain $n_{ei}(r)$ we invoke the symmetry argument of Cowan and Kirkwood (1958) and assert that

$$zn_{ei}(r) = n_{ie}(r). \quad (\text{A.33})$$

That is, that the form of the distribution of the ions about an electron is the same as that of the electrons about an ion. Thus

$$zn_{ei}(r) = n_{eo} \left[1 + e\beta\theta_e \varphi_i(r) \right]. \quad (\text{A.34})$$

We take $\mu_e = \mu_{ee} - e\varphi_e = \text{constant}$ and $\eta_e = \beta\mu_e$ to give to first order in $\varphi_e(r)$

$$n_{ee}(r) = n_{eo} \left[1 + e\beta\theta_e \varphi_e(r) \right]. \quad (\text{A.35})$$

Poisson's equation now becomes

$$\nabla^2 \varphi_e(r) = 4\pi e^2 \beta \theta_e n_{eo} \left[\varphi_e(r) - \varphi_i(r) \right]. \quad (\text{A.36})$$

From the symmetry requirement of equation (A.7) it is apparent that $\varphi_e(r) = C\varphi_i(r)$ where C is a constant. Substituting this into the above equation we find that $C = -\theta_e/z$ and we obtain the solution

$$\varphi_e(r) = -\frac{e\theta_e}{r} \exp(-\kappa r). \quad (\text{A.37})$$

The solutions φ_i and φ_e represent the mean electrostatic potential distributions about any particular ion or electron, respectively. Expanding the exponentials in equations (A.31) and (A.37) we have

$$\varphi_i(r) = \frac{ze}{r} (1 - \kappa r + \frac{1}{2}\kappa^2 r^2 - \dots)$$

and

$$\varphi_e(r) = -\frac{e\theta_e}{r} (1 - \kappa r + \frac{1}{2}\kappa^2 r^2 - \dots).$$

We now subtract off the self-potentials of the ion and the electron, ze/r and $-e\theta_e/r$, respectively, from these equations and let $r \rightarrow 0$ to obtain the residual electrostatic potential at the positions of each of the two particles arising from all of the other particles in the gas.

Denoting these potentials as $\varphi_i(0)$ and $\varphi_e(0)$ we have, respectively,

$$\varphi_i(0) = -ze\kappa \quad (\text{A.38})$$

and

$$\varphi_e(0) = e\theta_e\kappa. \quad (\text{A.39})$$

We observe that these solutions satisfy the symmetry requirements expressed by equations (A.7) and (A.8) in which the degeneracy parameter θ_e appears as the effective charge number of the electrons.

The contribution to the Helmholtz function of the gas resulting from the interactions between the particles is just the work done in charging up the particles of the gas at constant volume and temperature. For the ions we have

$$\begin{aligned}\frac{F_{ic}}{V} &= - n_{io} \int_0^e (ze' \kappa \cdot z) de' \\ &= - \frac{1}{3} n_{io} z^2 e^3 (4\pi\beta)^{1/2} (z^2 n_{io} + n_{eo} \theta_e)^{1/2}\end{aligned}$$

and for the electrons we have

$$\begin{aligned}F_{ec} &= - n_{eo} \int_0^e e' \theta_e \kappa de' \\ &= - \frac{1}{3} n_{eo} e^3 \theta_e (4\pi\beta)^{1/2} (zn_{io} + n_{eo} \theta_e)^{1/2}.\end{aligned}$$

The total electrostatic correction to the Helmholtz function $F_c = F_{ic} + F_{ed}$, is, then,

$$F_c = - \frac{V\kappa^3}{12\pi\beta}. \quad (A.40)$$

This result is in agreement with a similar result obtained by Kidder and DeWitt (1961).

REFERENCES

- Allen, C. W. 1963, Astrophysical Quantities (2d ed.; London: Athlone Press).
- Aller, L. 1950, Ap. J., 111, 173.
- Aller, L., Chamberlain, J., Lewis, E., Liller, W., McDonald, J., Potter, W., and Weber, N. 1952, Ap. J., 115, 328.
- Armstrong, B. H., Sokoloff, J., Nicholls, R. W., Holland, D. H., and Meyerott, R. E. 1961, J. Quant. Spectr. and Rad. Trans., 1, 143.
- Auman, J. R. 1966, Ap. J. Suppl., 14, 171.
- Brout, R., and Carruthers, P. 1963, Lectures on the Many-Electron Problem (New York: Interscience).
- Brush, S. G., Sahlin, H. L., and Teller, E. 1966, J. Chem. Phys., 45, 2102.
- Chandrasekhar, S. 1939, An Introduction to the Study of Stellar Structure (Chicago: University of Chicago Press).
- _____. 1958, Ap. J., 128, 114.
- Cowan, R., and Kirkwood, J. 1958, J. Chem. Phys., 29, 264.
- Cox, A. N. 1965, Stars and Stellar Systems, Vol. 8 (Chicago: University of Chicago Press).
- Cox, A. N., and Stewart, J. N. 1965, Ap. J. Suppl., 11, 22.
- Dalgarno, A., and Lane, N. F. 1966, Ap. J., 145, 623.
- Danielson, R. E., Woolf, N. J., and Gaustad, J. R. 1965, Ap. J., 141, 116.
- Debye, P., and Hückel, E. 1923, Z. F. Phys., 24, 185.
- Demarque, P. 1960, Ap. J., 132, 366.

- DeWitt, H. E. 1961, J. Nuclear Energy, C, 2, 27.
- _____. 1965, Lawrence Radiation Laboratory, Report UCRL-14102.
- Ecker, G., and Kröll, W. 1963, Phys. Fluids, 6, 62.
- Eggen, O. J. 1963, A. J., 68, 483.
- _____. 1965, A. J., 70, 19.
- _____. 1967, Ann. Rev. Astr. and Ap., 5, 105.
- _____. 1968, Ap. J. Suppl., 16, 49.
- Ezer, D., and Cameron, A. G. W. 1963, Icarus, 1, 422.
- _____. 1966, A. J., 71, 384 (also undated NASA report).
- Ferriso, C. C., Ludwig, C. B., and Thomson, A. L. 1966, J. Quant. Spectr. and Rad. Trans., 6, 241.
- Feynman, R. P., Metropolis, N., and Teller, E. 1949, Phys. Rev., 75, 1561.
- Fowler, R. H. 1936, Statistical Mechanics (Cambridge: Cambridge University Press).
- Fowler, R., and Guggenheim, E. A. 1956, Statistical Thermodynamics (Cambridge: Cambridge University Press).
- Gaustad, J. E. 1963, Ap. J., 138, 1050.
- Geltman, S. 1965, Ap. J., 141, 376.
- Gingerich, O. 1961, Ap. J., 134, 653.
- Gingerich, O. J., Latham, D. W., Linsky, J. L., and Kumar, S. S. 1967, Smithsonian Astrophysical Observatory Special Report No. 240.
- Glassgold, A. E., Hechrothe, W., and Watson, K. M. 1959, Phys. Rev., 106, 364.
- Harris, G. 1962, Phys. Rev., 125, 1131.
- Harris, G. M., and Trulio, J. 1961, J. Nuclear Energy, C, 2, 224.

- Haselgrove, C. B., and Hoyle, F. 1956, M.N.R.A.S., 116, 515.
- Hayashi, C. 1961, Pub. Astr. Soc. Japan, 13, 450.
- _____. 1966, Ann. Rev. Astr. and Ap., 4, 171.
- Hayashi, C., and Hōshi, R. 1961, Pub. Astr. Soc. Japan, 13, 442.
- Hayashi, C., and Nakano, T. 1963, Progr. Theoret. Phys., 30, 460.
- Hayashi, C., Hōshi, R., and Sugimoto, D. 1962, Progr. Theoret. Phys., Suppl. No. 22, p. 1.
- Hayashi, M. 1965, Pub. Astr. Soc. Japan, 17, 177.
- Heneyey, L., Forbes, J., and Gould, N. 1964, Ap. J., 139, 306.
- Heneyey, L., LeLevier, R., and Levée, R. 1955, P.A.S.P., 67, 154.
- Heneyey, L., Vardya, M. S., and Bodenheimer, P. 1965, Ap. J., 142, 841.
- Herzberg, G. 1950, Spectra of Diatomic Molecules (Princeton: D. Van Nostrand).
- Hubbard, W. B. 1966, Ap. J., 146, 858.
- Iben, I. 1965, Ap. J., 141, 993.
- John, T. L. 1966, M.N.R.A.S., 131, 315.
- Johnson, H. L. 1964, Bull. Tonantzintla and Tacubaya Obs., 3, 305.
- _____. 1965, Ap. J., 141, 170.
- _____. 1966, Ann. Rev. Astr. and Ap., 4, 193.
- Kidder, R. E., and DeWitt, H. E. 1961, J. Nuclear Energy, C, 2, 218.
- Kron, G. E. 1952, Ap. J., 115, 301.
- Kron, G. E., Gascoigne, S. C. B., and White, H. S. 1957, A. J., 62, 205.

- Kuiper, G. P. 1938, Ap. J., 88, 486.
- _____. 1963, Comm. Lunar and Planet. Lab., 1, 179.
- Kumar, S. S. 1963, Ap. J., 137, 1121.
- Landau, L. D., and Lifshitz, E. M. 1958, Statistical Physics (London: Pergamon Press).
- Limber, D. N. 1958a, Ap. J., 127, 363.
- _____. 1958b, Ap. J., 127, 387.
- Linsky, J. L. 1966, Paper presented at the Conference on the Evolution of Stars of Low Mass held at Indiana University, October, 1966.
- Luyten, W. J. 1968, M.N.R.A.S., 139, 221.
- Mayer, H. 1947, Los Alamos Scientific Laboratory, Report LA-647.
- Mayer, J. E., and Mayer, M. G. 1940, Statistical Mechanics (New York: John Wiley and Sons).
- McCammon, D., Münch, G., and Neugebauer, G. 1966, Ap. J., 147, 575.
- McDougall, J., and Stoner, E. C. 1938, Phil. Trans. R. Soc. London, 237, 67.
- McDowell, M. R. C., Williamson, J. H., and Myerscough, V. P. 1966, Ap. J., 143, 827.
- Mestel, L. 1950, Proc. Cambridge Phil. Soc., 46, 331.
- Montroll, E. W., and Ward, J. C. 1958, Phys. Fluids, 1, 55.
- Nakano, T. 1966 (private communication).
- Naur, P., and Osterbrock, D. 1953, Ap. J., 117, 306.
- Osterbrock, D. 1953, Ap. J., 118, 529.
- Parker, P. D., Bahcall, J. N., and Fowler, W. A. 1964, Ap. J., 139, 602.
- Popper, D. M. 1967, Ann. Rev. Astr. and Ap., 5, 85.
- Salpeter, E. 1952, Phys. Rev., 88, 547.

- _____. 1954, Australian J. Phys., 7, 373.
- _____. 1961, Ap. J., 134, 609.
- Schwarzschild, M. 1946, Ap. J., 104, 203.
- _____. 1958, Structure and Evolution of the Stars (Princeton, N. J.: Princeton University Press).
- Sears, R. L., and Brownlee, R. R. 1965, Stars and Stellar Systems, Vol. 8 (Chicago: University of Chicago Press), 575.
- Seitz, F. 1940, Modern Theory of Solids (New York: McGraw-Hill Book Co.).
- Somerville, W. B. 1965, Ap. J., 141, 811.
- Spinrad, H., and Newburn, R. L. 1965, Ap. J., 141, 965.
- Spinrad, H., Pyper, D. M., Newburn, R. L., Jr., and Younkin, R. L. 1966, Ap. J. 143, 291.
- Spitzer, L., Jr. 1968, Stars and Stellar Systems, Vol. 7 (Chicago: University of Chicago Press), 1.
- Stewart, J. C., and Pyatt, K. D., Jr. 1966, Ap. J., 144, 1203.
- Stromgren, B. 1952, A. J., 57, 65.
- Tolman, R. C. 1938, The Principles of Statistical Mechanics (Oxford: Oxford University Press).
- Vardya, M. S. 1960, Ap. J. Suppl., 4, 281.
- _____. 1962, Ap. J., 135, 303.
- _____. 1965, M.N.R.A.S., 129, 205.
- _____. 1966, M.N.R.A.S., 134, 347.
- Vardya, M. S., and Böhm, K. H. 1965, M.N.R.A.S., 131, 89.
- Weymann, R., and Moore, E. 1963, Ap. J., 137, 552.
- Williamson, R., and Duff, G. 1949a, M.N.R.A.S., 109, 46.
- _____. 1949b, ibid., p. 55.
- Woolf, N. J., Schwarzschild, M., and Rose, W. K. 1964, Ap. J., 140, 833.